

COMPRESSION RESPONSE AND MODELING OF  
INTERPENETRATING PHASE COMPOSITES  
AND FOAM-FILLED HONEYCOMBS

Except where reference is made to the work of others, the work described in this thesis is my own or was done in collaboration with my advisory committee. This thesis does not include proprietary or classified information.

---

Rahul Jhaver

Certificate of Approval:

---

Jeffrey C. Suhling  
Quina Professor  
Mechanical Engineering

---

Hareesh V. Tippur, Chair  
Professor  
Mechanical Engineering

---

Robert L. Jackson  
Assistant Professor  
Mechanical Engineering

---

George T. Flowers  
Dean  
Graduate School

COMPRESSION RESPONSE AND MODELING OF  
INTERPENETRATING PHASE COMPOSITES  
AND FOAM-FILLED HONEYCOMBS

Rahul Jhaver

A Thesis

Submitted to

the Graduate Faculty of

Auburn University

in Partial Fulfillment of the

Requirements for the

Degree of

Master of Science

Auburn, Alabama  
August 10, 2009

COMPRESSION RESPONSE AND MODELING OF  
INTERPENETRATING PHASE COMPOSITES  
AND FOAM-FILLED HONEYCOMBS

Rahul Jhaver

Permission is granted to Auburn University to make copies of this thesis at its discretion, upon request of individuals or institutions and at their expense. The author reserves all publication rights.

---

Signature of Author

---

Date of Graduation

## VITA

Rahul Jhaver was born in Nagpur, India in 1985. He obtained his Bachelor's degree in Mechanical Engineering from Anna University, Chennai, India in 2006 with first class. He started pursuing his Master of Science degree in Mechanical Engineering at Auburn University in August 2006. Since his enrollment in the M.S program, he has also worked as a Graduate Research Assistant, conducting research on the failure behavior of interpenetrating phase composites. He also worked as a Graduate Teaching Assistant for the undergraduate course of Mechanics of Materials at the mechanical engineering department

THESIS ABSTRACT

COMPRESSION RESPONSE AND MODELING OF

INTERPENETRATING PHASE COMPOSITES

AND FOAM-FILLED HONEYCOMBS

Rahul Jhaver

Master of Science, August 10, 2009  
(B.E., Anna University, 2006)

163 Typed Pages

Directed by Hareesh V. Tippur

Although multiphase materials with discrete, dispersed and/or embedded phases in a matrix have been evolving over the years, there are limitations in terms of the degree of concentration of the secondary phase that can be dispersed into the primary phase. Nature has addressed this by adopting a 3D interpenetrating network of phases as evident in skeletal tissues and some tree trunk microstructures. This observation has inspired a relatively new category of materials called Interpenetrating Phase Composites (IPC). Thus in an IPC constituent phases are interconnected three-dimensionally and topologically throughout the microstructure. Consequently, each phase of an IPC contributes its property to the overall macro scale characteristics while adding mechanical constraint synergistically.

In this thesis, the feasibility of processing a lightweight interpenetrating phase composite (IPC) made of aluminum and syntactic polymer foams is demonstrated.

A syntactic foam-filled aluminum honeycomb composite is also examined as a 2D variant of the IPC. Pressureless infiltration of uncured syntactic epoxy foam into an open-cell aluminum preform or a honeycomb structure is used for producing the composite systems. The compression characteristics of these novel materials relative to syntactic foams are studied. Different varieties of IPC foam and foam-filled honeycombs are prepared by varying the volume fraction of microballoons in the syntactic epoxy foam while keeping the volume fraction of the metallic network the same. Two variations of IPC foam are produced by using the aluminum preform in 'as-received' condition and after coating it with silane to increase adhesion between the metallic network and polymer foam. Uniaxial compression tests are then carried out on syntactic foam and foam-filled composites. The IPC foam and foam-filled honeycomb samples show enhancement in elastic modulus, yield stress and plateau stress when compared to the corresponding syntactic foam samples. Silane coated IPC foam samples in particular show significant improvements in these properties. The silane treated IPC foam consistently shows about 50% higher energy absorption relative to the corresponding syntactic foam. The maximum increase in the energy absorption for syntactic foam-filled honeycomb composite is found to be approximately 48%.

A unit-cell based 3D elastic-plastic finite element model is developed to predict the stress-strain response of the IPC foam. A space filling Kelvin cell (tetrakaidecahedron) is used to represent the microstructure of the IPC. In case of foam-filled honeycombs, 2D elastic-plastic analyses on 8 x 8 array of cells are carried out. Measurements are used to validate compression behavior of both IPC and foam-filled honeycomb models up to 40% strain. The measured elastic moduli of the syntactic foam and foam-filled composites are also compared with a few existing micromechanics models.

## ACKNOWLEDGEMENTS

In the first place, I would like to express my deepest and sincere gratitude to my advisor, Dr. Hareesh V. Tippur for his unflagging support, guidance, motivation and also introducing me to new concepts throughout this research work. Thanks are due to my thesis committee members Dr. Jeffrey Suhling and Dr. Robert Jackson for reviewing this work. I would like to thank my research group, Kailash, Chandru, Dong and Vinod for useful discussions and enjoyable moments in the lab. Thanks are also due to Madhu and Taylor, former students of our group for their suggestions and ideas during this research work. Thanks to Mr. Roy Howard in Materials Science Department for his help with the Scanning Electron Microscope. The financial support of this research by the U.S. Army Research Office (grants # W911NF-04-10257 and W911NF-08-1-0285) awarded to Dr. Hareesh Tippur is gratefully acknowledged

Finally, I would like to thank all my friends and colleagues for their support and encouragement at all times during my stay at Auburn. I owe my most sincere gratitude and gratefulness to my parents and brother for their enduring love and immense moral support. They have been a constant source of inspiration and motivation. I dedicate this work to them.

Style manual or journal used Discrete Mathematics (together with the style known as “auphd”). Bibliography follows van Leunen’s *A Handbook for Scholars*.

Computer software used The document preparation package Microsoft Word 2003. Microsoft Excel 2003 was used for preparing the graphs.



## TABLE OF CONTENTS

LIST OF FIGURES .....	xii
LIST OF TABLES .....	xvii
1. INTRODUCTION .....	1
1.1 Cellular solids: An overview .....	1
1.2 Advantages of foam-filled cellular solids .....	4
1.3 Interpenetrating phase composites(IPC) .....	5
1.4 Literature review .....	8
1.5 Objectives .....	12
1.5 Organization of the thesis .....	13
2. MATERIAL PREPARATION AND CHARACTERIZATION .....	15
2.1 Material description .....	15
2.1.1 Syntactic foam .....	16
2.1.2 Aluminum foam .....	17
2.1.3 Aluminum honeycomb .....	19
2.2 Material preparation .....	20
2.2.1 Mold preparation .....	21
2.2.2 Syntactic foam .....	22
2.2.3 Interpenetrating aluminum-syntactic foam composite .....	23
2.2.4 Syntactic foam-filled aluminum honeycomb composite .....	25
2.3 Microstructural characterization .....	26
2.3.1 Syntactic foam .....	26
2.3.2 Interpenetrating aluminum-syntactic foam composite .....	27
2.3.3 Syntactic foam-filled aluminum honeycomb composite .....	28
3. COMPRESSION CHARACTERISTICS OF SYNTACTIC FOAM .....	30
3.1 Experimental setup .....	30
3.2 Effect of specimen aspect ratio .....	32
3.3 Effect of volume fraction of microballoons .....	34
3.4 Energy absorption characteristics of syntactic foam .....	38
3.5 Effect of lubricant on stress-strain response of syntactic foam .....	41

4. COMPRESSION CHARACTERISTICS OF SYNTACTIC FOAM-FILLED COMPOSITES .....	45
4.1 Compression characteristics of IPC foam.....	46
4.1.1 Effect of volume fraction of microballoons.....	49
4.1.2 Energy absorption characteristics of IPC.....	54
4.2 Compression characteristics of syntactic foam-filled honeycombs.....	57
4.2.1 Effect of volume fraction of microballoons.....	57
4.2.2 Effect of direction of compression.....	64
4.2.3 Energy absorption characteristics of syntactic foam-filled honeycomb.....	67
5. FINITE ELEMENT MODELING OF SYNTACTIC FOAM-FILLED COMPOSITES.....	72
5.1 Material model.....	73
5.2 Finite element modeling of IPC foam.....	75
5.2.1 Development of unit cell model.....	75
5.2.2 FEA model description .....	77
5.2.3 Results.....	80
5.2.4 Effect of boundary conditions.....	85
5.3 Finite element modeling of syntactic foam-filled honeycombs.....	89
5.3.1 FEA model description .....	90
5.3.2 Results.....	95
6. MICROMECHANICS BASED ELASTIC MODULUS PREDICTION.....	100
6.1 Micromechanics model for elastic modulus prediction.....	101
6.1.1 Hashin-Shtrikman model .....	101
6.1.2 Tuchinskii model .....	102
6.1.3 Ravichandran model .....	103
6.2 Modulus prediction for syntactic foams .....	105
6.3 Modulus prediction for IPC .....	108
6.4 Modulus prediction for syntactic foam-filled honeycomb.....	110
7. CONCLUSIONS.....	112
7.1 Conclusions.....	112
7.2 Future work.....	116
BIBLIOGRAPHY.....	118

APPENDICES .....	122
A.    EFFECT OF CELL STRUCTURE ON ELASTIC-PLASTIC RESPONSE OF FOAM-FILLED COMPOSITES.....	123
A.1    Introduction.....	123
A.2    The approach: Voronoi tessellations.....	124
A.3    Irregularity parameter .....	125
A.4    FEA model description .....	127
A.5    Effect of cell irregularity on stress-strain response of composites .....	128
A.6    Effect of relative density on stress-strain response of composites .....	130
B.    MATLAB CODES.....	132

## LIST OF FIGURES

Figure 1.1:	Stress-Stain curve for an elastic solid and foam made from the same solid [1].....	2
Figure 1.2:	(a) aluminum honeycomb sandwich construction, (b) aluminum foam sandwich .....	3
Figure 1.3:	Examples of foam-filled cellular structures - (a) Interpenetrating aluminum-syntactic foam composite,(b) syntactic foam-filled aluminum honeycomb.....	4
Figure 1.4:	(a) Interpenetrating phase composite, (b) Traditional composite .....	6
Figure 1.5:	Schematic of a molecular scale IPN composite with two polymer chains .....	7
Figure 2.1:	Micrograph of microballoons .....	17
Figure 2.2:	Applications of foams [21] .....	18
Figure 2.3:	Aluminum honeycomb cell structure .....	19
Figure 2.4:	Mold fabrication process .....	21
Figure 2.5:	Preparation of syntactic foam .....	22
Figure 2.6:	Preparation of interpenetrating phase composite (IPC).....	24
Figure 2.7:	Preparation of syntactic foam-filled aluminum honeycomb composite .....	26
Figure 2.8:	Micrograph of epoxy syntactic foam with 30% $V_f$ of hollow glass microballoons .....	27
Figure 2.9:	(a) Cross-section of a lightweight IPC foam cylinder with open-cell Aluminum preform (9% relative density) infiltrated with epoxy-based syntactic foam. (b) Micrograph of the IPC foam showing the constituents. ....	28

Figure 2.10: Syntactic foam-filled aluminum honeycomb composite .....	28
Figure 3.1: Experimental setup for compression tests .....	31
Figure 3.2: Syntactic foam sample with coating of graphite powder .....	32
Figure 3.3: Stress-strain curves of syntactic foam with 20% volume fraction for two different aspect ratios.....	33
Figure 3.4: Stress-strain curves of syntactic foam with 20% volume fraction for three Samples having L/D=0.74 .....	34
Figure 3.5: Stress-Strain curves of syntactic foam (SF) with different volume fraction (20, 30, and 40) of microballoons.....	35
Figure 3.6: SEM images of a deformed syntactic foam sample with 30% $V_f$ of microballoons (a) at a strain of ~10%, (b) at a strain of ~60%, (c) higher magnification image showing fractured surface of microballoon Highlighted by dotted line in (b) (The sample is compressed in the vertical direction) .....	37
Figure 3.7: Comparison of energy absorption (up to 50% strain) for syntactic foams samples: (a) per unit volume (b) per unit mass.....	40
Figure 3.8: Stress-strain curves of syntactic foam with 20% volume fraction for different lubricants .....	41
Figure 3.9: Sequence of deformed configurations of SF-20 during compression experiments at a strain of: (a) 0%, (b) 4%, (c) 10%, (d) 24%, (e) 31%, (f) 43%, (g) 52 %, (h) 64% .....	43
Figure 3.10: Deformed SF-20 sample .....	44
Figure 4.1: Compression response of IPC foam: (a) uncoated (b) silane coated. (Data for three specimens are shown for IPC-S20 case to show experimental repeatability.) .....	47
Figure 4.2: SEM images of (a) silane coated IPC foam at a strain of 10%, (b) silane coated IPC foam at a strain of 58%, (c) uncoated IPC foam at a strain of 14%. (Compression is in the horizontal direction in (a) and in the vertical direction in (b) and (c). .....	48
Figure 4.3: Compression response of unfilled Aluminum foam used in this work [21].	49

Figure 4.4: Comparison of stress-strain response of syntactic foam, IPC foam with uncoated preform and IPC foam with silane coated preform for (a) 20% volume fraction, (b) 30% volume fraction, (c) 40% volume fraction of microballoons.....	51
Figure 4.5: Comparison of energy absorption (up to 50% strain) for syntactic foams and IPC foam samples: (a) per unit volume (b) per unit mass.....	56
Figure 4.6: Compression response of syntactic foam-filled honeycomb composite. compression along (a) L-direction, (b) W-direction .....	58
Figure 4.7: Deformation sequence for a SFH-30 sample at a applied strain of of (1):0%, (2):3.2%, (3):5.8%, (4):8.8%, (5):12.6%, (6):16%, (7):24.6%, (8):30.2%, (9):36%, (10):42% .....	61
Figure 4.8: Compression response of SFH-20 with uncoated honeycomb preform and silane coated preform .....	63
Figure 4.9: Comparison of stress-strain response of syntactic foam, Syntactic foam-filled honeycomb for (a) 20% volume fraction, (b) 30% volume fraction, (c) 40% volume fraction of microballoons .....	66
Figure 4.10: Comparison of energy absorption (up to 50% strain) for syntactic foams and Syntactic foam-filled honeycomb samples: (a) per unit volume (b) per unit mass.....	69
Figure 4.11: Comparison of energy absorption (up to 50% strain) for syntactic foams, IPC foam and syntactic foam-filled honeycomb samples.....	70
Figure 5.1: Schematic of a unit cell model of Kelvin cell (Color rendition is for clarity only).....	76
Figure 5.2: Finite element model development: (a) Idealization of IPC foam structure using Kelvin cells (b) Unit cell model used to represent aluminum-syntactic foam IPC. ....	77
Figure 5.3: Finite element model of undeformed unit cell with boundary conditions used while simulating the uniaxial compression of IPC foam.....	78
Figure 5.4: Finite element model of undeformed unit cell with mesh (Different colors/shades show metallic ligaments embedded in the syntactic foam cubic cell.) .....	79

Figure 5.5: Comparison of numerical and experimental results for IPC foam with (a) 20% volume fraction, (b) 30% volume fraction, (c) 40% volume fraction of microballoons .....	82
Figure 5.6: Finite element results for unit cell model for IPC-S30 at 40% strain. (a) Deformed and undeformed unit cell with von-Mises stress contours (b) Deformed unit cell with equivalent plastic strain contours (c) Deformed unit cell with displacement contours in the $u_3$ ( $u_z$ ).....	84
Figure 5.7: Periodic finite element mesh on a pair of opposite faces.....	87
Figure 5.8: Effect of boundary condition on stress-strain response of IPC.....	89
Figure 5.9: Geometry of honeycomb specimen used in analysis .....	90
Figure 5.10: Loads and boundary conditions used during the analysis.....	93
Figure 5.11: (a) Finite element mesh of the model (b) enlarged view showing finite element mesh of the composite.....	94
Figure 5.12: Sequence of deformation at applied strain of (1): 1.8%, (2):5.4%, (3): 8.2%, (4): 14.6%, (5):32.8%, (6)40% .....	96
Figure 5.13: Comparison of numerical and experimental results for Syntactic foam-filled honeycomb composites (a) 20% volume fraction, (b) 30% volume fraction, (c) 40% volume fraction of microballoons.....	98
Figure 6.1: Schematic representation of phase geometry for a Tuchinskii model [13]	103
Figure 6.2: Schematic representation of cell geometry for a Ravichandran model [13]	104
Figure 6.3: Variation of measured young's moduli with microballoon volume fraction .....	105
Figure 6.4: Comparison between predicted and measured values of elastic modulus for syntactic foams. (a) Hashin-Shtrikman and Ravichandran bounds, (b) Tuchiniskii bounds .....	107
Figure A.1: (a) Set of random points, (b) Voronoi diagram for that set of points .....	124
Figure A.2: Syntactic foam-filled honeycomb composite with varying degree- of- irregularity: (a): $\alpha =0$ , (b) $\alpha =0.2$ , (c) $\alpha =0.4$ , (d) $\alpha =0.6$ .....	126
Figure A.3: Effect of cell irregularity on stress-strain response of the composite .....	128

Figure A.4: Effect of cell irregularity on elastic modulus of the composite .....129

Figure A.5: Effect of relative density on stress-strain response of the composite .....131



## LIST OF TABLES

Table 2.1:	Properties of constituents .....	23
Table 3.1:	Properties of syntactic foam .....	36
Table 4.1:	Properties of IPC Foam (20, 30, 40 designation denotes $V_f$ of microballoons in the syntactic foam).....	53
Table 4.2:	Properties of syntactic foam-filled honeycomb composite (20, 30, 40 designation denotes $V_f$ of microballoons in the syntactic foam.) .....	62
Table 5.1:	Comparison of finite element results with experiments (based on true stress- strain data).....	83
Table 6.1:	Comparison between measured and predicted values of elastic modulus for the IPC foam based on different micromechanics models .....	109
Table 6.2:	Comparison between measured and predicted values of elastic modulus for the syntactic foam-filled honeycomb composite based on different micromechanics models.....	111

# CHAPTER 1

## INTRODUCTION

### 1.1 Cellular solids: An overview

Cellular materials are drawing a great deal of attention in view of their attractive engineering properties. They are lightweight and stiff and have very good energy-absorbing characteristics making them excellent candidates for structural applications. They also have attractive thermal characteristics (often used to cool electronic equipment and as heat exchangers in engines). A typical cellular solid is made up of an interconnected network of solid struts which form the edges of cells in case of two-dimensional honeycomb structures and faces of cells in case of three-dimensional foams. The cell geometry is the one that characterizes the overall mechanical behavior of cellular material. Such materials are common in nature; wood, cancellous bone and coral are a few examples. Honeycomb-like materials, made up of parallel, prismatic cells, are used for lightweight aerospace structural components. Polymer and glass foams have low thermal conductivity and hence have been used as insulating material in applications ranging from disposable coffee cups to material for booster rocket of the space shuttle. Cellular solids have also been effectively used as packaging materials to absorb shock.

The cellular structure of these materials enables them to undergo large compressive strains while holding the peak force to a minimum when compared with a monolithic solid from which it is made. The energy in these materials is dissipated primarily through cell wall bending, buckling and collapse but the stress is generally limited by an extended plateau region of the stress-strain curve as seen in Fig1.1.

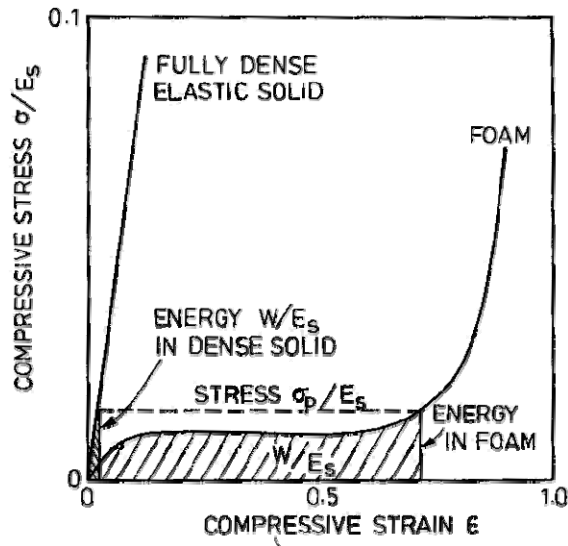
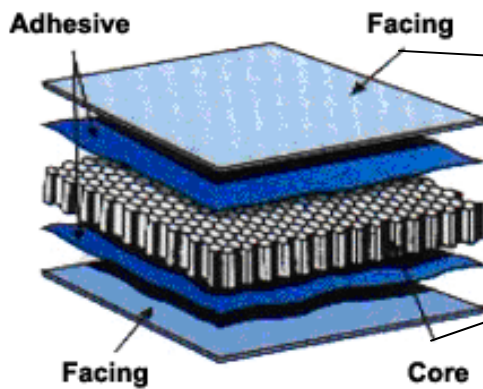


Figure 1.1: Stress-Strain curve for an elastic solid and foam made from the same solid [1]

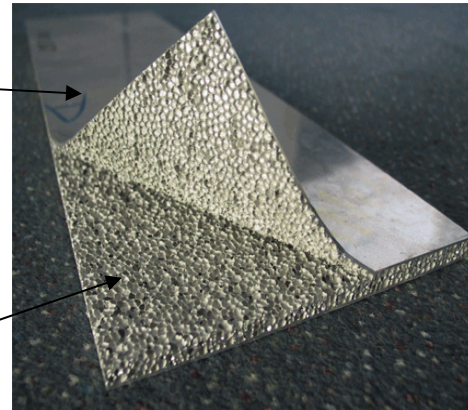
By choosing the right cell wall material and relative density, the foam can be tailored to give an optimum combination of properties for a given packaging application. Foams and honeycombs are also commonly used as core materials in sandwich construction. The purpose of a core in a composite laminate is to increase the flexural stiffness of a structure by effectively 'thickening' it with a low-density core material. In fig.1.2 an example of a lightweight and high strength sandwich construction using aluminum honeycomb and foam as core material is shown. The partially torn off face sheet in Fig.1.2(b) reveals the bonding between foam and sheet in Fig.1.2(a). The use of

foams as core material can provide a dramatic increase in stiffness for very little additional weight. Recent advances in material processing methods to mold complex geometries allow greater design flexibility of structural parts. Foamed polystyrene and polyvinyl chloride are extensively used for floating structures and as flotation devices in boats. Aluminum foam is also extensively used in automotive, aerospace, marine, railway, civil engineering and medical industries due to high stiffness-to-weight ratio, vibration damping capacity and non-inflammability characteristics. Foam-filled columns or sandwich panels have replaced conventional dense metal used in rotating printing rolls and in rapidly moving platforms in order to reduce their inertia and damp out vibrations. All these uses exploit the special combination of properties offered by cellular solids, properties which are ultimately a derivative of their cellular structure [1].



Ref: <http://engineeredmaterialsinc.com/composites.htm>

(a)



Ref: <http://sandwichmater.com/sheet.htm>

(b)

Figure 1.2: (a) aluminum honeycomb sandwich construction, (b) aluminum foam sandwich

## 1.2 Advantages of foam-filled cellular solids

Relative density of cellular solid is the single most important structural characteristic which controls the properties of foams and honeycomb structures. Foam filling is often preferable to increasing the wall thickness in order to enhance the required properties of the cellular solids. Foam filling of honeycomb and other open-cellular materials further increases the range of applications to meet some of the most stringent design applications in which honeycombs or other single-material structural foams alone cannot be used. While most of the compressive performance depends on the honeycomb cell structure, the foam-fill acts as an effective reinforcement for the cell walls of the honeycomb material by preventing premature bending and buckling failure under compression and also increases the surface area for dissipating compressive forces. The wide range of alternatives in honeycomb cell sizes and relative densities ensure many possibilities for the preparation of this composite.

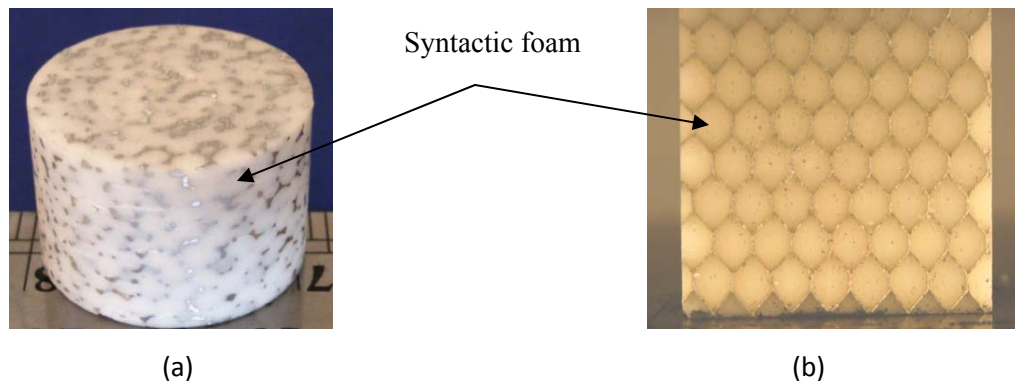


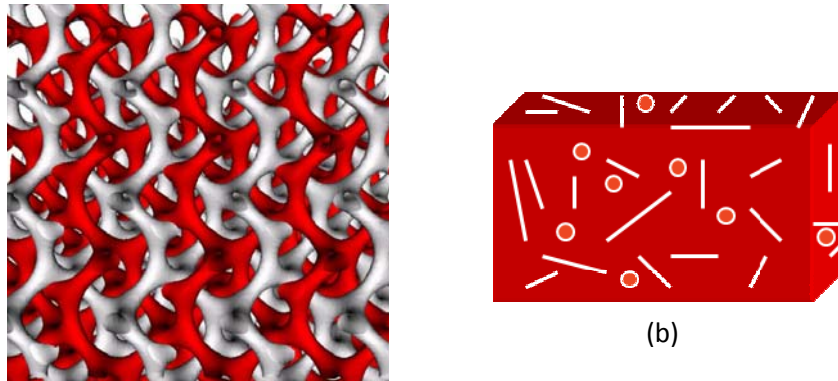
Figure 1.3: Examples of foam-filled cellular structures - (a) Interpenetrating aluminum-syntactic foam composite, (b) Syntactic foam-filled aluminum honeycomb

In situations when weight is a concern, a low-density rigid foam can be used for making foam-filled honeycombs since the mechanical performance of foam-filled honeycomb is largely correlated to the type and density of the constituents used. Figure 1.3 shows two types of syntactic foam-filled composites that were studied in this work. Thermoplastic, Nomex or aluminium honeycombs are often used as core materials in sandwich constructions and can be filled with low strength and stiffness foam for low load applications. On the other hand, high strength and stiffness foam can be used for application such as aircraft structures. Such components are damage tolerant and easy to integrate into a space frame. The final composite core provides the strength of the honeycomb combined with the workability of the foam. The foam-filled composites also have a high strength to weight ratio.

### **1.3 Interpenetrating phase composites (IPC)**

The continued demand for lighter, stiffer, stronger and tougher structural components requires development of novel materials. Heterogeneous materials with discrete, dispersed and/or embedded phases in a matrix material (fiber reinforced composites, particulate composites, functionally graded materials, syntactic foams, etc.) are found suitable for many structural applications. There are, however, limitations in terms of the degree of concentration of the secondary phase that can be dispersed into the primary phase and the degree of inter connectivity between the phases. Nature overcomes these limitations by adopting 3-D interpenetrating microstructure as evident in skeletal tissue and botanical systems. This observation has inspired a relatively new category of

materials called interpenetrating phase composite/s or IPC (also called co-continuous composites). The IPC are multiphase materials in which the constituent phases are interconnected three-dimensionally and topologically throughout the microstructure (and hence sometimes are referred to as “3–3” composites). That is, both matrix and reinforcement phase/s interpenetrate all over the microstructure, in all the three spatial dimensions, as depicted schematically in Fig. 1.4(a). Thereby the two constituents in their stand alone state would have an open-cell microstructure. Hence, IPC are uniquely different from traditional composites comprising of a matrix with one or more reinforcing filler phases (long fibers, whiskers, particles, microballoons, etc.) where such a complete interpenetration does not occur, as can be seen in Fig. 1.4(b).



(a)  
Figure 1.4: (a) Interpenetrating phase composite, (b) Traditional composite

Consequently, each phase of an IPC contributes its property to the overall macro scale characteristics synergistically. For example, if one constituent provides strength and toughness, the other might enhance stiffness, thermal stability, acoustic insulation and/or dielectric characteristics. For instance, in a polymer-ceramic IPC, ceramic phase offers

stiffness whereas the polymer phase increases the failure strain of the composite synergistically. Additionally, it is also possible to tailor residual stresses in the constituents to produce advantageous macro scale response in a metal–ceramic IPC. The tensile residual stresses in the metallic phase and compressive ones in the ceramic phase delays crack initiation and strengthens the IPC. Examples of such systems include Corning's Vycor™ glass and the Lanxide Corporation's DIMOX™ material. Based on the occurrence of phase interpenetration at different length scales, IPC can be classified as molecular, micro or meso varieties. Figure 1.5 shows a blend of two or more cross-linked polymers which are interlaced but not covalently bonded to each other and cannot be separated unless chemical bonds are broken. This is an example of a molecular scale IPC and is called an Interpenetrating Polymer Network (IPN).

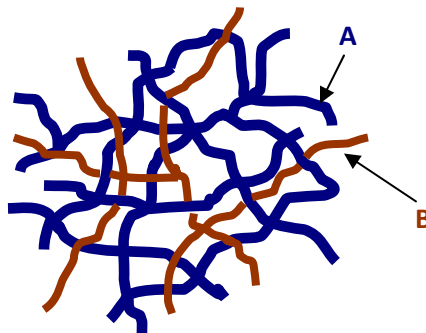


Figure 1.5: Schematic of a molecular scale IPN composite with two polymer chains

Among the many potential mechanical benefits of IPC, the ones regarding fracture and energy dissipation characteristics are noteworthy. In traditional polymeric or ceramic fiber composites with aligned fibers, stiffness and strength advantages are limited to only the fiber direction as crack propagation along the fibers cannot be



effectively resisted. On the contrary, the 3D interconnectivity of phases in a IPC could mitigate failure effectively while offering beneficial macro scale isotropy.

#### **1.4 Literature review**

The literature review in the context of the present research can be classified into parts: (a) foam-filled honeycombs and (b) open-cell 3-D scaffolds/preforms. There are a relatively few reported results available on the former. The work by Wu et al. [2] highlights the improvements in the mechanical properties of honeycomb core by filling it with rigid polyurethane foam. This foam-filled honeycomb was then used to construct sandwich panels with graphite/epoxy composite face sheets. The results of low velocity impact tests showed the sandwich panel with foam-filled honeycomb core to have a higher impact resistance and also the impact-inflicted core crushing was found to be highly localized when compared with the unfilled honeycomb core. Vaidya et al. [3] carried out low velocity impact tests on foam-filled honeycomb core with graphite and S2-glass fabric face sheets. Low-cost resin infusion molding process was used for the preparation of foam-filled honeycomb core sandwich composites. The results of the low velocity impact tests showed the sandwich composite with S2-glass face sheet to possess more damage tolerance when compared to the composite with graphite face sheets. Low velocity and high velocity impact response of honeycomb core with fully filled polyurethane foam and partially filled syntactic foam having carbon-epoxy face sheets is reported by Vaidya et al. [4]. Vacuum assisted resin transfer molding process was used to produce the sandwich panels. The results showed that the ballistic limit for the partial

foam-filled sandwich plate increased by 74% and the sandwich composite with full filling of its cells with polyurethane foam had 73% increase in the ballistic limit when compared to that of the unfilled core samples.

Some of the conceptual underpinnings and possible material processing strategies for IPC are reviewed by Clarke [5]. He has noted that interpenetrating phase microstructures are commonly found in biological systems including mammalian bones and trunks and limbs of plants. Yet, very few synthetic counterparts, with a few exceptions such as Vycor<sup>TM</sup> ('thirsty') glass from Corning Corporation are available at the moment. It is suggested in this review that a possible approach for producing metal/ceramic IPC composites would be to slip cast a ceramic slip into an open-cell polymer foam and fire the product to burn away the polymer leaving behind a ceramic negative structure to be infiltrated with a desired molten metal. The work by Breslin et al. [6] outlines material processing and characterization of aluminum/alumina IPC using a liquid phase displacement reaction method. These authors have successfully displaced Si from SiO<sub>2</sub> using aluminum to obtain the desired IPC. The resulting IPC is shown to have excellent mass density, thermal conductivity and CTE characteristics without compromising stiffness or fracture toughness. The elastic-plastic behavior of this IPC is studied by Daehn et al. [7] using experimental and finite element methods. It is shown to have a bilinear stress-strain response. Polymer networks made by a photo-cross-linking method are reported by Imagawa and Qui [8]. The thermal expansion behavior of alumina/aluminum IPC is reported by Skirl et al. [9]. They used a pressure infiltration technique to introduce aluminum into slip cast and then sintered alumina. These authors

suggest that tensile and compressive residual stresses in alumina and aluminum phases, respectively, contribute favorably to the overall thermal coefficient of expansion. They report an increase in failure strain as the metal content increases in the composite. Veenstra et al. [10] also developed polymer blends (poly(ether-ester)/PS and SEBS/PP) with interpenetrating microstructures and compared their mechanical properties to the ones based on the same polymers processed with a droplet/matrix morphology. A significantly higher tensile modulus without a notable drop in the tensile and impact strengths when compared to the one obtained from dispersed blends is reported. They have also modeled elastic modulus of the blended structures using different micromechanics approach. Finite element modeling of a two phase interpenetrating microstructures to study elastic, strength and thermal properties is reported by Wegner and Gibson [11]. They have also evaluated these properties for the case of non-interpenetrating structures and have reported an enhancement in thermo-mechanical characteristics of composite with interpenetrating microstructure. In a recent work on graphite/aluminum IPC Etter et al. [12] examined flexural strength and fracture toughness at room temperature and at 300°C. Their global measurements indicate a 200% improvement in both these characteristics for IPC over the un-infiltrated material at room temperature and at elevated temperatures no significant drop in properties is seen. Estimation of elastic properties of alumina/aluminum IPC structures using micromechanics approach is the focus of the work reported by Moon et al. [13]. In the range 5-97% volume fraction of alumina, 'effective medium approximation' method is shown to be the most suitable. Fatigue behavior of graphite/aluminum IPC is studied by

Mayer and Papakyriacou [14]. They attempted to improve the low fracture toughness of polycrystalline graphite using infiltration by lightweight metals such as aluminum. A 30% increase in the cyclic strength and a 10% increase in the endurance limit (at  $10^9$  cycles) are reported. Static compression and energy absorption of metal–polymer IPC are examined by Liu and Gong [15]. They infiltrated polyethylene or epoxy into an open-cell aluminum network to prepare IPC. A fivefold increase in energy absorption by aluminum/epoxy IPC relative to unfilled aluminum foam and a 2.5 fold increase relative to aluminum/Polyethylene IPC are reported. A new method for the preparation of metal-ceramic IPC is suggested by Kim et al [16]. They propose a two-stage processing method including preparation of composite powder precursors by reaction in a metal matrix and subsequent compaction of as-synthesized nanostructured powders. Han et al. [17] investigated the thermal shock behavior of TiB<sub>2</sub>–Cu IPCs using numerical and experimental methods. TiB<sub>2</sub>–Cu IPCs were prepared by a novel technique of combustion synthesis. The maximum thermal stress was found to be at 2 seconds and took place at the periphery of the top surface. The experimental results show that the TiB<sub>2</sub>–Cu IPCs has a good thermal shock resistance, and no cracks were found by plasma arc heating method. The work by Rio et al. [18] demonstrates a new method for creating a high-temperature co-continuous composite. In this method first, silica is reacted in liquid aluminum. This creates a highly aligned, near single crystal alumina structure that has about 25% open volume that is filled with aluminum. This open space is subsequently re-infiltrated with a refractory metal (NiAl or a nickel alloy), creating an interpenetrating phase or co-continuous composite. The results showed that unlike

traditional composites co-continuous composites were quite resistant to thermal cycling damage.

## **1.5 Objectives**

The following are the main objectives of the current work:

- Process lightweight interpenetrating aluminum-syntactic foam composite and syntactic foam-filled honeycomb composite by infiltrating uncured epoxy-based syntactic foam into an open-cell aluminum preform, resulting in IPC foam and by infiltrating the syntactic foam into a aluminum honeycomb structure, resulting in a foam-filled honeycomb composite.
- Prepare different varieties of these composites by varying the volume fraction of microballoons in the syntactic foam from 20% to 40% while keeping the volume fraction of the metallic network the same.
- Two variations of the interpenetrating aluminum-syntactic foam composite are produced. In first case the aluminum preform is used in 'as-received' condition and for second case the aluminum preform is coated with silane to increase adhesion between the metallic network and polymer foam.
- Study the compression characteristics of these composites and highlight the effect of volume fraction of microballoon on the stress-strain response of the composites.
- Compare the compression response and energy absorption characteristics of these composites with the conventional syntactic foams and explain the differences in the mechanical properties with the aid of micro structural analysis.

- Predict the elastic modulus of syntactic foam and the interpenetrating aluminum-syntactic foam composite using micromechanics models and compare them with measurements.
- Develop a Kelvin cell based 3D elasto-plastic finite element model to capture both linear and nonlinear characteristics of the interpenetrating phase composite.
- Model stress-strain response of the foam-filled honeycomb composite by developing a finite element based numerical model to represent the actual experimental model.
- Examine the effect of direction of compression on the stress-strain response of syntactic foam-filled honeycomb composite.
- Study the effect of cell shape on the elastic-plastic properties of the syntactic foam-filled honeycomb composite by using Voronoi tessellation technique to generate composite with random cell structures.

## **1.6 Organization of the thesis**

Including the present, this thesis is divided into seven chapters. The first chapter identifies the materials of interest along with the motivation for this research and also an overview of previous studies in this area. Chapter 2 presents details of material preparation for the syntactic foam and syntactic foam-filled composites. This chapter also details the mechanical characterization of the composites using scanning electron microscopy. Chapter 3 discusses the compression response and energy absorption characteristics of syntactic foams. The effect of volume fraction of microballoons on

stress-strain response of syntactic foam is also discussed in this chapter. Compression response of syntactic foam-filled composites is discussed in chapter 4. In this chapter, relevant mechanical properties of syntactic foam based interpenetrating phase composites and filled honeycomb composites are compared with that of syntactic foam and possible explanations for the differences are provided with the aid of microstructural analysis. The details of finite element models capable of capturing the stress-strain response of the interpenetrating aluminum-syntactic foam composite and the syntactic foam-filled aluminum honeycomb composite is presented in chapter 5. Chapter 6 discusses various micromechanics models used to predict the elastic properties of composites. Finally, chapter 7 presents summary and conclusions of this research work. A brief presentation of the effect of randomized cell structures generated using voronoi tessellations is presented in the appendix.

## **CHAPTER 2**

### **MATERIAL PREPARATION AND CHARACTERIZATION**

The focus of this chapter is on processing and characterization of homogeneous syntactic epoxy foams and syntactic foam-filled composites. This chapter is divided into two sections. The first section describes preparation of homogeneous syntactic epoxy foams, aluminum-syntactic foam composites with an interpenetrating architecture and the syntactic foam-filled aluminum honeycomb composites. In the second section details on microstructural analysis of these composites using scanning electron microscopy is presented.

#### **2.1 Material description**

The syntactic foam is used as the reference material in this study. A pressureless infiltration technique is used to prepare syntactic foam-filled composites. The interpenetrating architecture is produced by infiltrating uncured epoxy-based syntactic foam into open-cell aluminum preforms. The syntactic foam-filled aluminum honeycomb composites are produced by infiltrating the syntactic foam into an expanded aluminum honeycomb structure.



### **2.1.1 Syntactic foam**

A class of foams called syntactic foams is considered for structural applications in recent years [19, 20]. These foams can be distinguished from conventional variety by the way they are manufactured. Unlike traditional foams which are produced by gasification of a matrix material, syntactic foams are produced by mechanical blending of hollow polymer, ceramic or metal microballoons (hollow microspheres) in a polymer or metal matrix. Thus porosity in a syntactic foam is due to the 'filler' phase and results in closed-cell structure. Additionally, unlike conventional foams, the porosity in syntactic foam can be varied by controlling the size and volume fraction of the microballoons. Further distinction of these foams is that porosity in these materials is often microscopic and offers the potential advantages due to high surface area to volume ratio. Microscopic porosity also results in macroscopic isotropy useful for simpler mechanical design.

The range of engineering applications of syntactic foams has increased in recent years due to advances in processing methods offering greater choices in microballoon wall-thickness and diameter as well as the materials with which they are made of. These foams have been extensively used by naval and marine equipment manufacturers for marine platforms, buoys and in submersibles. They are also used in civil and industrial engineering as imitation wood and building construction materials for their high shear stiffness and specific strength. Due to the high specific energy absorption and impact resistance, syntactic foams have the potential for use as core materials of sandwich structures. syntactic foams made of glass and carbon micro-/nano-spheres are used in aerospace structures, missile heads and heat shields for space vehicles.

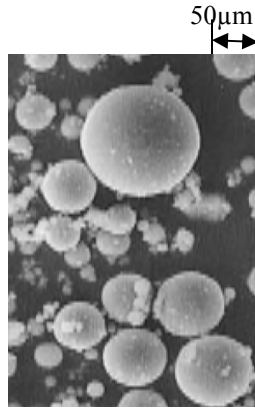


Figure 2.1: Micrograph of microballoons

They are also employed in electronics and telecommunications due to superior thermal and dielectric properties. Figure 2.1 shows a micrograph of hollow soda-lime glass microballoons used in this study.

### **2.1.2 Aluminum foam**

Metals such as aluminum can be foamed into either open-cell or closed-cell foams, resulting in a microstructure consisting of an interconnected network of solid struts or walls. Like soap suds or beer foam, the original bubbles that form the foam are a three-dimensional, perfectly packed array of similar sized bubbles where each bubble has the maximum volume for the minimal surface area and surface energy. Each bubble is typically a 14-facet polyhedra or a solid shape called a tetrakaidecahedron [21]. Unlike honeycombs, this cellular structure is nearly identical in all the three spatial directions, and is therefore considered isotropic. Since all the structural ligaments or struts are interconnected, the pores in open-cell foams are also interconnected, enabling fluids to pass freely into and out of the foam structure. While technically designated as open-

celled foams, these materials are also occasionally called porous metals. The Pore size, relative density and foam material are the three independent characteristics of a foam useful for engineering design. Aluminum foams have a number of advantages in terms of strength, weight, thermal properties, energy dissipation, vibration and noise absorption, toxicity and recyclability.



Figure 2.2: Applications of foams [21]

Due to these characteristics aluminum foams have found applications in heat exchanger, cryogenic tanks, filters, optical mirrors, missile baffles, gas diffused discs, composite structures etc. Figure 2.2 shows a few molded foam parts that are used by industries for various applications.

### 2.1.3 Aluminum honeycomb

An aluminum honeycomb is a two-dimensional array of periodic microstructure which packs to fill a planar area and is made primarily by an expansion method. The fabrication process using the expansion method begins with stacking sheets of (aluminum) material on which adhesive node lines are printed/deposited. The adhesive lines are then cured to form a HOBE<sup>®</sup> (Honeycomb Before Expansion Block). The HOBE block is then expanded after curing to give the final product. The expanded sheets are trimmed to the desired L dimension (ribbon direction) and W dimension (transverse to the ribbon) as shown in Fig 2.3. The aluminum honeycomb used in this study is also shown in the figure. The in-plane mechanical response of honeycomb is dependent on whether it is loaded in the W or L direction. The out-of-plane stiffness and strengths (T direction) are much larger when compared to the in-plane properties. This is one of the reasons why aluminum honeycomb is used as a core material for sandwich constructions.

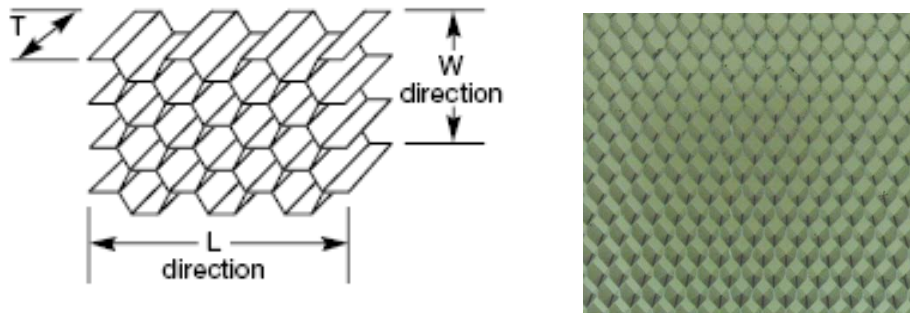


Figure 2.3: Aluminum honeycomb cell structure

As a structural core material honeycombs find applications in a variety of aerospace vehicles and supporting equipment where sandwich structures are used to obtain rigid lightweight panels offering aerodynamically smooth surfaces, and fatigue resistant structures. Honeycombs crush at nearly a constant stress level (dependent on the core material and density) and hence its energy absorption capacity is predictable, making it ideal for mechanical energy dissipation applications. When used in this manner, the core is often pre-crushed slightly to remove the compressive peak in the load-deflection curve. The same structural properties are also used for commercial applications such as tools, snow and water skis, bulkheads, and floors [22]. Other non-structural uses include directional air/fluid flow control and RF shielding. An aluminum honeycomb is widely used in structural applications because of its high strength-to-weight and stiffness-to-weight ratios when compared to other materials and configurations.

## **2.2 Material preparation**

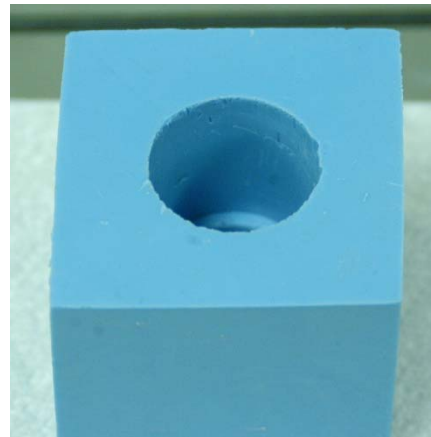
Two types of syntactic foam based composites were prepared by infusing the syntactic foam into open-cell aluminum foam and aluminum honeycomb structures. The volume fraction of microballoons used in these composites ranged from 20% to 40%. Other details on material preparation are described in the sub-sections below:

### 2.2.1 Mold preparation

A mold had to be prepared for making cylindrical specimens for compression testing. The preparation of a mold to cast these cylindrical foam specimens consisted of the following steps. First a master specimen, made of aluminum and with dimensions slightly greater than the final specimen dimensions, was machined. Next, the master was placed inside a cardboard well as shown in Fig.2.4(a). A two-part silicone rubber (Plastil 7360 RTV manufactured by Polytek Corporation) was then mixed and poured into the mold.



(a)



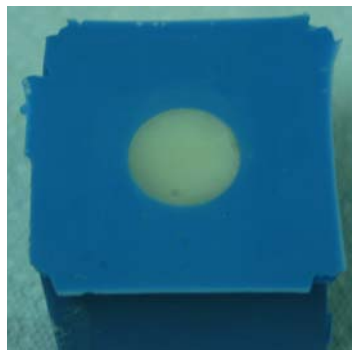
(b)

Figure 2.4: Mold fabrication process

It was then allowed to cure at room temperature for 36 hours after which the master specimen was removed from the mold. The resulting cavity (see Fig.2.4(b)) in the rubber mold is used subsequently for casting foam specimens.

### 2.2.2 Syntactic foam

Epoxy-based syntactic foams containing different volume fractions (20%, 30% and 40%) of hollow soda-lime glass microballoons were processed. The method involved heating epoxy resin to 50°C for ~45 minutes. A predetermined amount of microballoons (spherical hollow balloons of mean diameter ~60µm and wall-thickness ~600 nm) were added into epoxy resin and the mixture was carefully stirred ensuring uniform distribution of the filler. Subsequently, an amine based curing agent was introduced and stirring was continued. The mixture was then placed in a vacuum chamber and evacuated down to -75 kPa (gage) pressure. Once this pressure was reached the vacuum was released and the chamber was returned to atmospheric conditions.



(a)



(b)

Figure 2.5: Preparation of syntactic foam

This process was repeated (about 8–10 times) until no air bubbles were observed in the mixture. (This method of cyclic vacuuming of the mixture was found to be more effective when compared to holding the vacuum continuously for a set period of time.) When the

mixture showed a tendency to gel, it was transferred into a silicone rubber mold with a blind cylindrical cavity. The increased viscosity of the mixture prevented segregation of microballoons due to buoyancy forces. The mixture was then cured at room temperature for a period of 48 hours and rested for over a week to obtain a macroscopically homogeneous and isotropic solid. The cylindrical sample was then machined to the required dimensions as shown in fig. 2.5(b). Unless specified otherwise, in this work, the sample length and diameter were 20mm and 26.7mm respectively.

Properties	Neat Epoxy <sup>§</sup>	Microballoons <sup>#</sup>
Elastic Modulus (MPa)	3200	-
Bulk Density (kg/m <sup>3</sup> )	1175	125
Poisson's ratio	0.34	-

Table 2.1: Properties of constituents

### 2.2.3 Interpenetrating aluminum-syntactic foam composite

Many different strategies have been proposed in the literature to process co-continuous composites including powder metallurgy [23], squeeze casting [24,12], stir casting [25], and molten metal infiltration [9]. In this work pressureless infiltration technique was used. A commercially available open-cell aluminum foam (made of Al 6101-T6; pore density = 40 ppi, relative density = 9%, manufactured by ERG Inc., USA)

---

<sup>§</sup> supplied by Beuhler, Inc., under the trade name 'Epo-Thin'

<sup>#</sup> supplied by 3M Corp., under the trade name K-1 microballoons



was used as the scaffold for the Interpenetrating Phase Composite (IPC) foam. The preform has a uniform cell size distribution resulting in an isotropic mechanical response at macro scales. The manufacturing of the IPC foam consisted of the following steps. A silicone rubber mold was first prepared with a blind cylindrical well (see Fig. 2.4) of dimensions close to the final sample dimensions. The syntactic foam (prepared as described in section 2.2.2) was then poured into the rubber mold just before the mixture started to gel. Subsequently a cylindrical aluminum preform of the required dimensions was slowly lowered into the cavity previously filled with uncured syntactic foam. This ensured good percolation of the uncured syntactic foam mixture into all the cells of the preform. The resulting IPC foam was then cured at room temperature for 48 hours before removing from the mold. The cylindrical sample was subsequently machined to a length of 20mm and diameter 26.7mm (Fig. 2.6(b)).

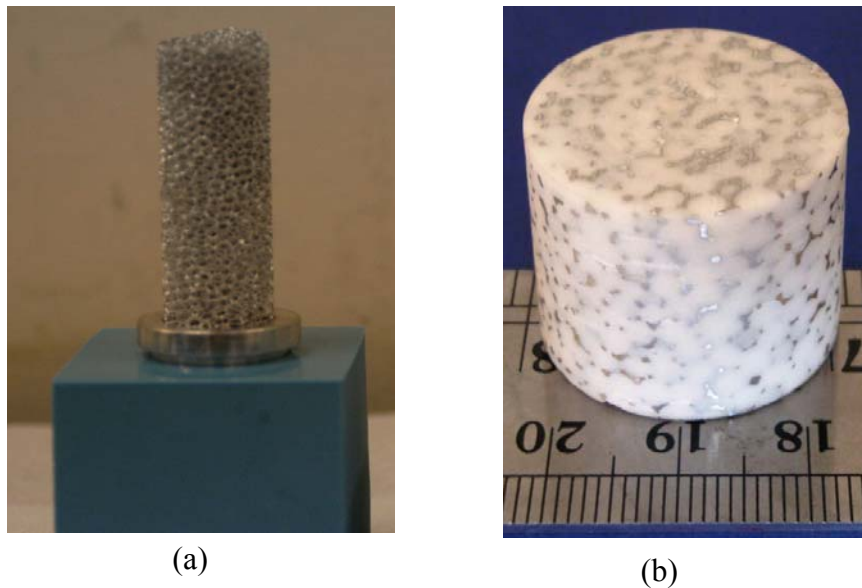


Figure 2.6: Preparation of interpenetrating phase composite (IPC)

Two different types of cylindrical IPC foam specimens were prepared. In the first type, the aluminum preform was used in ‘as-received’ state after degreasing it with laboratory grade alcohol. In the second type, the surface of the degreased aluminum preform was coated with amino silane, aminopropyltrimethoxysilane ( $\text{H}_2\text{NC}_2\text{H}_4\text{NHC}_3\text{H}_6\text{Si}(\text{OCH}_3)_3$ ). This coating was to enhance adhesion between syntactic epoxy foam and the aluminum ligaments whereas the former produced a relatively weaker adhesion between polymer and metal phases of the IPC foam.

#### **2.2.4 Syntactic foam-filled aluminum honeycomb composite**

Commercially available aluminum honeycomb (made of AL 5052; cell size = 3.125 mm, density =  $192 \text{ kg/m}^3$ , manufactured by Hexcel corporation, USA) core was also infused with syntactic foam. A silicone rubber mold was first prepared with a well of dimensions nearly close to the final sample dimensions (Fig. 2.7(a)). The syntactic foam (prepared as described in section 2.2.2) was then poured into the rubber mold just before the mixture started to gel. Subsequently a pre-cut aluminum honeycomb (of dimensions close to that of the well) was slowly lowered into the cavity previously filled with uncured syntactic foam. This ensured good percolation of the uncured syntactic foam mixture into all the cells of the honeycomb material. The resulting composite was then cured at room temperature for 48 hours before removing from the mold for machining. The sample was subsequently machined to dimensions of  $25.4\text{mm} \times 25.4\text{mm} \times 16\text{mm}$  (Fig. 2.7(b)). Different varieties of syntactic foam-filled composites were prepared by varying

the volume fraction of microballoons in the syntactic foam from 20%-40% while keeping the volume fraction of the metallic network the same.

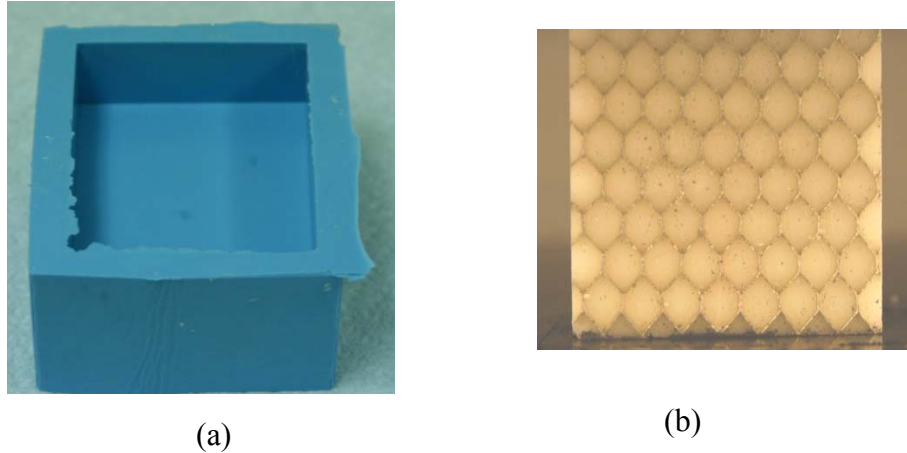


Figure 2.7: Preparation of Syntactic foam-filled aluminum honeycomb composite

### 2.3 Microstructural characterization

A scanning electron microscope was used to examine the surfaces of the cast composite specimens. The samples were first polished and then sputter coated with gold in order to make the surface conductive.

#### 2.3.1 Syntactic foam

The SEM image of polished surface of epoxy-based syntactic foam with 30% volume fraction of microballoons made by dispersing hollow soda-lime glass microballoons in the epoxy matrix is shown in Fig. 2.8. Random but uniform distribution of microballoons in the epoxy matrix can be seen from the figure. From the micrograph it can also be seen that the microballoons show a relatively broad size variation.

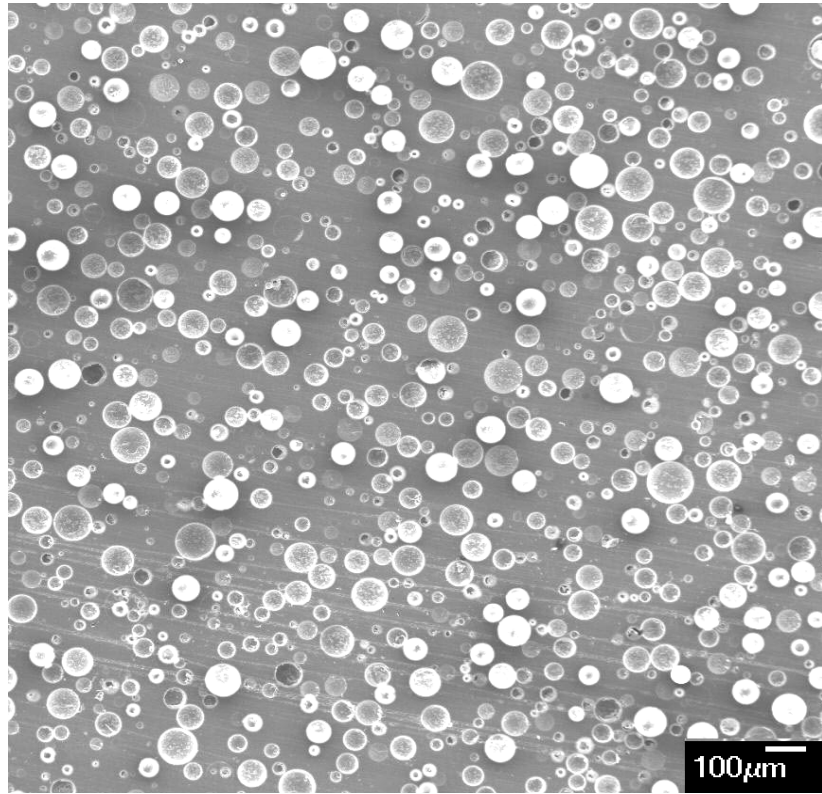


Figure 2.8: Micrograph of epoxy syntactic foam with 30%  $V_f$  of hollow glass microballoons

### 2.3.2 Interpenetrating aluminum-syntactic foam composite

The cross-section of cast cylindrical IPC foam is shown in Fig. 2.9(a). The photograph reveals aluminum cell walls (shiny gray ligaments) interconnecting pockets (white) of syntactic foam throughout. A micrograph of an undeformed IPC foam specimen 30% volume fraction of microballoons obtained using a scanning electron microscope is shown in Fig. 2.9(b). It clearly shows aluminum ligaments surrounded by microballoons dispersed in the epoxy matrix. The metal-polymer foam interfaces are crisp and continuous suggesting a good bond between the two. The microstructure does

not show any evidence of distortions in the aluminum ligaments caused by the curing process.

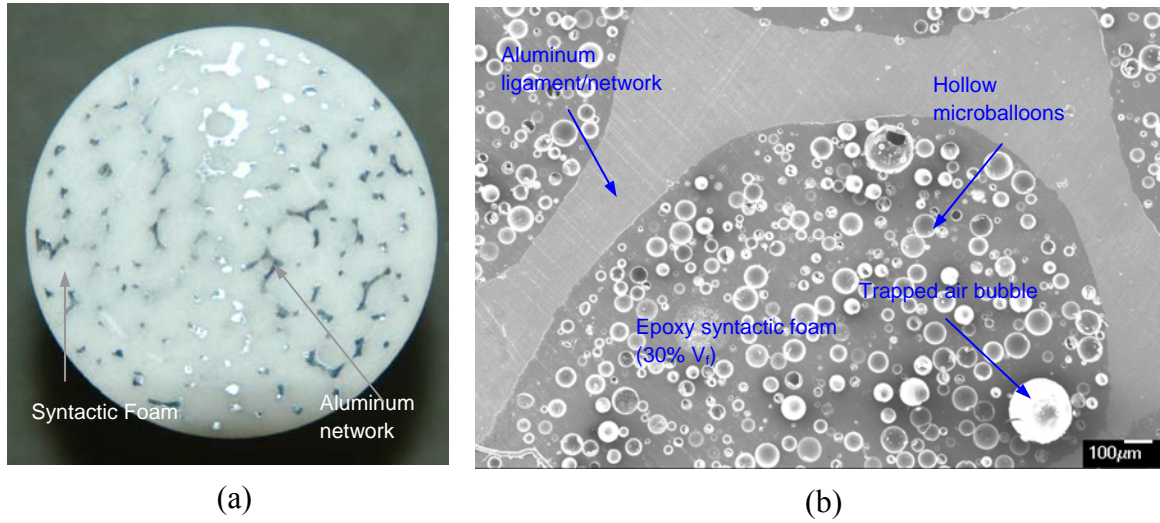


Figure 2.9: (a) Cross-section of a lightweight IPC foam cylinder with open-cell aluminum preform (9% relative density) infiltrated with epoxy-based syntactic foam. (b) Micrograph of the IPC foam showing the constituents.

### 2.3.3 Syntactic foam-filled aluminum honeycomb composite

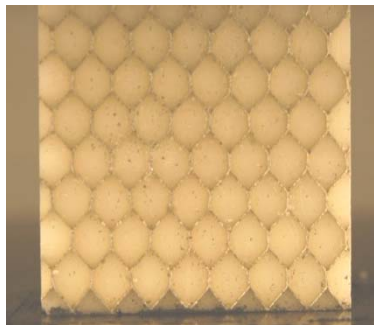


Figure 2.10: Syntactic foam-filled aluminum honeycomb composite

The photographed image of a machined syntactic foam-filled aluminum honeycomb composite containing 30% volume fraction of microballoons is shown in the Fig. 2.10. The microstructure shows good bonding between the aluminum honeycomb network and the syntactic foam phases also there are no visible cracks on the surface.

## **CHAPTER 3**

### **COMPRESSION CHARACTERISTICS OF SYNTACTIC FOAM**

The energy absorption characteristics of epoxy-based syntactic foams are presented in this chapter. The effect of volume fraction of microballoons on the stress-strain response of syntactic foams is also discussed. Compression tests were carried out on syntactic foam samples with 20%, 30% and 40% volume fraction of microballoons. The effect of specimen aspect ratio and lubrication of platen/specimen interface on the stress-strain response of foams is also noted.

#### **3.1 Experimental setup**

A series of compression tests were carried out on syntactic foam and syntactic foam-filled composite specimens at room temperature using a MTS universal testing machine. The photograph of the set up is shown in Fig.3.1. The testing machine was fitted with a 100 kN load cell. The tests were performed according to ASTM standard D-695 for plastics. The specimen to be tested was placed between the two compression platens of the testing machine. The top platen was moved at a constant rate as determined by the prescribed crosshead speed during tests and the bottom platen was fixed. A cross-head speed of 1.25 mm/min was used during the tests. Dry graphite powder was used as the lubricant between the two platens and the specimen surfaces to minimize friction.

A photograph of syntactic foam sample with a coating of dry graphite powder on its surface is shown in Fig 3.2.

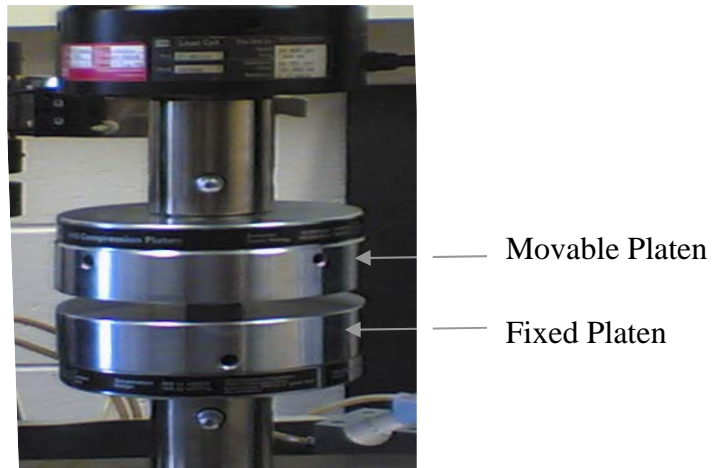
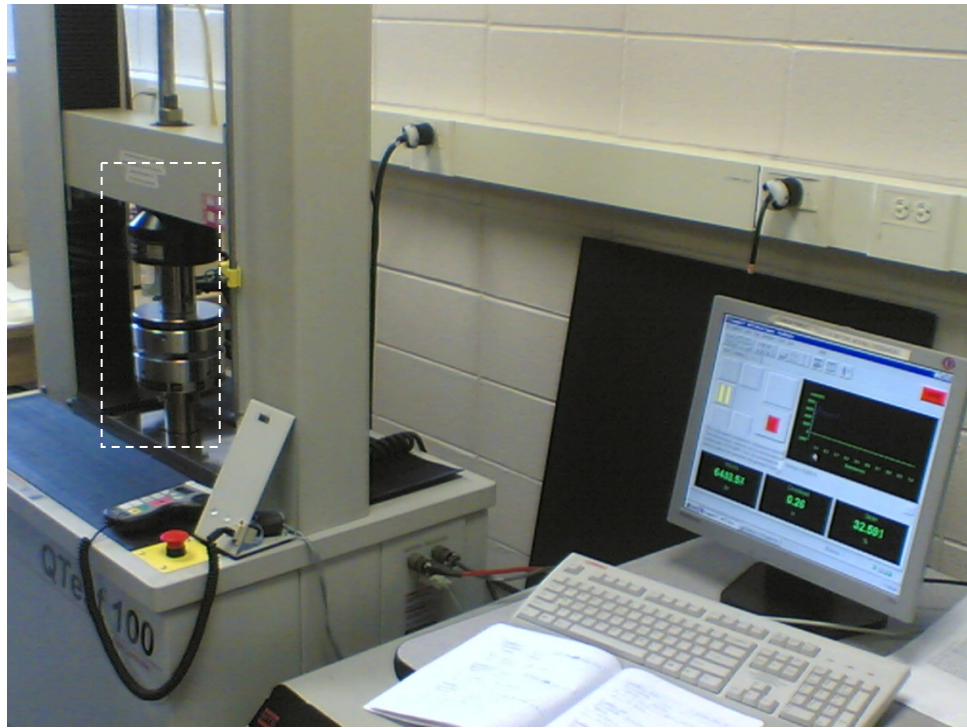


Figure 3.1: Experimental setup for compression tests



### 3.2 Effect of specimen aspect ratio

The aspect ratio of the sample could influence the material response in compression tests. A large aspect ratio (say,  $> 2$ ) has the draw back of susceptibility to bending and buckling deformation modes. On the other hand, a low aspect ratio ( $< 0.5$ ) could affect the measured response due to a combination of specimen edge effects and frictional effects. In light of this, uniaxial compression tests were performed on syntactic foam samples of two different specimen length ( $L$ ) to diameter ( $D$ ) ratios – 0.74 and 0.85. (The aspect ratio was altered by changing the length of the specimen while keeping the specimen diameter unchanged.)



Figure 3.2: Syntactic foam sample with coating of graphite powder

The measured engineering stress-strain responses for syntactic foam specimens with 20% microballoon volume fraction and the two aspect ratios are shown in Fig. 3.3. It is interesting to note that unlike conventional cellular structures and honeycombs, macro scale stress-strain responses for syntactic foams tend to be rather smooth due to microscopic porosity. The two curves overlap on each other and are in close agreement. The values of elastic modulus in each case is  $1594 \pm 50$  MPa and yield stress is  $55.7 \pm 2$

MPa. The results being nearly the same for both the cases, the effect of the two  $L/D$  ratios is insignificant and hence in all subsequent tests a  $L/D$  ratio of 0.74 was used. A similar observation has been made by Song, et al., [26] who note that increasing the  $L/D$  ratio to 2 resulted in a lower compressive strength of the syntactic epoxy foams by  $\sim 4.5\%$ . They attributed this reduction to size-dependent defect distribution in their specimens. For this reason  $L/D < 1$  was used during this study. A detailed study of the effect of aspect ratio on the failure behavior and compressive properties of syntactic foam has also been reported by Gupta, et al., [27].

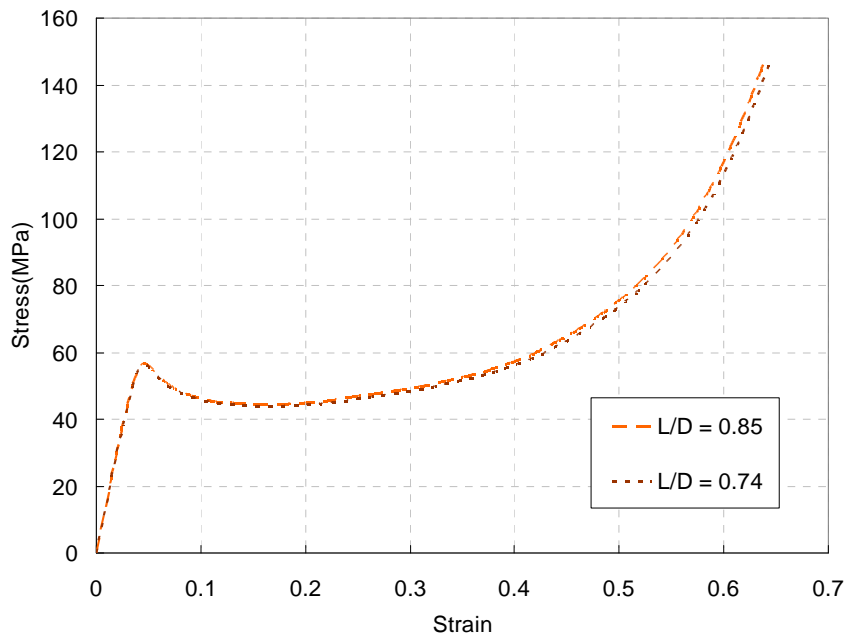


Figure 3.3: Stress-strain curves of syntactic foam with 20% volume fraction for two different aspect ratios

Next, the repeatability of compressive stress-strain responses of syntactic foam samples was studied. In Fig. 3.4, engineering stress-strain curves for three different

samples having aspect ratio ( $L/D$ ) of 0.74 made from 20% volume fraction of microballoons in epoxy resin is shown. The stress-strain responses essentially follow each other and very good repeatability is evident from the figure.

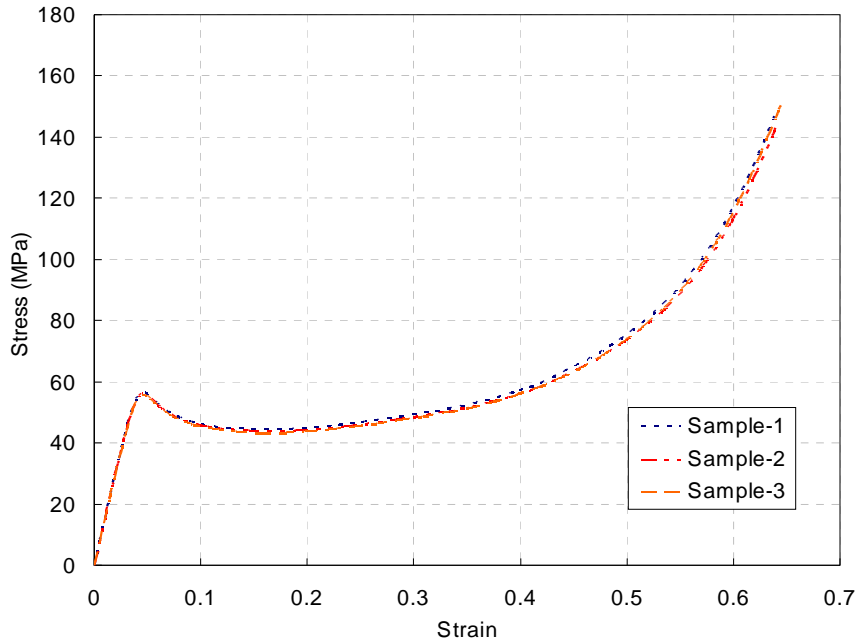


Figure 3.4: Stress-strain curves of syntactic foam with 20% volume fraction for three samples having  $L/D = 0.74$

### 3.3 Effect of volume fraction of microballoons

The influence of volume fraction ( $V_f$ ) of microballoons on stress-strain response of syntactic foam was also studied. A few representative stress-strain responses for three  $V_f$  - 20%, 30% and 40% - are shown in Fig. 3.5. In these curves a linear elastic response is seen initially. The compressive stress decreases with increasing strain as evident from the softening response following yield stress. This is followed by a plateau of nearly constant stress where progressive crushing of microballoons occurs. Further increase in

load results in densification seen as the region of monotonically rising stress, consistent with the observations reported in the previous works [26-28] on syntactic foams. These responses are similar to the compression response of structural foams in general.

An increase in the volume fraction of microballoons resulted in a reduction of elastic modulus as well as the compressive strength (see, Table 3.1). The elastic modulus and compressive strength decreased from 1595 MPa and 55.7 MPa, respectively for 20% volume fraction case to 1260 MPa and 36.7 MPa for 40% volume fraction case. The foam samples SF-20 (designation implies syntactic foam with 20%  $V_f$  of microballoons), SF-30 ( $V_f = 30\%$ ) and SF-40 ( $V_f = 40\%$ ) show a linear elastic response up to strains of approximately 0.028, 0.031, 0.039, respectively.

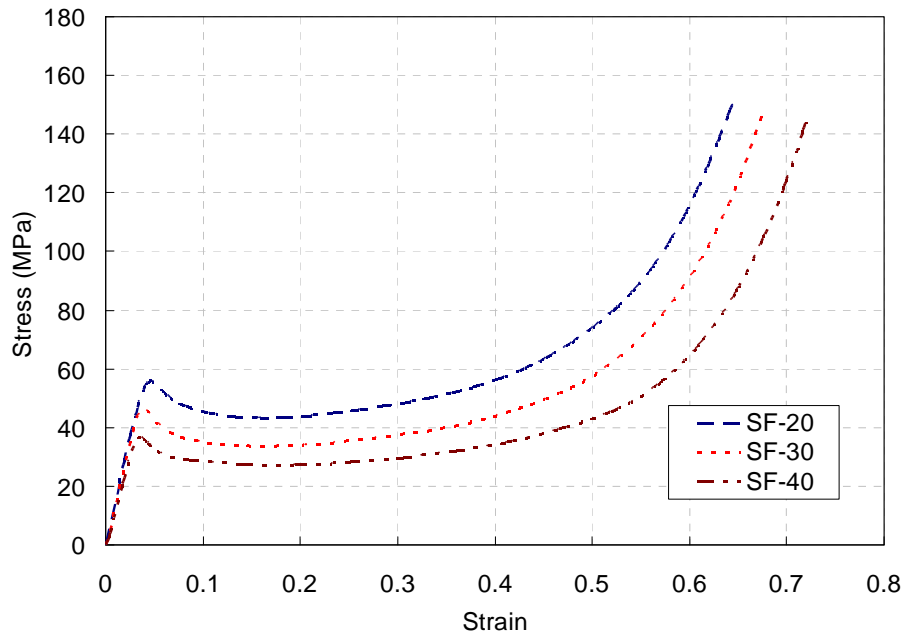


Figure 3.5: Stress-Strain curves of syntactic foam (SF) with different volume fraction (20, 30, and 40) of microballoons.

The plateau stress values in the three cases are 42 MPa, 33 MPa and 27 MPa for SF-20, SF-30 and SF-40, respectively. That is, the plateau stress decreases with increasing volume fraction of microballoons and is consistent with the trends reported by Kim, et al., [28]. The onset of densification for the three cases is in the strain range of 0.3-0.5 with the lower value corresponding to the lower volume fraction of microballoons. Beyond this strain, stress increases with increasing strain. All specimens showed formation of inclined cracks at advanced stages of deformation suggesting shear localization. This is consistent with previously published results [27, 29] for syntactic foams.

Foam designation	Volume fraction of microballoons (%)	Density (kg/m <sup>3</sup> )	Compressive strength (MPa)	Elastic modulus (MPa)
SF-20	20	931 ±4	55.7 ±2.2	1594.7 ±35
SF-30	30	821 ±6	46.3 ±1.4	1447.6 ±28
SF-40	40	701 ±4	36.7 ±1.8	1260.5 ±42

Table 3.1: Properties of Syntactic foam

In order to explain the failure behavior of syntactic foams, deformed specimens were sectioned and microscopically examined at a few select strain levels. Figure 3.6 shows SEM images of a syntactic foam sample (with 30% volume fraction of microballoons). In these, the direction of compression is along the vertical axis. In Fig. 3.6(a) and (b) micrographs of deformed specimens at 10% and 60% strain are shown. In Fig. 3.6(c) an enlarged view of an isolated crushed microballoon, highlighted in Fig.

3.6(b), is shown. It can be clearly seen from the images that the initial softening response is due to the onset of crushing of microballoons. A good interfacial bonding between microballoons and matrix has produced clearly visible fragments of crushed microballoon adhering to the surrounding matrix.

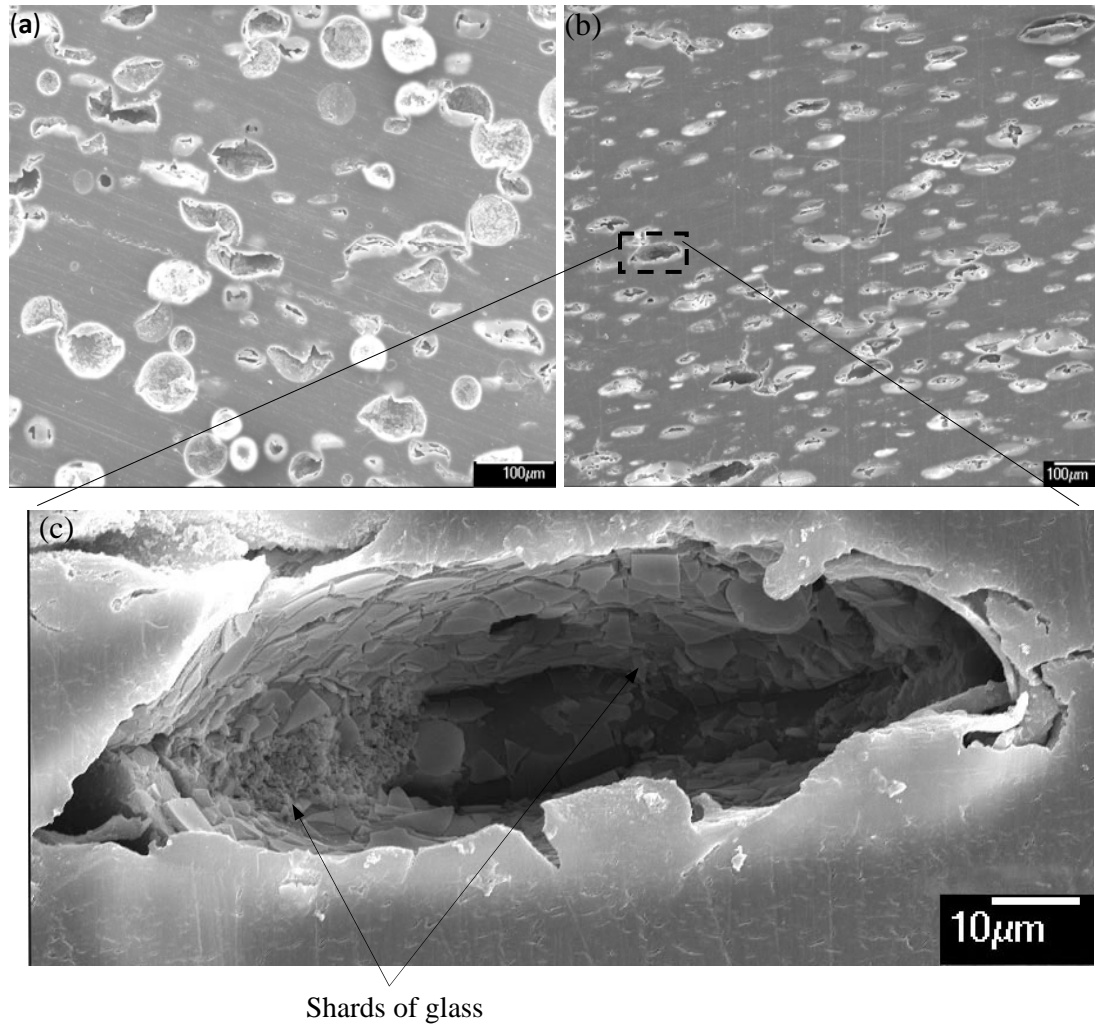


Figure 3.6: SEM images of a deformed syntactic foam sample with 30%  $V_f$  of microballoons (a) at a strain of ~10%, (b) at a strain of ~60%, (c) higher magnification image showing fractured surface of microballoon highlighted by dotted line in (b). (The sample is compressed in the vertical direction)

This suggests that interfacial debonding between microballoons and matrix is not a major contributor in the observed global material response shown in Fig. 3.5. A bias in the direction of fractured microballoons at lower levels of deformation can be seen in Fig. 3.6(a). With further deformation of the sample, microballoons fracture completely, leading to densification response seen in stress-strain curves. Failure of microballoons along inclined planes (relative to the loading direction) also indicates shear localization.

### 3.4 Energy absorption characteristics of syntactic foams

Conventional cellular materials have found applications in automotive and packaging industries due to their excellent energy dissipation characteristics. The cellular structure of these materials enables them to undergo large deformations in compression, enabling them to absorb considerable amounts of energy [1]. Syntactic foams are a class of structural foams in which the porosity is due to the filler phase (microballoons). This results in a closed-cell structure of the composite and hence it is important to evaluate the energy absorption characteristics of this composite. The energy absorbed per unit volume ( $U$ ) can be found by evaluating the area under the stress-strain curve:

$$U = \int_0^{\varepsilon} \sigma(\varepsilon) d\varepsilon \quad (3.1)$$

where  $\sigma(\varepsilon)$  denotes uniaxial stress as a function of strain.

The energy absorbed by the syntactic foam samples up to 50% strain are plotted as histograms in Fig. 3.7. The syntactic foam with 20% (SF-20) volume fraction of

microballoons is found to have the highest value of energy absorption when compared to 30% (SF-30) and 40% (SF-40) cases, in that order. The energy absorbed per unit volume increases by 61% for the syntactic foam with 20% volume fraction of microballoons when compared to the corresponding syntactic foam sample with 40% volume fraction of microballoons. This also shows that with increasing volume fraction of microballoons in syntactic foam, there is a steep increase in the value of energy absorbed per unit volume. The energy absorbed per unit mass is also plotted in Fig. 3.7(b). From the plots it can be seen that with increasing volume fraction of microballoons there is a relatively smaller decrease in this value and is nearly constant for all the volume fractions, varying between 0.026-0.022 MJ/kg.



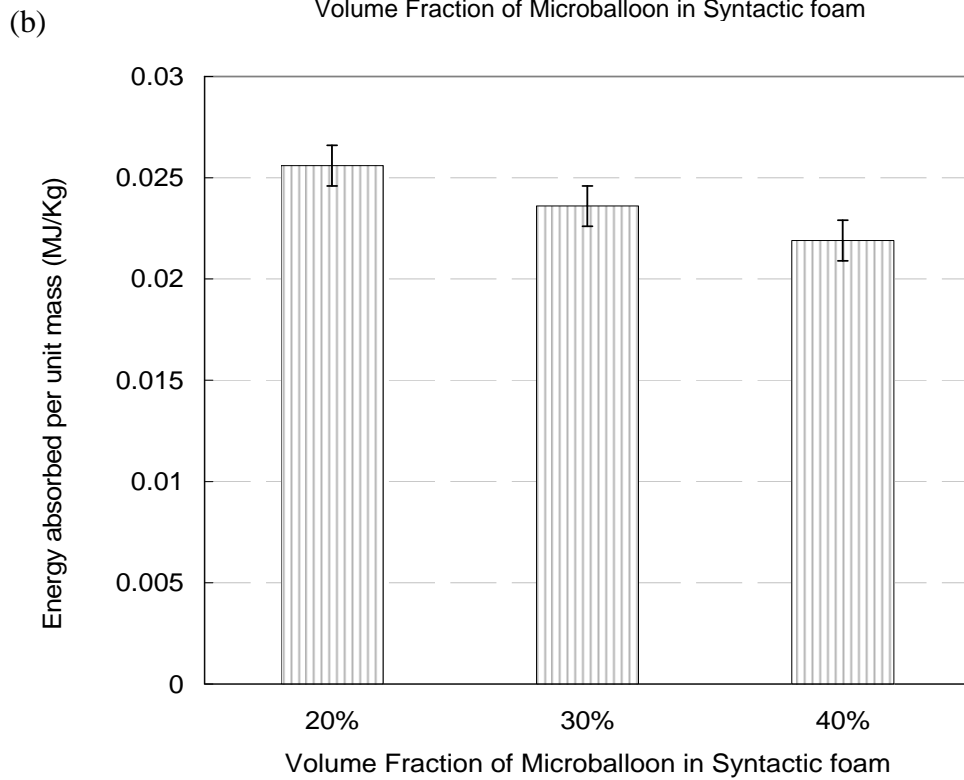
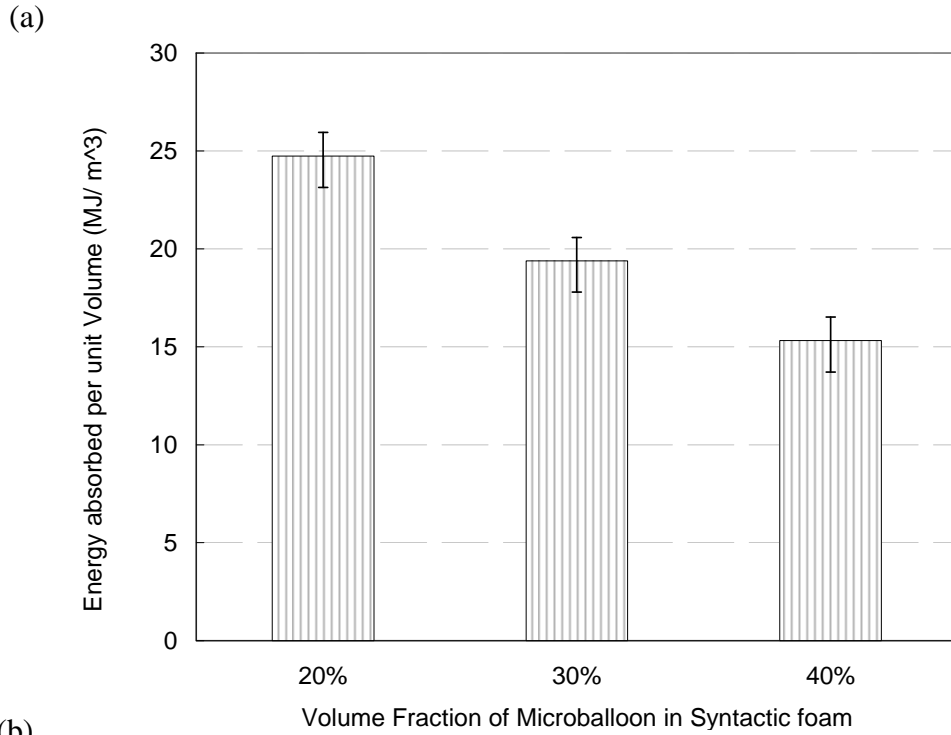


Figure 3.7: Comparison of energy absorption (up to 50% strain) for syntactic foams samples: (a) per unit volume (b) per unit mass.

### 3.5 Effect of lubricant on the stress-strain response of syntactic foam

Dry graphite powder was used as lubricant for most part of this study. Some experiments were also carried out by using grease as a lubricant. The stress-strain response of syntactic foam with 20% volume fraction of microballoons obtained using grease and powdered graphite as lubricant are plotted in Fig.3.8 . Figure 3.9 shows a sequence of photographs for a syntactic foam sample with 20% volume fraction of microballoons using grease as the lubricant between the platens and specimen surfaces.

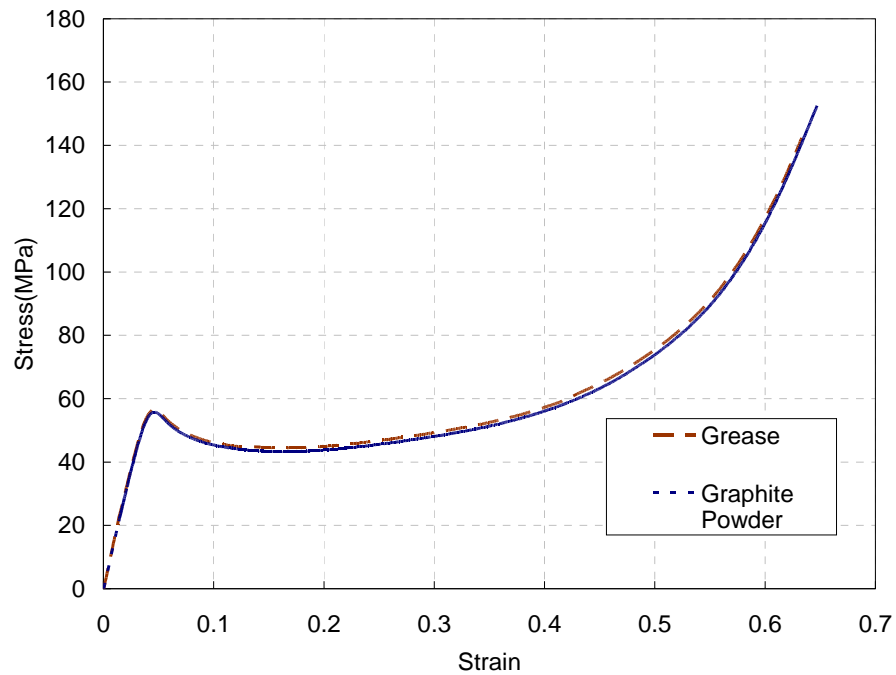


Figure 3.8: Stress-strain curves of syntactic foam with 20% volume fraction for different lubricants



(a)



(b)



(c)

42



(d)



(e)



(f)



(g)



(h)

Figure 3.9: Sequence of deformed configurations of SF-20 during compression experiments at a strain of: (a) 0%, (b) 4%, (c) 10%, (d) 24%, (e) 31%, (f) 43%, (g) 52 %, (h) 64%

From Fig.3.8 it can be clearly seen that the overall response of the syntactic foam sample is the same for both the cases. However, with the use of graphite powder as a lubricant a slight barreling at the edges of the sample was seen. A deformed sample from this experiment is shown in Fig. 3.10. Dark material on the upper (and lower) circular faces are due to graphite solid lubricant powder. From Figs 3.9(h) and 3.10 it can be seen that failure in all these specimens involved the formation of inclined cracks at  $\sim 45^\circ$  to the loading direction suggesting shear type of failure.



Figure 3.10: Deformed SF-20 sample

## **CHAPTER 4**

### **COMPRESSION CHARACTERISTICS OF SYNTACTIC FOAM-FILLED COMPOSITES**

In this chapter, the compression response and energy absorption characteristics of syntactic foam-filled composites are described. The first part of this chapter presents experimental results for syntactic foam-based interpenetrating phase composites (IPC). In the second part experimental results for epoxy syntactic foam-filled aluminum honeycombs are discussed. The samples are tested in uniaxial compression and failure responses are examined relative to those for conventional syntactic foams with corresponding volume fraction of microballoons. Also, possible explanations for the differences are provided with the aid of microstructural analysis.

Two variants of foam-filled composites are produced. In the first case an open-cell aluminum preform or an aluminum honeycomb is used in 'as-received' condition. In the second case, the preform or the honeycomb is treated with silane to enhance the adhesion between the polymer foam and metal ligaments. The effect of silane coating on the overall response of the foam-filled composites is also examined.

#### 4.1 Compression characteristics of IPC foam

Figure 4.1 shows typical stress-strain curves for different IPC foam samples. These plots correspond to samples made of aluminum preforms infiltrated with syntactic foam containing 20%, 30% and 40% volume fractions of microballoons. Figure 4.1(a) shows responses for IPC foam samples when the aluminum preform was used in uncoated condition whereas plots in Fig. 4.1(b) are for IPC foam counterparts with silane treated preforms. In Fig. 4.1(b) three results for one particular type of IPC foam (20% syntactic foam with silane treated preform) are shown to demonstrate a high degree of repeatability of these tests.

The overall compression response of IPC foams has similarities with the ones obtained for pure syntactic foam specimens (described in the previous chapter). These plots (Fig. 4.1) also show three distinct regions, typical of foam behavior. Initially there is a linear elastic response. The stress plateau region following the onset of nonlinearity is characterized by progressive bending of aluminum ligaments of the IPC foam. This in turn results in crushing of microballoons present in between the metallic ligaments. The SEM images of silane coated IPC foam (with 30% volume fraction of microballoons and sample compressed in the horizontal direction) shown in Fig. 4.2 supports this observation. With further increase in load, the stress increases more rapidly (compared to pure syntactic foam counterparts). This can be explained by the micrograph in Fig. 4.2(b) (compression is along the vertical direction) where compaction of crushed microballoons and deformation of aluminum preform is clearly evident.

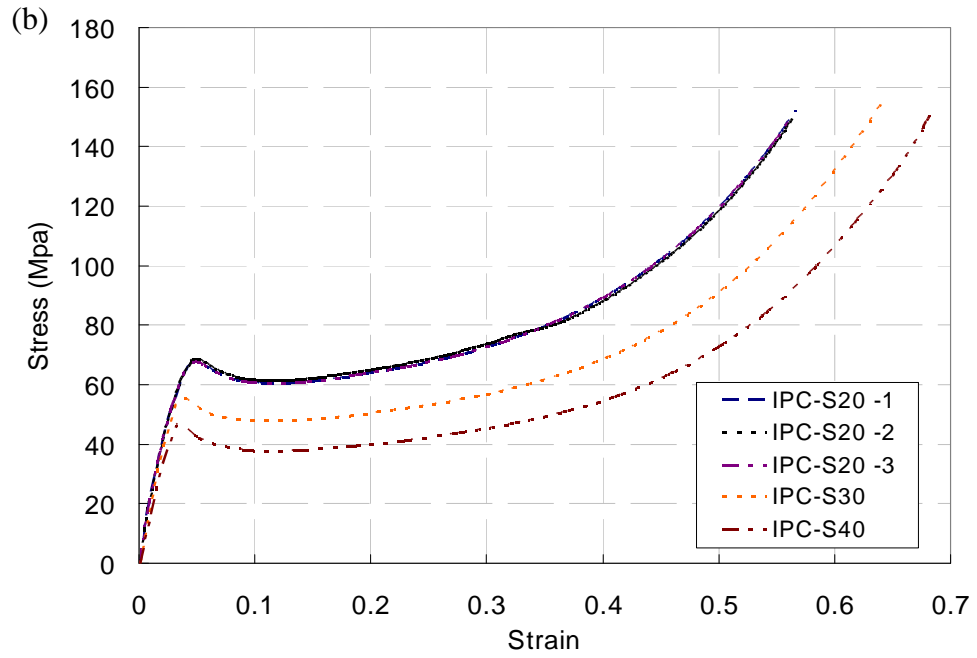
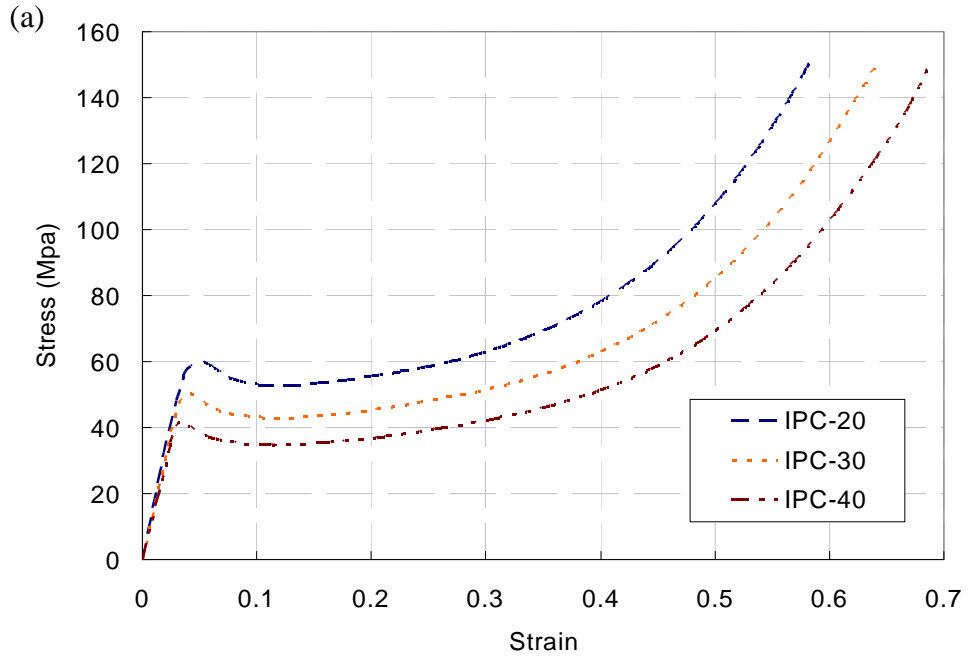


Figure 4.1: Compression response of IPC foam: (a) uncoated (b) silane coated. (Data for three specimens are shown for IPC-S20 case to show experimental repeatability.)



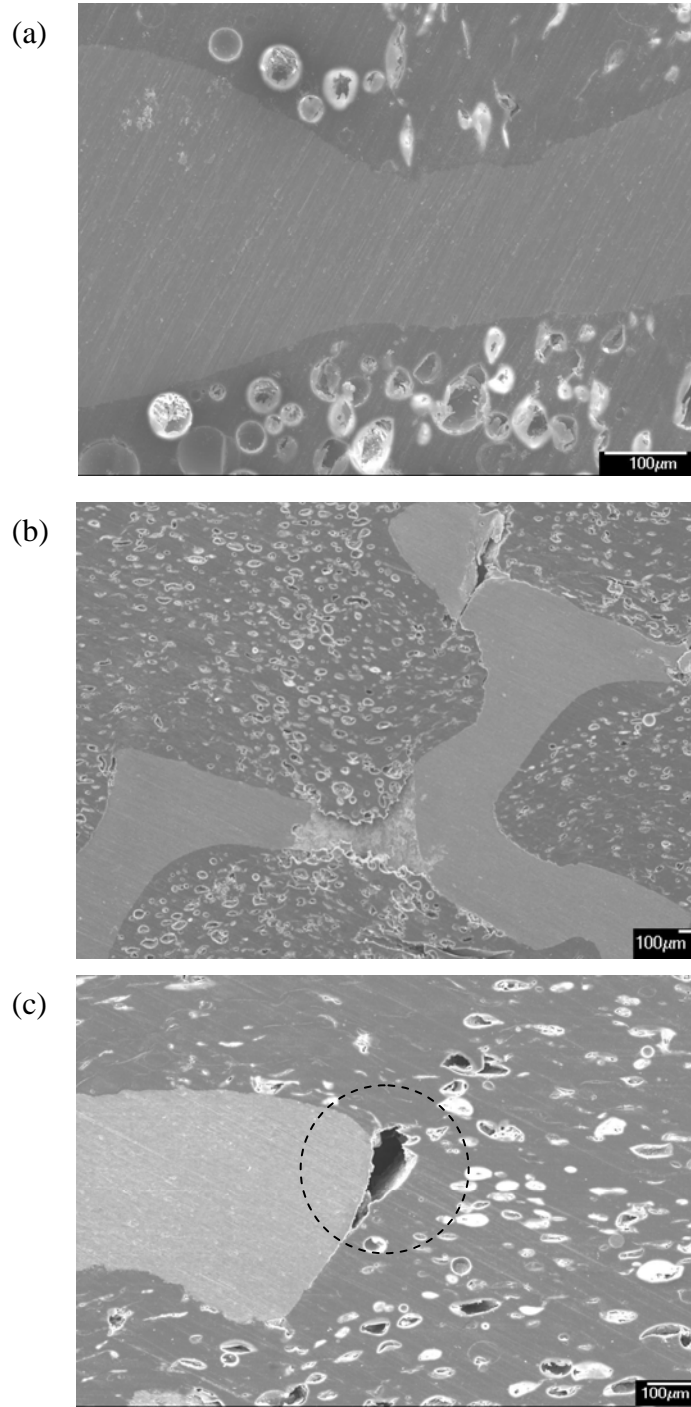


Figure 4.2: SEM images of (a) silane coated IPC foam at a strain of 10%, (b) silane coated IPC foam at a strain of 58%, (c) uncoated IPC foam at a strain of 14%. (Compression is in the horizontal direction in (a) and in the vertical direction in (b) and (c).

The behavior is dependent on many factors with the density (dependent on the volume fraction of the microballoons in the current IPC foam) of the composite being the most important. The SEM image in Fig. 4.2(c) is that of uncoated IPC foam compressed to about 14% strain. It clearly reveals the effect of weaker adhesion between the metal and polymer phases as evident from an isolated debond highlighted in the micrograph. Such debonds are generally absent even at relatively high strain levels when silane coated preform is used (see Fig. 4.2(b)).

#### 4.1.1 Effect of volume fraction of microballoons

For comparison, the compression response of an unfilled aluminum preform [21] is shown in Fig. 4.3. It has an elastic modulus of ~93 MPa (Young's modulus of bulk aluminum is 70 GPa) and a plateau stress of ~2.5 MPa without any noticeable softening at the onset of cell collapse .

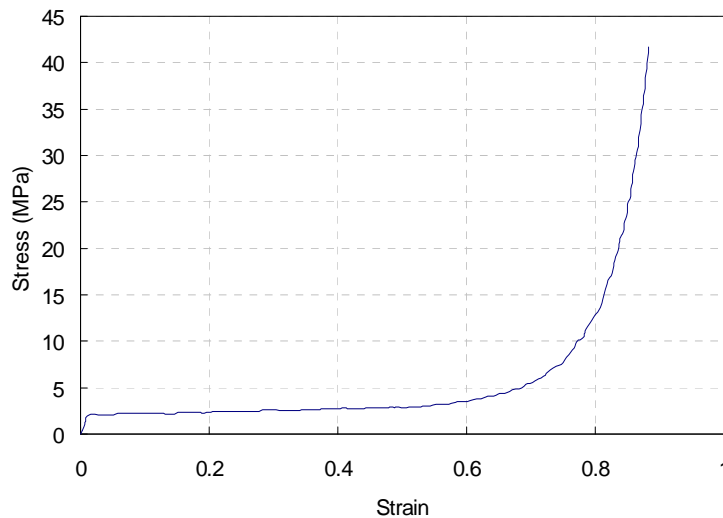
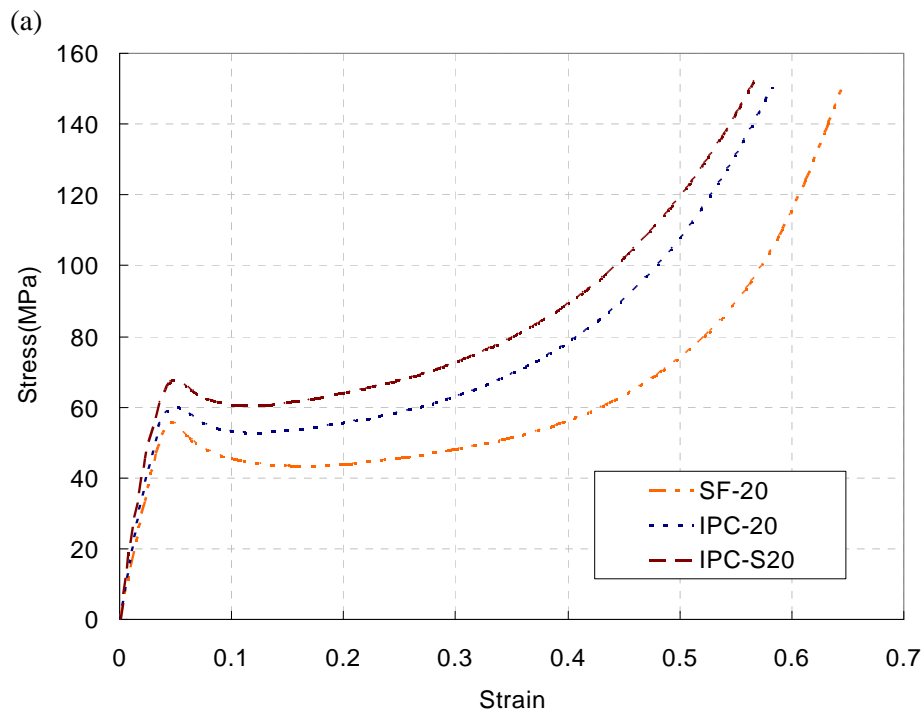


Figure 4.3: Compression response of unfilled aluminum foam used in this work [21]

This is unlike the response of syntactic foam samples (see, Fig. 3.4) which have a noticeable softening at the onset of nonlinearity.

When responses of pure syntactic and IPC foams with the same volume fraction of microballoons (Fig.4.4) are compared, IPC foams show an increase in the plateau stress by as much as 15-20 MPa (depending upon the volume fraction of the microballoons in the infiltrated syntactic foam), much higher than that expected from the aluminum preform. Synergistic mechanical constraint between the aluminum ligaments of the preform and pockets of infused syntactic foam are responsible for this favorable response. That is, aluminum ligaments are laterally supported by the syntactic foam pockets preventing them from premature bending/buckling as in an unfilled preform. On the flip side, pockets of syntactic foam are reinforced by the metallic ligaments against an early collapse of microballoons.



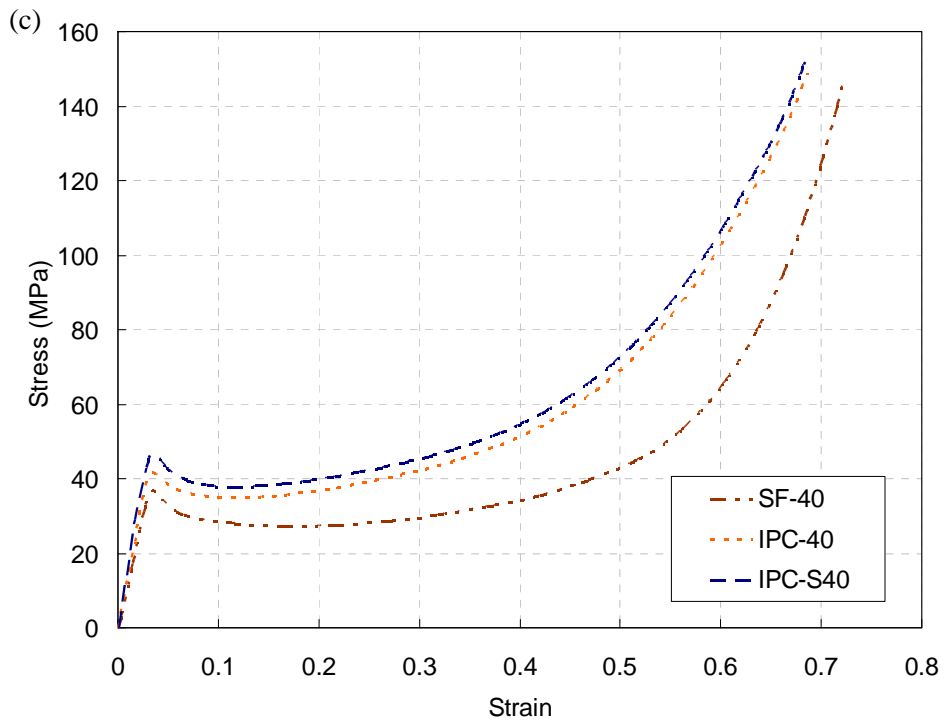
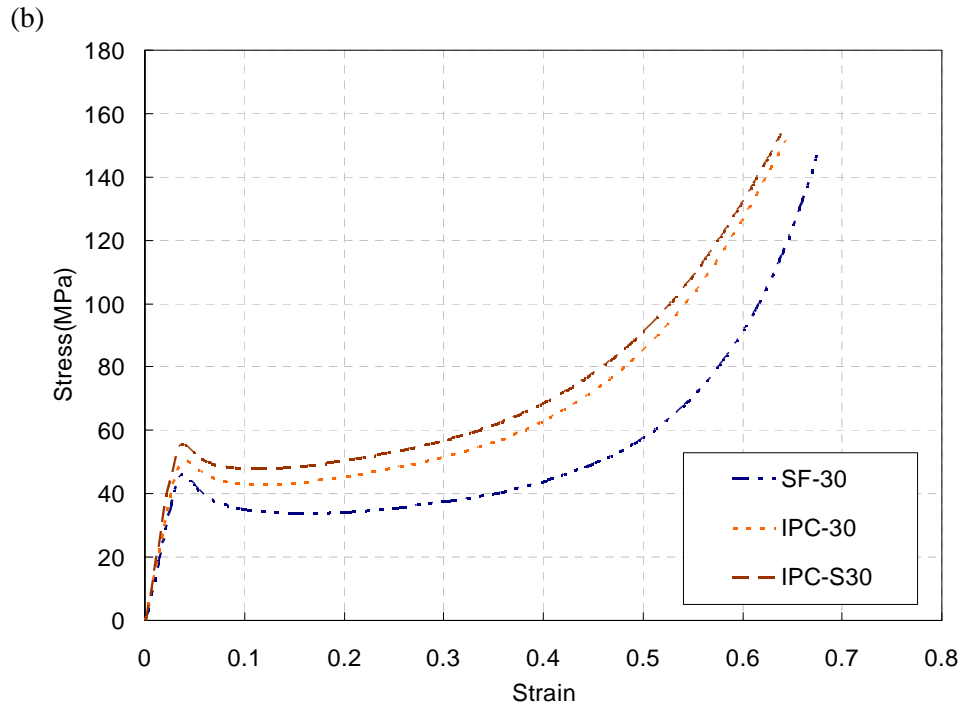


Figure 4.4: Comparison of stress-strain response of syntactic foam, IPC foam with uncoated preform and IPC foam with silane coated preform for (a) 20% volume fraction, (b) 30% volume fraction, (c) 40% volume fraction of microballoons

Another interesting comparison between the responses of IPC foam with silane coated and uncoated aluminum ligaments can be made from Figs. 4.4(a), (b) and (c). The characteristics such as yield stress, plateau stress and compaction response all seem to favor silane coated IPC foam over uncoated IPC foam and the pure syntactic foam, in that order. This is largely attributed to the reduction of microscopic debonds between aluminum ligaments and syntactic foam as deformation progresses in case of coated IPC foam.

The elastic modulus of the composite was determined using the initial linear portion of the measured stress-strain curves. The elastic modulus and the upper yield stress for IPC foam made from uncoated and coated aluminum preforms are quantified in Table 4.1 and are found to monotonically decrease with increasing volume fraction of microballons in the syntactic foam. This behavior is consistent with the corresponding values of pure syntactic foam (see, Table 3.1). From Table 4.1 it can also be noted that the elastic modulus and yield stress of IPC foam with silane coating is higher when compared to the corresponding uncoated preform for all volume fractions of microballoons in syntactic foam. As noted earlier, the increase in elastic modulus and compressive strength of silane coated preform can be attributed to improved wettability, which in turn enhances adhesion between the metal and polymer phases. The IPC foam is also found to have improved the mechanical properties when compared with those for the respective syntactic foams.

In Figs. 4.4(a)-(c), data for syntactic foam and the corresponding IPC foam samples with uncoated and silane coated preforms is examined comparatively for 20%,

30% and 40% volume fraction of microballoons. There is a substantial increase in all the relevant characteristics of IPC foam samples when compared to that for pure syntactic foam samples. The increase in the elastic modulus for IPC foam with silane coated preform was found to be about 33%, 28%, 35% for the composites IPC-S20, IPC-S30, IPC-S40, respectively, when compared to the corresponding pure syntactic foam. (The corresponding increases are nearly constant after factoring into account experimental scatter in the data.) The relative increase in the compressive strengths for the three composites were 21.2%, 19.7%, 24.8%, respectively, relative to the corresponding syntactic foam samples.

IPC foam with uncoated preform				IPC foam with silane coated preform			
IPC designation	Density (kg/m <sup>3</sup> )	Compressive Strength (MPa)	Elastic Modulus (MPa)	IPC designation	Density (kg/m <sup>3</sup> )	Compressive Strength (MPa)	Elastic Modulus (MPa)
IPC-20	1008 ±12	59.9 ± 2.5	1821 ± 17	IPC-S20	1036 ±13	67.5 ± 2.3	2123 ± 32
IPC-30	937 ± 8	50.5 ± 1.8	1573 ± 12	IPC-S30	954 ± 12	55.4 ± 3.6	1852 ± 27
IPC-40	861 ±12	41.5 ± 2.6	1442 ± 28	IPC-S40	879 ± 18	45.8 ± 1.9	1702 ± 26

Table 4.1: Properties of IPC Foam  
(20, 30, 40 designation denotes  $V_f$  of microballoons in the syntactic foam)

From Fig. 4.4 it can also be seen that treating the preforms with silane results in an increase in plateau stress for the same three IPC foams when compared to the corresponding uncoated versions IPC-20, IPC-30 and IPC-40, respectively. Also the percentage increase is a maximum for IPC-S20 which is approximately 14% and it decreases with increasing volume fraction of microballoons to a value of about 8% for IPC-S40. That is, there is diminishing return in terms of compression characteristics due to silane treatment as volume fraction of microballoons increase In the composite.

#### 4.1.2 Energy absorption characteristics of IPC

Conventional cellular materials have found applications in automotive and packaging industries due to their superior energy dissipation characteristics. The cellular structure of these materials enables them to undergo large deformations in compression, enabling them to absorb considerable amounts of energy [1]. The energy absorbed per unit volume ( $U$ ) can be found by evaluating the area under the stress-strain curve

$$U = \int_0^{\varepsilon} \sigma(\varepsilon) d\varepsilon \quad (4.1)$$

where  $\sigma(\varepsilon)$  denotes uniaxial stress as a function of strain.

The energy absorbed up to 50% strain is plotted as histograms in Fig. 4.5. The syntactic foam with 20% (SF-20) volume fraction of microballoons is found to have the highest value of energy absorption when compared to 30% (SF-30) and 40% (SF-40) cases, in that order. Similar trend can also be seen for IPC foams with silane coated and uncoated aluminum preforms. Approximately 50% increase in the absorbed energy per

unit volume of silane coated IPC foam samples relative to the conventional syntactic foams is evident from Fig. 4.5(a). Specifically, 48%, 53% and 49% increase in the absorbed energy per unit volume for IPC-S20, IPC-S30 and IPC-S40 relative to the conventional syntactic foam samples SF-20, SF-30 and SF-40, respectively, is indicative of the potential of IPC foams for energy dissipation applications. On the other hand, for IPC foam samples with an uncoated preform, the absorbed energy was modestly lower and was found to be 31%, 37%, 40% for IPC-20, IPC-30 and IPC-40 relative to SF-20, SF-30, and SF-40, respectively. The presence of aluminum preform increases the overall weight of the composite and hence specific energy absorption (energy absorbed per unit mass) was also calculated. From Fig. 4.5(b), the increase in the value of energy absorption per unit mass for IPC-S20 is found to be about 33% when compared to the corresponding syntactic foam case (SF-20). This value decreases to about 28% and 23% for IPC-S30 and IPC-S40 when compared to syntactic foam cases SF-30 and SF-40, respectively. This also shows that with increasing volume fraction of microballoons in syntactic foam, the percentage increase in the value of specific energy absorption reduces.

From the stress-strain plots shown in Fig. 4.4 for various volume fractions of microballoons in syntactic foam, it can be seen that coating the aluminum preform with silane results in improved compression characteristics of the IPC foam resulting in higher values of compressive strength and elastic modulus relative to the uncoated IPC foam. There is also an increase in energy absorption per unit mass of IPC foam with silane coated aluminum preform when compared to the uncoated preform.



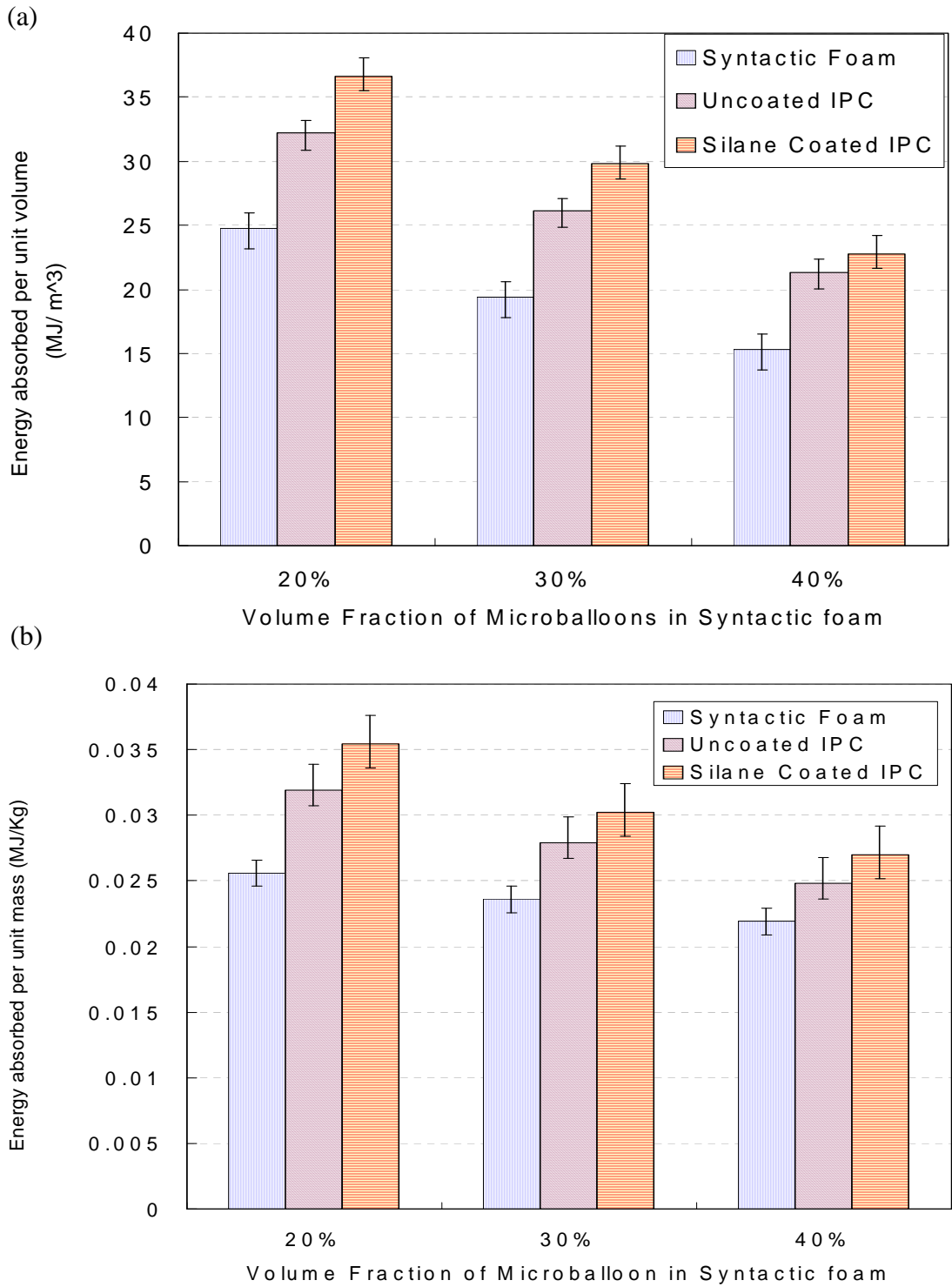


Figure 4.5: Comparison of energy absorption (up to 50% strain) for syntactic foams and IPC foam samples: (a) per unit volume (b) per unit mass.

## **4.2 Compression characteristics of syntactic foam-filled honeycombs**

Many commercial honeycombs are made by expanding strip-glued sheets. As a result each cell has two cell walls of double wall thickness (Fig.2.3). The doubling of this pair of cell walls results in the anisotropic mechanical response of honeycomb. That is, the overall response differs based on whether it is loaded in the L (longitudinal) or W (width) direction.

### **4.2.1 Effect of volume fraction of microballoons**

The compression response of the foam-filled honeycomb composite containing 20%, 30% and 40% volume fractions of microballoons is shown in Fig. 4.6. In Figs. 4.6(a) and (b) the stress-strain responses when compressed in the L and W directions, respectively, are shown. From these plots, it can be seen that the compression responses of these two are similar to that of IPC foams in terms of the presence of three distinct regions. The linear elastic region is followed by a plateau of nearly constant stress and a densification region of steeply rising stress. Each region is associated with a different mechanism of deformation identified by photographing the foam-filled honeycomb composites during loading. The compressive behavior can be explained with the help of Fig. 4.7 where the sequence of specimen deformation for the case of syntactic foam with 30% volume fraction of microballoons is shown. Upon loading, following an elastic region, the cell walls of the aluminum honeycomb network undergo bending which in turn leads to the onset of crushing of microballoons present in that cell. With further increase in load the deformation starts to localize in a narrow zone of cells near the centre of the specimen.

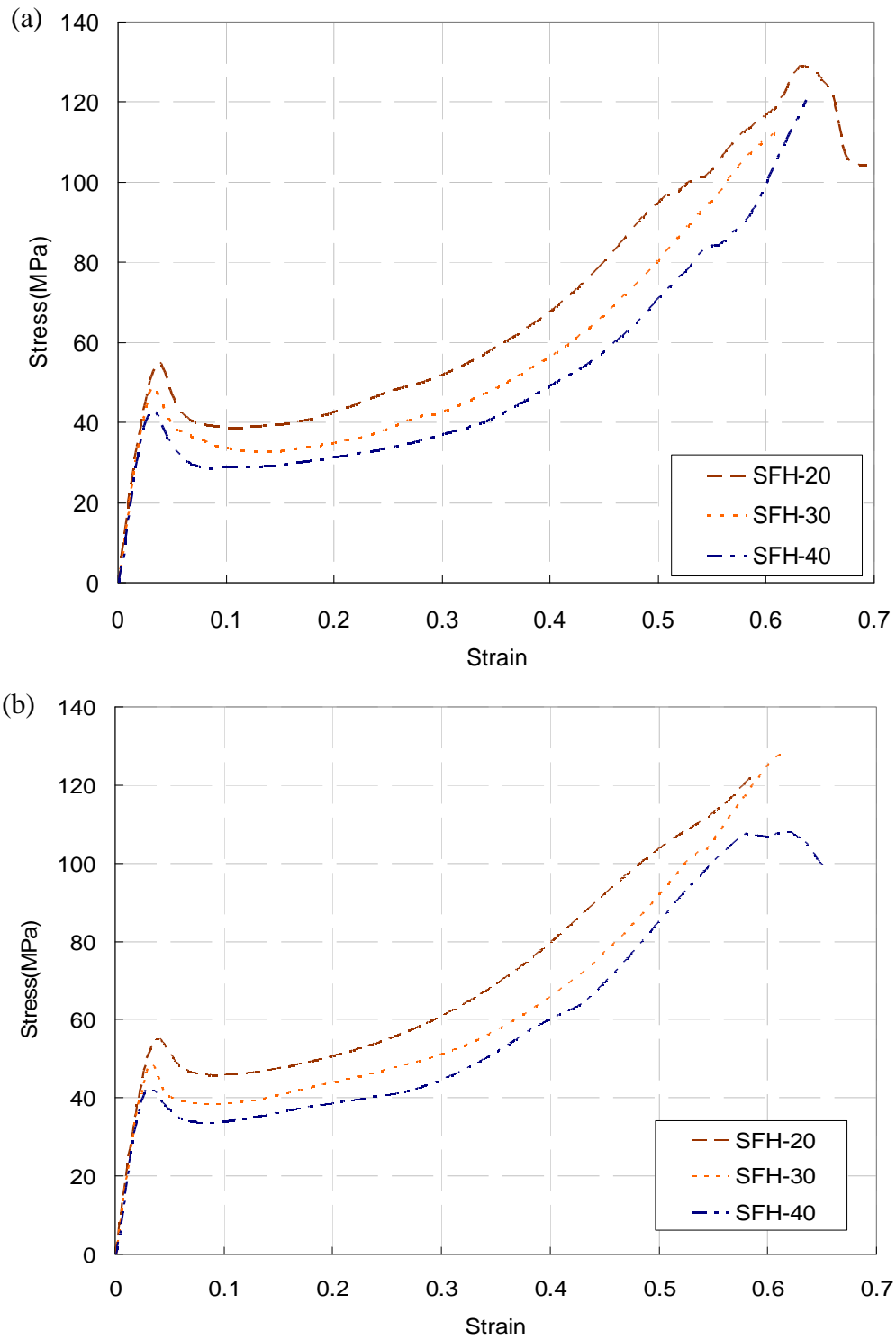
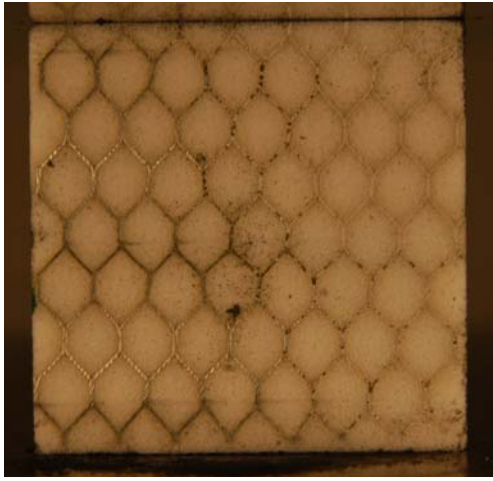


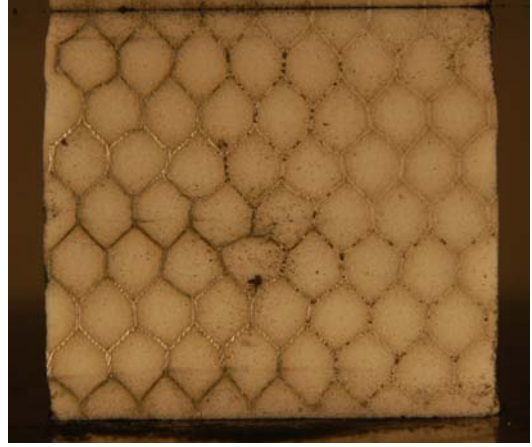
Figure 4.6: Compression response of syntactic foam-filled honeycomb composite. compression along (a) L-direction, (b) W-direction

In this regime, individual cells undergo deformation in a shear dominant mode. At this stage the sample deforms at a relatively constant stress as strain increases resulting in a stress plateau region characterized by progressive collapse of cells. The deformation then spreads from the centre outwards towards the free edges of the specimen. Once this pattern develops, crushing spreads from the collapsed zone to the neighboring cells which leads to a complete collapse of the cells at a relatively faster rate. Upon completion of cell collapse, densification begins as seen by the region with a steeply rising stress.

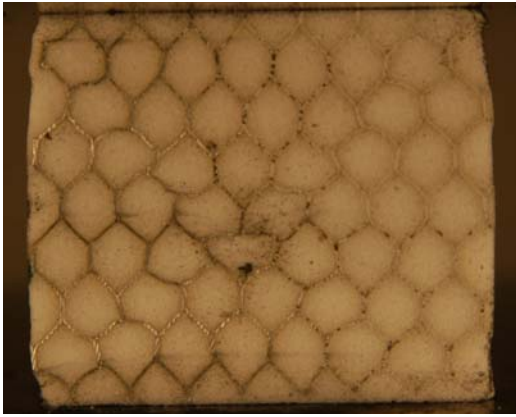
From Figs. 4.6(a) and (b) it can be seen that an increase in volume fraction of microballoon leads to a decrease in yield strength, elastic modulus and plateau stress. The onset of densification occurs at much lower strain values when the volume fraction of microballoons in the syntactic foam is low. These trends are consistent with that observed in case of syntactic foam and IPC foam samples. Also, these results show that the elastic response of syntactic foam-filled honeycomb composite is nearly identical in the two directions. (This is unlike the orthotropic response of unfilled honeycombs in the L- and W - directions, as reported in [30].) Elastic modulus and plateau stress for foam-filled honeycomb composite compressed along L and W directions is reported in Table 4.2. The elastic modulus of the composite is found to decrease from 2027 MPa for the sample with 20% volume fraction of microballoons to 1695 MPa for the one with 40% volume fraction of microballoons.



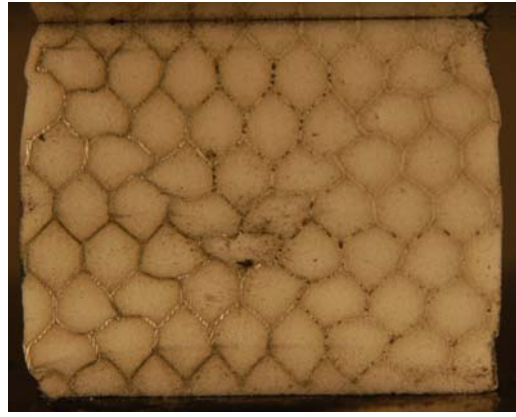
1



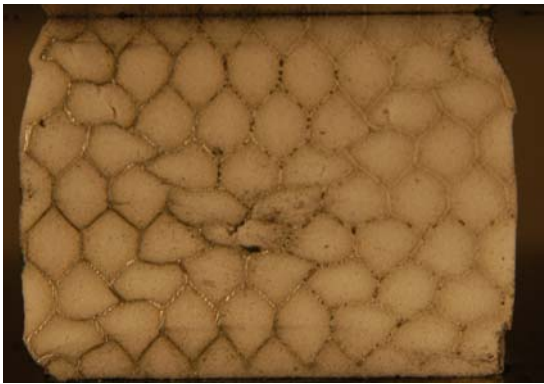
2



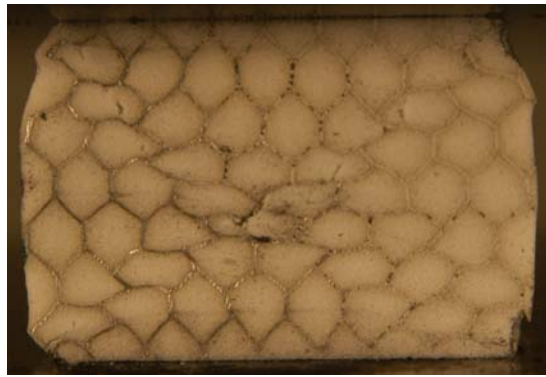
3



4

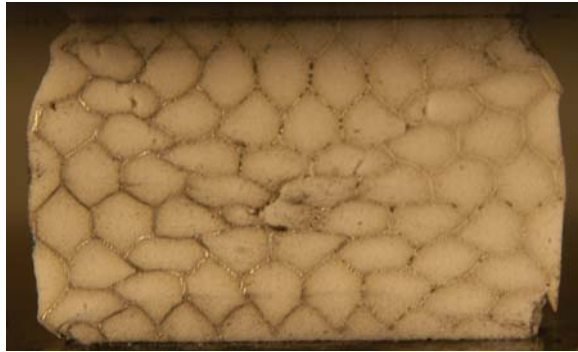


5

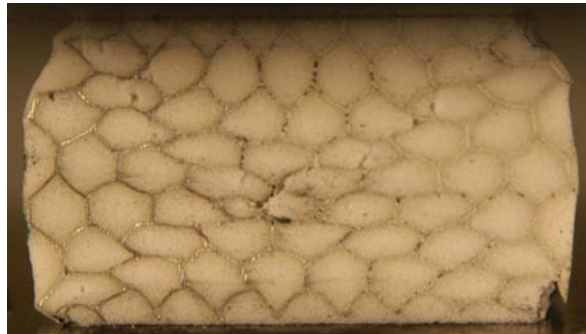


6

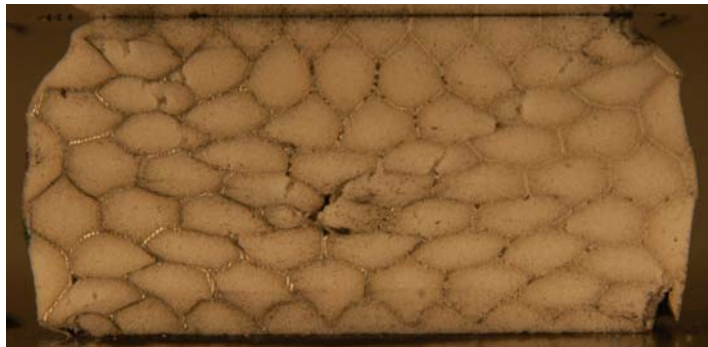
7



8



9



10



Figure 4.7: Deformation sequence for a SFH-30 sample at a applied strain of (1):0%, (2):3.2%, (3):5.8%, (4):8.8%, (5):12.6%, (6):16%, (7):24.6%, (8):30.2%, (9):36%, (10):42%

The values of plateau stress and the yield strength are also found to monotonically decrease by 22% and 26%, respectively, with increasing volume fraction of microballoons in the syntactic foam along both L and W directions. The graphs also show that densification strain increases with increasing volume fraction of microballoons and hence is not as rapid for the sample with 40% volume fraction of microballoons when compared to the ones with the lower volume fractions. With increasing density the resistance to cell wall bending and crushing of microballoons goes up, and hence results in higher modulus and plateau stress.

Composite designation	Density (kg/m <sup>3</sup> )	Elastic Modulus (MPa)	L-Direction	W-Direction
			Plateau Stress (MPa)	Plateau Stress (MPa)
SFH-20	1023 ± 8	2027 ± 18	38.58 ± 2.3	45.45 ± 2.6
SFH-30	921 ± 10	1989 ± 20	33.84 ± 1.7	38.59 ± 2.0
SFH-40	828 ± 14	1695 ± 22	28.74 ± 1.8	34.06 ± 1.6

Table 4.2: Properties of syntactic foam-filled honeycomb composite (20, 30, 40 designation denotes  $V_f$  of microballoons in the syntactic foam)

A few tests were also carried out on samples made by infusing syntactic foam into silane coated honeycomb structures. In Fig. 4.8 the results for the foam-filled silane coated honeycomb samples with 20% volume fraction of microballoons compressed along the L-direction is compared with that of the corresponding uncoated honeycomb. The results show that there is no significant difference between the compression

responses of the two cases and this can be explained with the help of Fig. 4.7 where the sequence of deformation of the foam-filled composite with uncoated honeycomb preform is shown. From this figure it can be clearly seen that a good bonding between the metal (aluminum) and the polymer (syntactic foam) phase leads to the formation of shear bands that propagate within the sample as it continues to deform with increasing load. Also, the sample does not show any significant oozing out of syntactic foam in the out-of-plane direction which further supports this observation. The formation of surface cracks at higher loads shows that because of good bonding between the individual phases these cracks are able to propagate through the specimen.

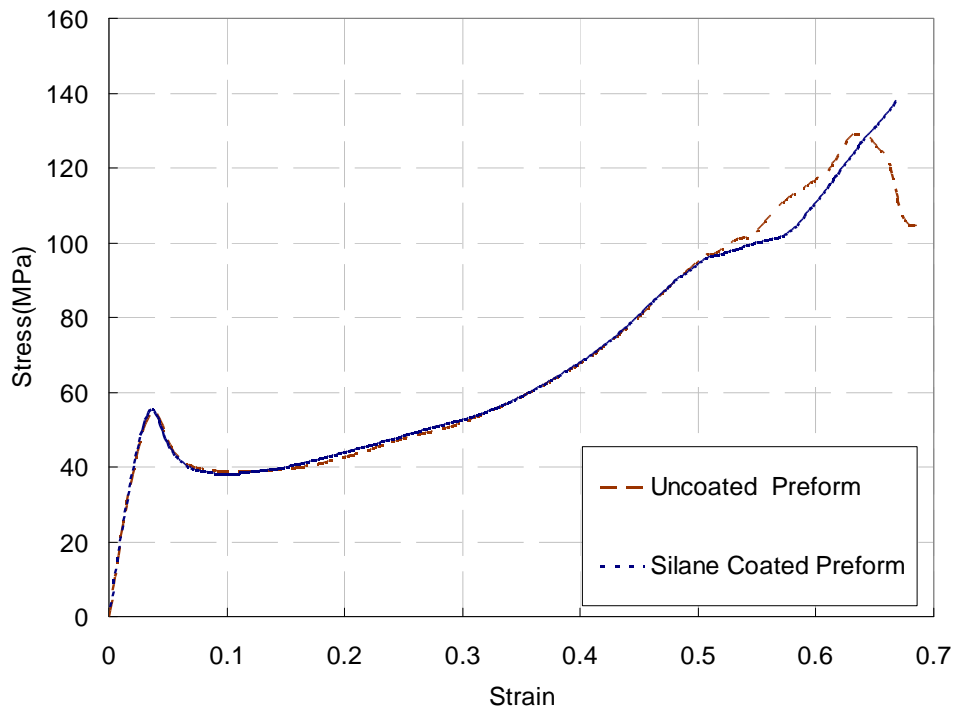


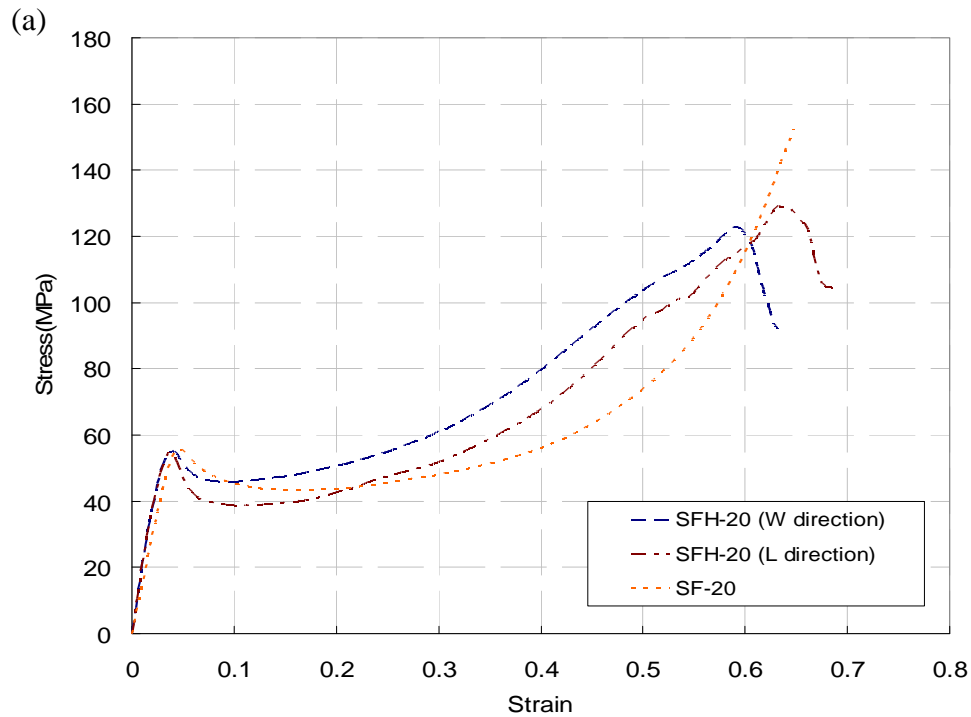
Figure 4.8: Compression response of SFH-20 with uncoated honeycomb preform and silane coated preform



#### 4.2.2 Effect of direction of compression

Unlike the open-cell metallic foams used for making IPC samples, the compressive response of honeycomb structures depends on whether it is compressed along the L- or W-direction. The compression response of syntactic foam and syntactic foam-filled honeycomb composites with the same volume fraction of microballoons is compared in Fig. 4.9. The graphs show that foam-filled honeycomb composites have the same elastic modulus and approximately the same yield stress in both the directions of compression. That is, the linear elastic response is essentially isotropic and the deviations in the two responses occur only at very large strains in the post yielding region. For a particular volume fraction of microballoons, the foam-filled honeycomb is found to have a higher plateau stress for W-direction compression when compared to the one in the L-direction and the percentage increase is 17.8%, 14.0% and 18.5% for 20%, 30% and 40% volume fraction of microballoons in syntactic foam, respectively. The difference in the plateau stresses can be attributed to the non-uniform deformation and propagation of a shear band of deformed cells through the sample when it is compressed in L- or W- directions. From Fig. 4.9(a) it can be seen that the syntactic foam has a modestly higher yield stress when compared to the syntactic foam-filled honeycomb with 20% volume fraction of microballoons. However, this trend shifts with increasing volume fraction of microballoons and the yield stress of the syntactic foam-filled honeycomb increases by ~6 MPa when compared to the syntactic foam with 40% volume fraction of microballoons. The increase in the volume fraction of microballoons in the foam also leads to significant improvements in the yield stress and plateau stress of the foam-filled

honeycombs when compared to the syntactic foam. Hence the syntactic foam-filled honeycomb with 40% volume fraction of microballoons has maximum improvement in its properties when compared to the other two volume fractions. The introduction of aluminum honeycomb web into the syntactic foam prevents the microballoons from an early collapse. This aspect is strongly manifested in the response of the syntactic foam containing 40% volume fraction of microballoons. That is, the syntactic foam-filled honeycomb with 40% volume fraction of microballoon in syntactic foam shows significant improvements in compression response along both L- and W- directions when compared to the corresponding syntactic foam sample.



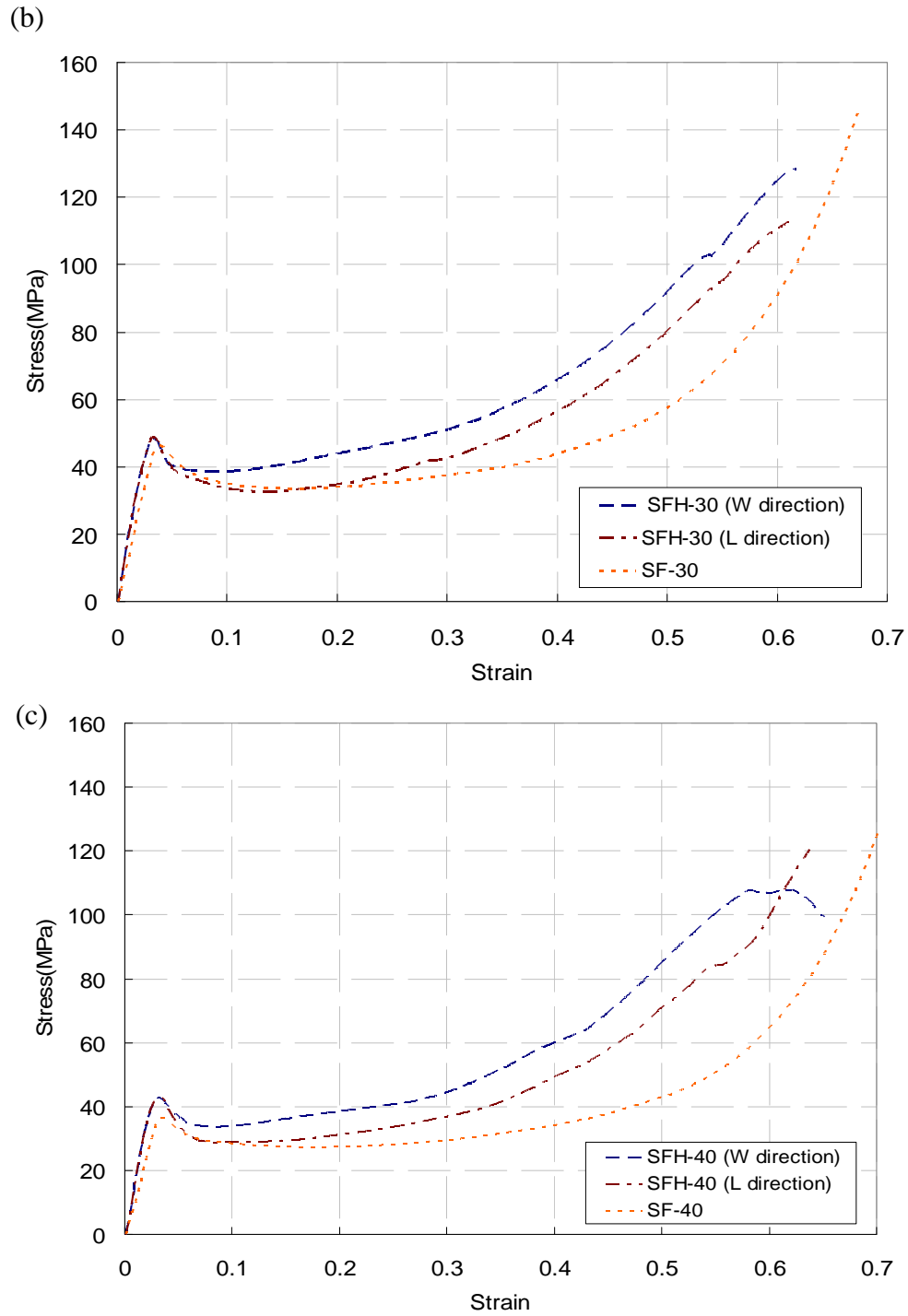


Figure 4.9: Comparison of stress-strain response of syntactic foam, Syntactic foam-filled honeycomb for (a) 20% volume fraction, (b) 30% volume fraction, (c) 40% volume fraction of microballoons

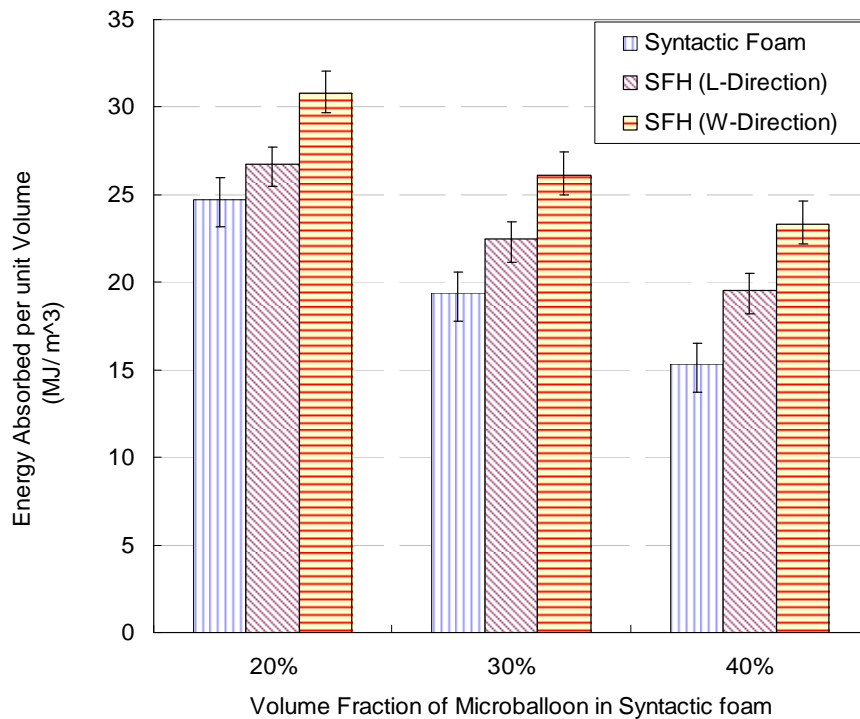
### 4.2.3 Energy absorption characteristics of syntactic foam-filled honeycomb

The energy absorbed by the syntactic foam and the syntactic foam-filled honeycombs up to 50% strain is plotted as histograms in Fig. 4.10. The histograms show foam-filled honeycombs to have enhanced energy absorption characteristics when compared to the corresponding syntactic foam samples made with the same volume fraction of microballoons. The foam-filled honeycomb composite with 20% volume fraction of microballoons, SFH-20, is found to have the highest value of energy absorption when compared to SFH-30 and SFH-40 samples. From Fig. 4.9 it can be seen that foam-filled honeycombs have higher values of plateau stress for the W-direction compression when compared to the L-direction compression. They show 15.1%, 16.4% and 19.5% increase in energy absorption per unit volume of SFH-20, SFH-30 and SFH-40 honeycombs, respectively, when compressed in the W-direction compared to the corresponding values for the L-direction. Foam-filled honeycomb with 20% volume fraction of microballoons (SFH-20) has 24% improvement in energy absorption per unit volume when compared to the corresponding syntactic foam sample and this value increases to 34% and 52% for syntactic foam-filled honeycomb composite with 30% (SFH-30) and 40% volume fraction of microballoons, respectively, when compared to the corresponding syntactic foam samples (foam-filled honeycombs are compressed along the W-direction).

The energy absorbed per unit mass is also evaluated and is plotted in Fig. 4.10(b). From this figure it can be seen that syntactic foam-filled honeycombs compressed along the L-direction show a relatively small improvement in the energy absorption when

compared to the corresponding pure foam samples. This value, however, increases for foam-filled honeycomb composites compressed along the W-direction and the percentage increase is approximately 17%, 20% and 28% for SFH-20, SFH-30 and SFH-40 when compared to the corresponding pure foam samples. The graph also shows that the foam-filled honeycombs with 30% volume fraction of microballoons (SFH-30) and the one with 40% volume fraction of microballoons (SFH-40) have a relatively small difference in their values of energy absorption per unit mass and is  $\sim 0.8$  KJ/Kg for the L-direction and  $\sim 0.21$  KJ/kg for the W-direction.

(a)



(b)

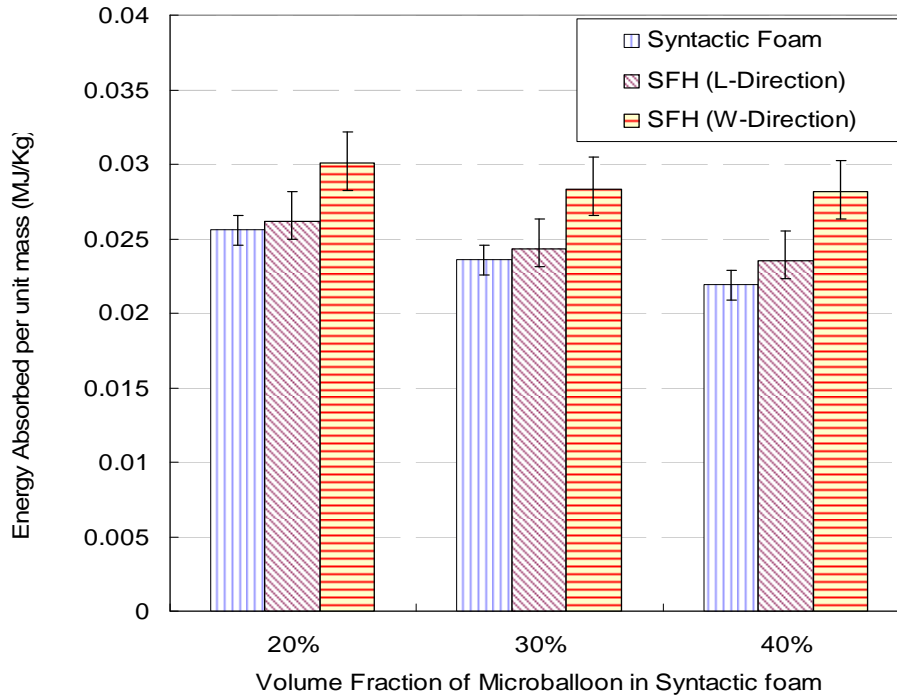


Figure 4.10: Comparison of energy absorption (up to 50% strain) for syntactic foams and Syntactic foam-filled honeycomb samples: (a) per unit volume (b) per unit mass.

Another comparison can be made from Figs. 4.5 and 4.10. From these it can be seen that the IPC foam has higher values of energy absorption per unit mass and per unit volume when compared to the corresponding syntactic foam-filled honeycomb composites, which clearly shows that the interpenetrating architecture of the interpenetrating phase composite enhances the compression response of the syntactic foam by a greater margin. The energy absorption per unit mass for the syntactic foam and syntactic foam-filled composites is plotted for comparison purposes in Fig.4.11, where it can be seen that the IPC foam with 20% volume fraction of microballoons has

approximately 15% higher energy absorption when compared to the syntactic foam-filled honeycomb composite. This value is ~6% for the case of 30% volume fraction of microballoons.

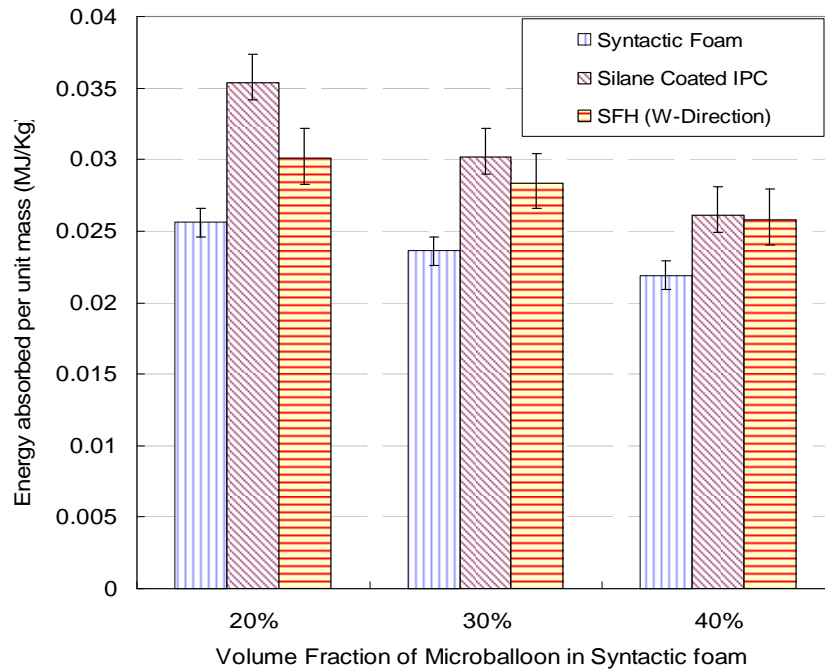


Figure 4.11: Comparison of energy absorption (up to 50% strain) for syntactic foams, IPC foam and syntactic foam-filled honeycomb samples

Also, this trend is found to be consistent for the case of 40% volume fraction of microballoons but the percentage increase is found to be relatively less ~2%. In fig.4.11 the energy absorption characteristics of syntactic foam-filled honeycomb composite when it is compression along W-direction is considered for comparison with IPC. It should be noted that foam-filled honeycomb composite has a significantly lower value of energy absorption when it is compressed along the L-direction and hence was not considered for comparison purposes with IPC in the above figure. The IPC samples consistently have ~

50% higher energy absorption per unit volume and ~33% higher energy absorption per unit mass for various volume fraction of microballoons which is also not the case with syntactic foam-filled honeycombs which have ~24%, ~34% and ~48% higher energy absorption per unit volume for SFH-20, SFH-30 and SFH-40 samples respectively when compressed along the W-direction. The maximum increase in the energy absorption per unit mass for the foam-filled honeycombs is found to be ~26% for SFH-40 sample when it is compressed along the W-direction and this value is also found to be lower when compared to the IPC samples.



## **CHAPTER 5**

### **FINITE ELEMENT MODELING OF SYNTACTIC FOAM-FILLED COMPOSITES**

This chapter describes modeling and simulation of the compressive behavior of syntactic foam-filled composites. The finite element models for Interpenetrating Phase Composite (IPC) foam composites and syntactic foam-filled honeycomb composites are developed in SOLIDEDGE® and MATLAB® software environments, respectively. These models were then imported into ABAQUS/Standard structural analysis software to carry out finite element analyses. A rate independent plasticity model based on associated plastic flow rule and von-Mises yield criterion with isotropic hardening was used to model plasticity of both aluminum and syntactic foam phases of the composite. The overall stress-strain relations of the two types of composites were determined using measured stress–strain responses for the individual phases.

In the first part of this chapter details on the development of a Kelvin cell-based finite element model capable of capturing the salient features of the experimental observations is presented for IPC foam. The numerical results of this unit cell based 3-D elasto-plastic finite element analysis are compared with experimentally obtained true stress-strain curves. The second part of this chapter describes computational modeling of syntactic foam-filled honeycomb composites.

Finite element analysis was used to simulate experiments performed on syntactic foam-filled honeycomb composite. Once the simulations were validated by the experimental data, additional insight on the in-plane mechanical behavior of foam-filled honeycomb composites was sought.

## **5.1 Material model**

A rate independent plasticity model in ABAQUS® was used to model plastic behavior of both aluminum and syntactic foam phases. Most materials of engineering interest initially respond elastically. Within the elastic regime, deformation is fully recoverable upon removal of load. When the stress exceeds the yield value, the deformation is no longer fully recoverable when load is removed. Plasticity theories model mechanical response of materials as they undergo such non-recoverable deformations. These theories, although developed primarily to model ductile behavior of metals, they are also shown to be effective for modeling inelastic behavior of soils, concrete, rock, ice, crushable foams, as well. These materials behave in very different ways. For example, large values of hydrostatic pressure cause very little inelastic deformation in metals whereas even small hydrostatic pressures can cause significant, non-recoverable volume changes in soils. Nonetheless, the fundamental concepts of plasticity theories being sufficiently general, models based on these concepts have been developed successfully for a wide range of materials.

Most of the plasticity models are based on “incremental” theories in which strain rate is decomposed into an elastic part and a plastic (inelastic) part. The incremental plasticity models are usually formulated in terms of

- Yield surface, which generalizes the concept of yield load into a test function that can be used to determine if the material responds purely elastically at a particular state of stress, temperature, etc.
- Flow rule, which defines the inelastic deformation that occurs if the material point is no longer responding purely elastically, and
- Evolution laws that define hardening - the way in which the yield and/or flow definitions change as inelastic deformation occurs.

The experimental test data is converted into true stress and logarithmic plastic strain using Eqns. 5.1 and 5.2 which are then used as the input for the plasticity model:

$$\sigma_{true} = \sigma_{nom} (1 + \varepsilon_{nom}) \quad (5.1)$$

$$\varepsilon_{ln}^{pl} = \ln(1 + \varepsilon_{nom}) - \frac{\sigma_{true}}{E} \quad (5.2)$$

In this work, the plasticity model based on associated plastic flow and von Mises yield criterion with isotropic hardening was used to model plasticity of both metallic and syntactic foam phases. The Mises yield surface was used to define isotropic yielding. In the associated plastic flow rule the direction of flow was the same as the direction of the outward normal to the yield surface and in isotropic hardening the yield surface is

assumed to maintain its shape, while its size increases or decreases as plastic straining occurs . The isotropic hardening means that the yield function is written as

$$f(\sigma) = \sigma^0(\varepsilon^{pl}, \theta) \quad (5.3)$$

where  $\sigma^0$  is the equivalent (uniaxial) stress,

$\varepsilon^{pl}$  is the work equivalent plastic strain, and

$\theta$  is temperature.

## 5.2 Finite element modeling of IPC foam

In order to model stress-strain characteristics of IPC foams finite element method was utilized and the results were validated by those obtained from experiments discussed earlier. To understand the mechanical behavior of the IPC foam on hand, it would be appropriate to consider models with randomly interpenetrating 3-D structures, similar to the one studied experimentally. However, in view of practical considerations of modeling the complexities of the metallic preform and syntactic foam, a unit cell based analysis was carried out.

### 5.2.1 Development of unit cell model

Previous structural foam researchers [31-33] have successfully used space filling Kelvin cells [34] to represent an open-cell microstructure. These investigators have demonstrated the ability of these cells used in conjunction with the finite element method to capture the behavior of open-cell foams. A Kelvin cell is a tetrakaidecahedron, a 14-sided polyhedron comprised of six squares and eight hexagonal faces. In the present

work, the initial modeling of a Kelvin cell was done using SOLIDEDGE®. Figure 5.1 shows the Kelvin cell that is used to represent the aluminum foam in this work. The actual cross-section of aluminum ligaments of the perform/scaffold used in experiments was close to a triangular shape and hence was approximated as an equilateral triangle in the simulations for simplicity.

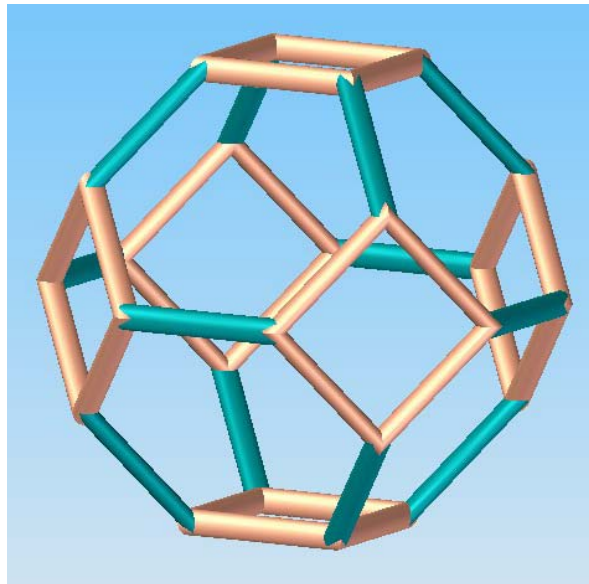


Figure 5.1: Schematic of a unit cell model of Kelvin cell.  
(Color rendition is for clarity only)

The space inside and outside this cell was filled with syntactic foam, assumed to be a macroscopically homogeneous and isotropic solid medium for modeling purposes. This results in an interpenetrating structure, representative of the IPC foam on hand. The unit cell model used to represent the IPC foam is shown in Fig. 5.2. All the ligaments of the Kelvin cell have the same length ( $L$ ) and the cell height in this case is  $h = 2\sqrt{2} L$ .

The cross sectional area of ligaments was decided such that the overall volume fraction of the aluminum foam in the IPC is approximately 9%, same as that of the preform used in the experiments.

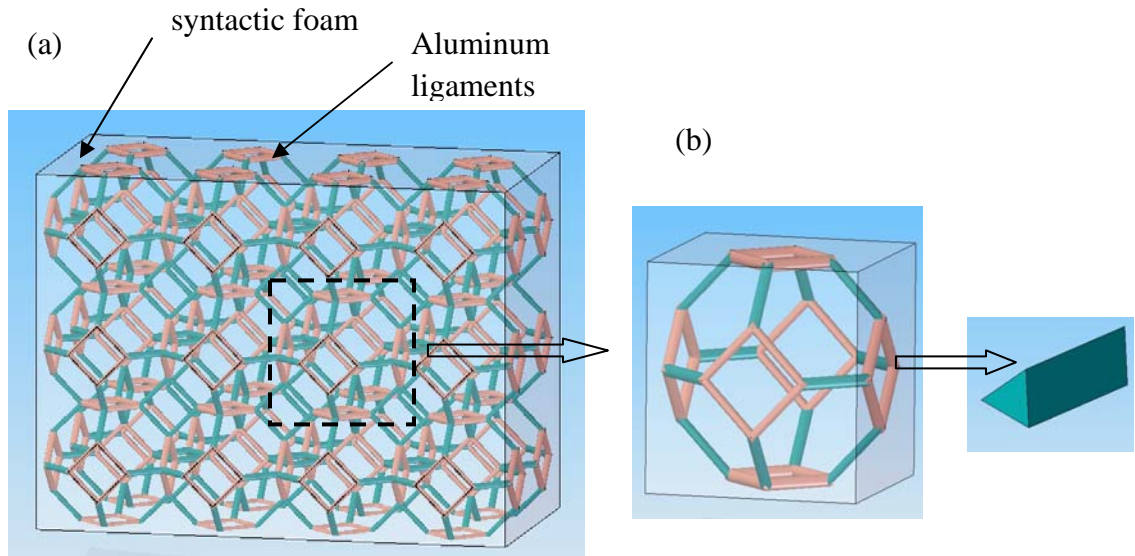


Figure 5.2: Finite element model development: (a) Idealization of IPC foam structure using Kelvin cells (b) Unit cell model used to represent aluminum-syntactic foam IPC.

### 5.2.2 FEA model description

Finite element analyses were carried out using ABAQUS/Standard structural analysis software. A four node tetrahedron element (element type C3D4) in ABAQUS with linear interpolation was used to discretize the unit cell. The model had a total of 86865 elements and 16111 nodes. A mesh convergence study was performed using different element sizes (average sizes - 0.0825mm, 0.152mm and 0.325mm) and it was found that the element size of 0.152 mm was sufficient for achieving good convergence, and hence was used in all the simulations. The elastic constants of aluminum and the

respective syntactic foam (from experiments) were assigned to the two phases of the IPC foam.

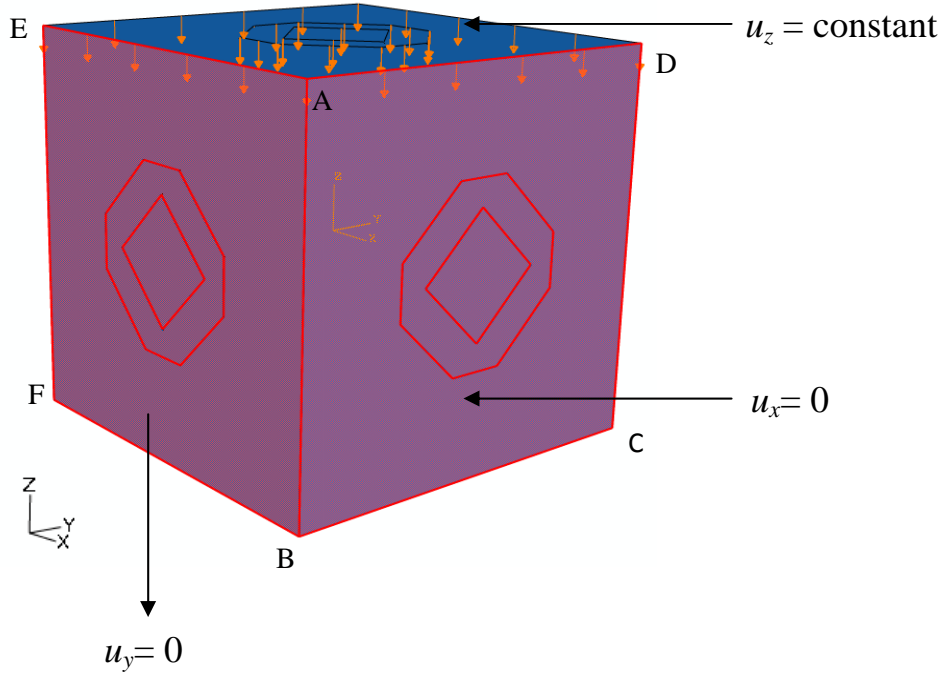


Figure 5.3: Finite element model of undeformed unit cell with boundary conditions used while simulating the uniaxial compression of IPC foam.

The plasticity model described in the previous section was used to model plasticity of both metallic and syntactic foam phases. Since the applied strains were greater than the elastic limit ( $\sim 40\%$  in this work), geometrical nonlinearity was also incorporated into the analysis. The stress-strain response of aluminum Al-6101 (Young's modulus = 69 GPa,  $\nu = 0.35$ , yield stress = 172 MPa at 0.2% strain and ultimate stress = 200 MPa (at 15% strain) based on Alcoa Inc. datasheet) was assigned to all the elements representing the metallic ligaments. The measured stress-strain responses for syntactic

foams made with different volume fractions of microballoons were used to model the infiltrating material surrounding the ligaments of the unit cell.

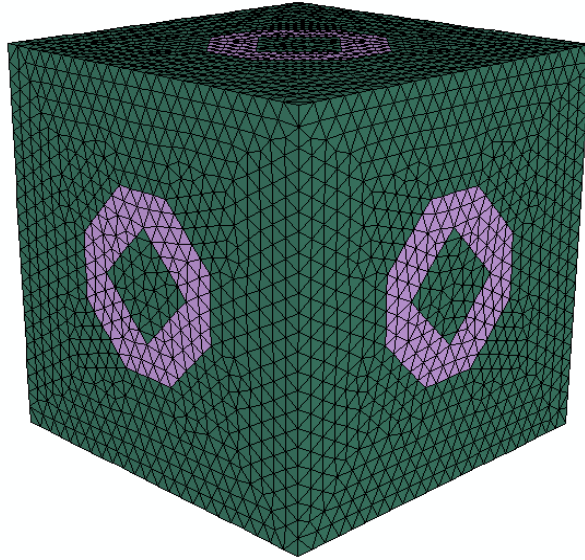


Figure 5.4: Finite element model of undeformed unit cell with mesh (Different colors/shades show metallic ligaments embedded in the syntactic foam cubic cell.)

The model was subjected to uniaxial compression by displacing the nodes uniformly on the top face of the cell in the  $z$ -direction, as shown in Fig. 5.3. The nodes on the other lateral faces of the unit cell were constrained in the respective outward directions but were free to displace in the in-plane directions. All the prescribed boundary conditions are shown in Fig. 5.3, where displacements of nodes on the face ABCD along the  $x$ -direction is zero and similarly displacements of nodes on the face ABEF along the  $y$ -direction is zero. Figure 5.4 shows the finite element mesh of the model used in this study. Previous foam mechanics researchers have used either displacement constraints or periodic boundary conditions in their studies and therefore the effect of boundary

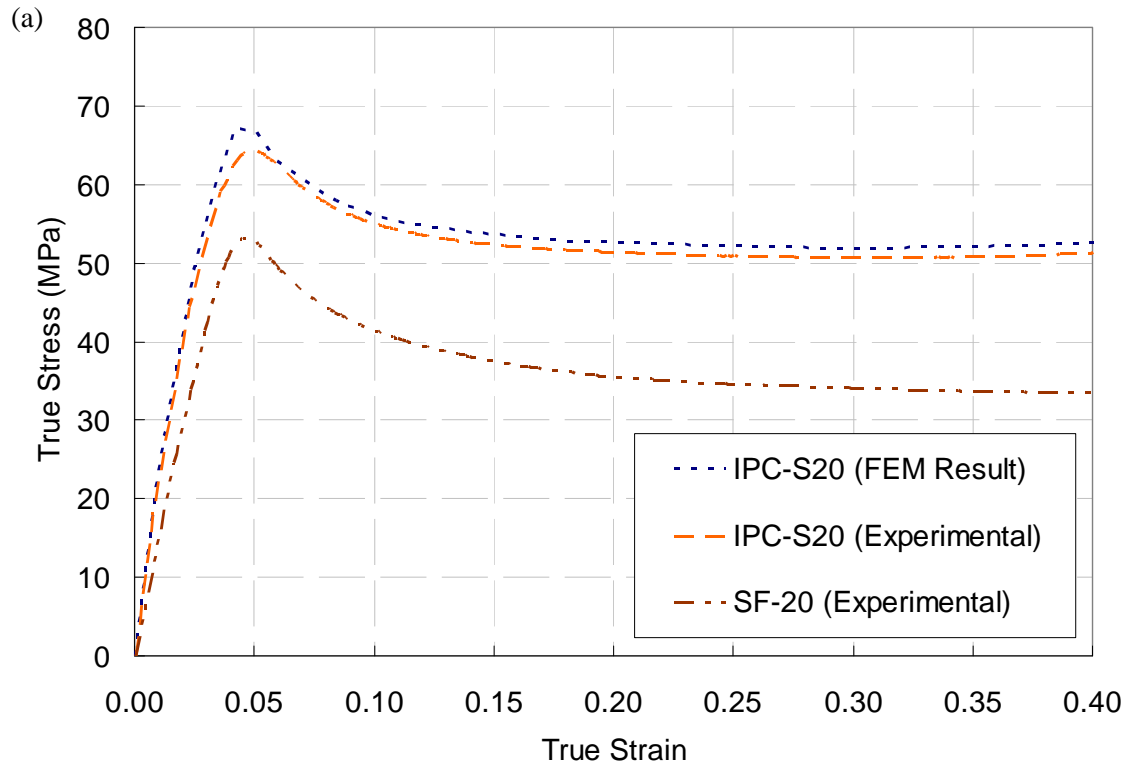


condition on the stress-strain response of the IPC foam is also discussed in the next section.

### **5.2.3 Results**

The uniaxial compressive behaviors of IPC foam with different volume fractions of microballoons (20%, 30% and 40%) in syntactic foam were simulated and the results were compared with the corresponding ones from experiments. In Fig. 5.5, the finite element results for IPC foam with 20%, 30% and 40% volume fraction of microballoons in syntactic foam are compared with experimentally obtained true stress-strain responses. It should be noted that results from the simulation are compared with that for the silane coated IPC samples due to the idealization of perfect bonding between the two phases in case of the finite element analysis. The measured stress-strain response of the corresponding syntactic foam samples with the same volume fraction of microballoons is also shown for comparison. It can be seen that the simulations indeed capture the measured IPC foam behavior very well. In the post-yield regime, the simulations seem to slightly over predict the measurements attributed primarily to the idealization of uniform and defect free bonding between aluminum and syntactic foam phases. The assumption of uniform cross-sectional area for all ligaments throughout the unit cell could be an additional contributor to this over prediction. From Fig. 5.5 it can also be seen that the simulations seem to predict more accurate results for the IPC with 20% volume fraction of microballoons when compared to IPC with 30% and 40% volume fraction of microballoons. This could be due to the fact that syntactic foam is modeled as an

isotropic and homogeneous material during the finite element analysis. The results also clearly show that the Kelvin cell model successfully captures the overall behavior of the IPC composite. Table 5.1 lists the values of elastic modulus, compressive strength and plateau stress of the IPC foam obtained from finite element simulations for all the three cases. Again, from the results it is evident that the predictions are slightly higher in all cases when compared to measurements.



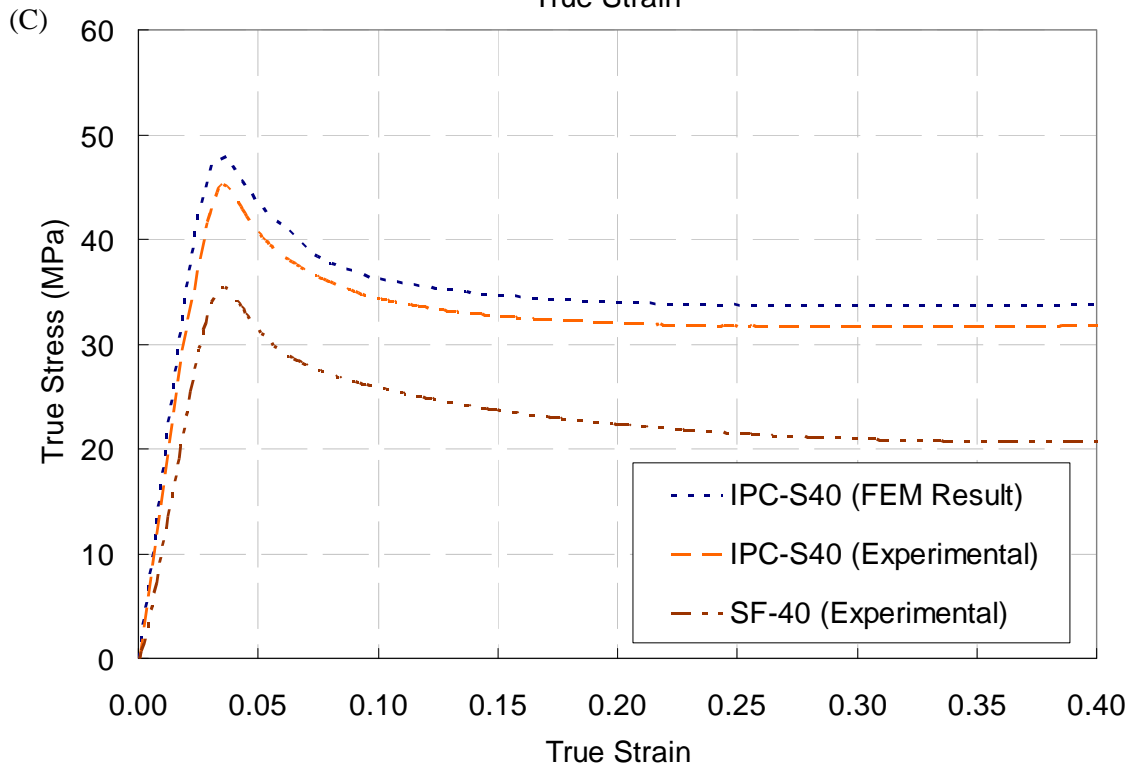
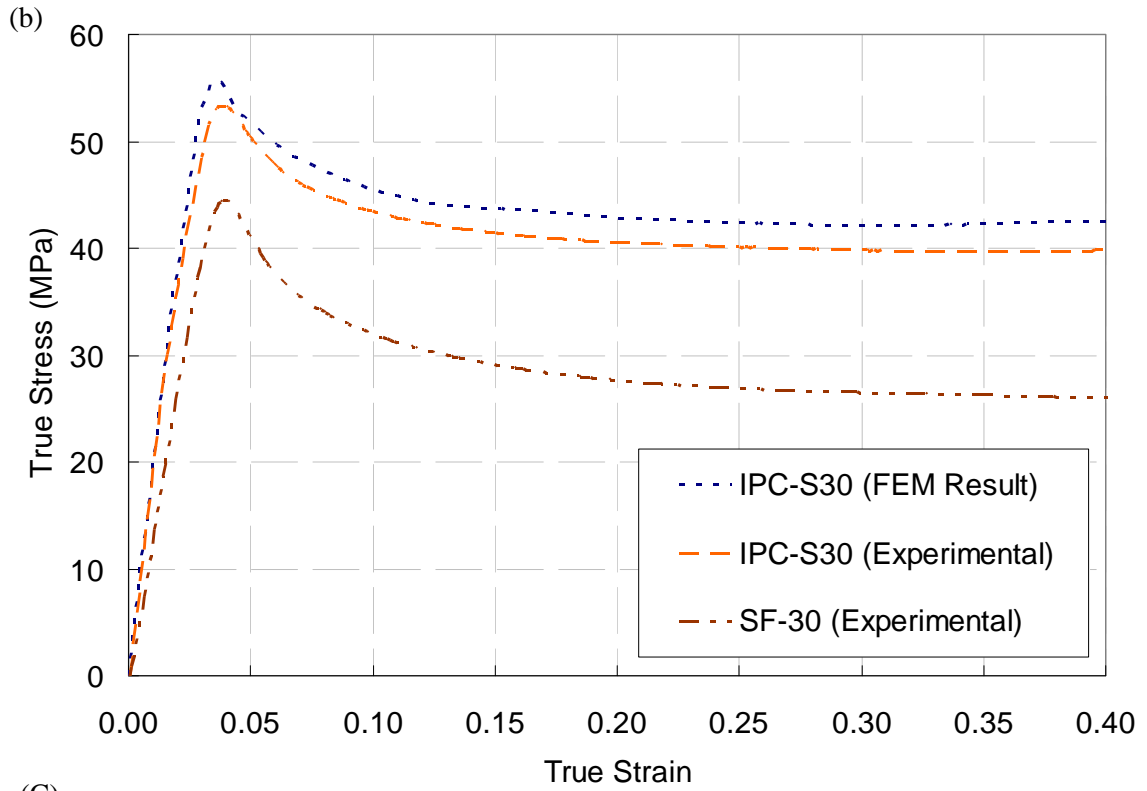


Figure 5.5: Comparison of numerical and experimental results for IPC foam with (a) 20% volume fraction, (b) 30% volume fraction, (c) 40% volume fraction of microballoons

A few representative results from finite element simulations for IPC-S30 case are shown in Figs. 5.6(a)-(c). In Fig. 5.6(a), von-Mises stress contours are depicted on the unit cell and on an interior planar section denoted by A-B at an imposed strain of 40%. As expected, the ligaments experience higher stresses compared to the surrounding syntactic foam. From the contours of equivalent plastic strain (Fig. 5.6(b)) it can be seen that the strain levels are higher for the syntactic foam when compared to that in the aluminum phase as syntactic foam has lower yield strength when compared to the preform ligaments. Further, non-uniformity of strains through the cross-section of the unit cell is clearly evident.

IPC Designation	Finite Element Results			Experimental Results		
	Elastic Modulus (MPa)	Compressive Strength (MPa)	Plateau Stress (MPa)	Elastic Modulus (MPa)	Compressive Strength (MPa)	Plateau Stress (MPa)
IPC-S20	2204	67.8	52.0	2109	64.2	50.8
IPC-S30	1938	55.8	41.9	1843	53.2	40.2
IPC-S40	1792	47.9	33.7	1689	45.0	31.7

Table 5.1: Comparison of finite element results with experiments (based on true stress- strain data)

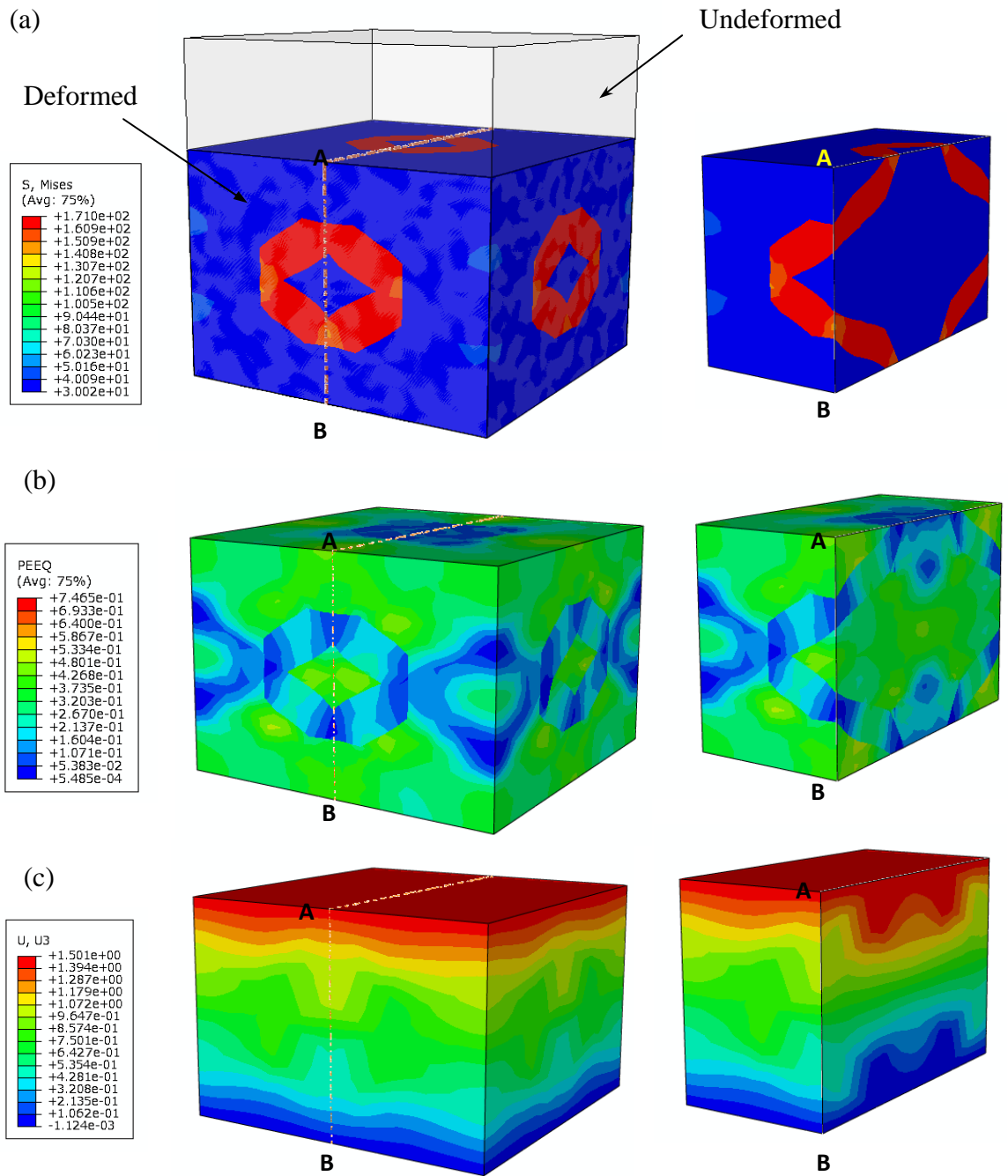


Figure 5.6: Finite element results for unit cell model for IPC-S30 at 40% strain. (a) Deformed and undeformed unit cell with von-Mises stress contours (b) Deformed unit cell with equivalent plastic strain contours (c) Deformed unit cell with displacement contours in the  $u_3$  ( $u_z$ )

In Fig. 5.6(c), displacement contours in the direction of the imposed strain ( $u_z$ ) is shown. The presence of aluminum ligaments in the unit cell clearly perturbs the uniformity of displacements as evident from the contours on and within the cell. A Kelvin cell based 3D elasto-plastic finite element model is developed by adopting unit cell analysis approach to examine the feasibility of predicting both the elastic and plastic characteristics of the IPC foam. This analysis is aimed at validating the case of silane treated preform where adhesion between the ligaments and foam can be assumed to be relatively strong. The numerical model based on measured compression response of the corresponding syntactic foam and aluminum is able to successfully capture the overall IPC foam behavior.

#### **5.2.4 Effect of boundary conditions**

Many researches [35-37] have used spatially periodic boundary conditions to study the mechanical behavior of cellular solids in view of the periodicity of their microstructures. Thus periodic boundary conditions are also used in the current unit cell analysis and the effect of boundary condition on the stress-strain response of the IPC foam was studied. In the current work, the periodic boundary conditions were applied according to the procedure described in Ref. [37]. The three pairs of opposite bounding faces of the cell were represented as  $(\partial R_{i1}, \partial R_{i2})$   $i = 1, 2, 3$ .

The boundary conditions corresponding to an average strain for a periodic cell can then be expressed as

$$\mathbf{u}_{i1} - \mathbf{u}_{i2} = \mathbf{u}_{i1}^{ref} - \mathbf{u}_{i2}^{ref} \quad (5.4)$$

where  $(\mathbf{u}_{i1}, \mathbf{u}_{i2})$  is the displacement of points on each pair of faces denoted by  $(\partial R_{i1}, \partial R_{i2})$  and  $(\mathbf{u}_{i1}^{ref}, \mathbf{u}_{i2}^{ref})$  are displacements of conjugate points on opposite sides chosen as reference points.

A finite element mesh on the two opposite faces of the unit cell is shown in Fig. 5.7 where  $\mathbf{u}_{i1}^{ref}$  and  $\mathbf{u}_{i2}^{ref}$  are the displacements of the corresponding *matching nodes*. In the current analysis the aluminum ligaments are modeled using a symmetric Kelvin cell described above and thus each pair of opposite bounding faces of the cell have the same in-plane displacements. In order for a unit cell to be periodic, all outer faces must fulfill a periodicity condition. That is, every node on the outer face must have an equivalent node on the corresponding opposite (negative) outer face. As long as periodicity conditions can be formulated for a given cell, then the same cell can be used to represent the microstructure. In Fig. 5.7, two opposite sides of the same pair of the model are shown. From this figure it can be clearly seen that for every node on one face there is a corresponding matching node on the other face of the model. The mesh of the finite element model thus generated had a matching node for each pair of surfaces. This periodic mesh had reduced integration hexahedral elements type C3D8 in ABAQUS® on the outer faces of the model while four node tetrahedron element (element type C3D4) in ABAQUS® with linear interpolation in the inner regions of the unit cell. The model had

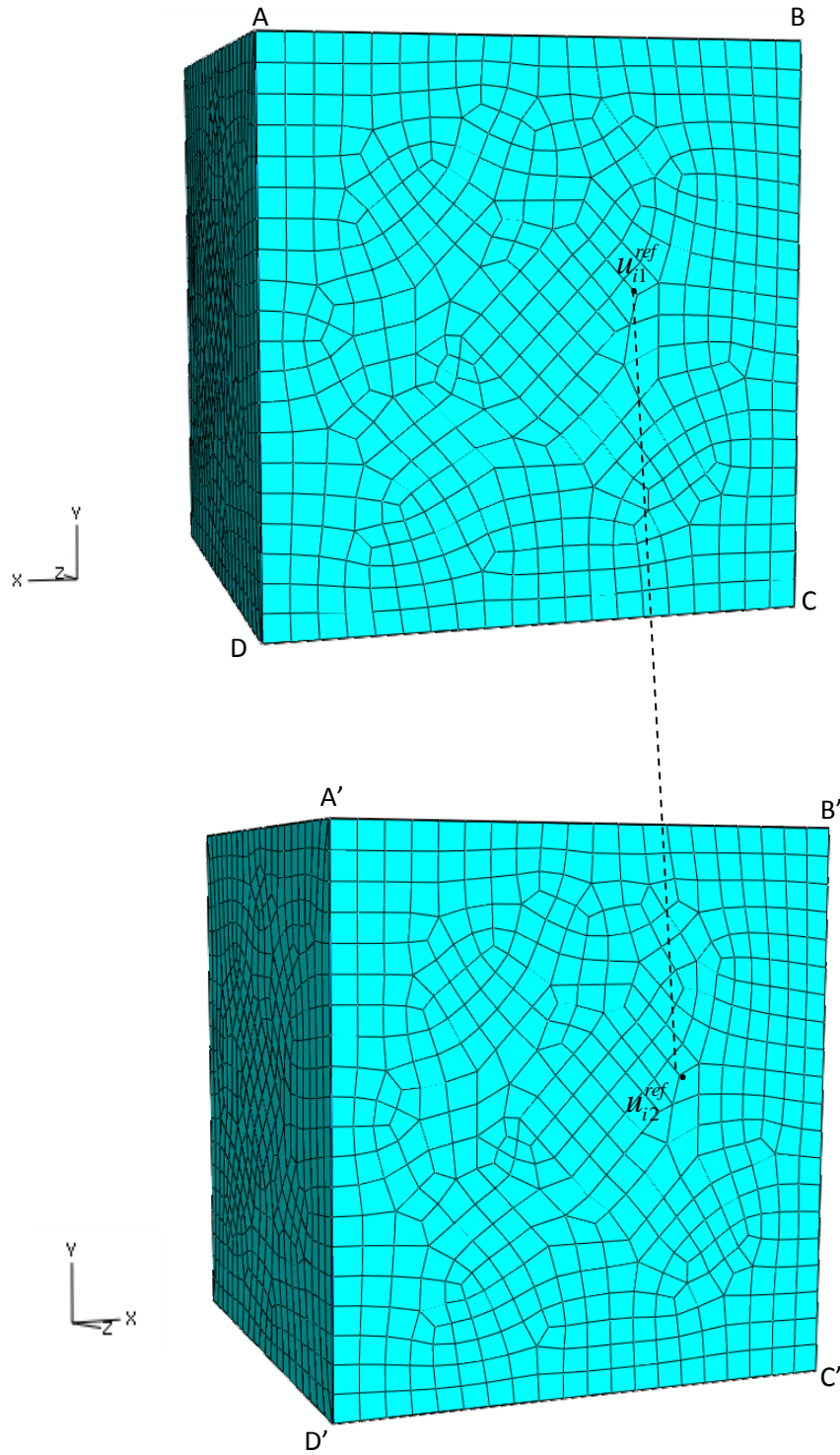


Figure 5.7: Periodic finite element mesh on a pair of opposite faces.



a total of 94887 elements. The initial meshing of the model was done using commercially available HYPERMESH® software and the model was then imported into ABAQUS® for carrying out the finite element simulations. In ABAQUS®, the periodic boundary conditions were implemented by using the EQUATION option, where equations were formed to tie equivalent points on the opposite faces of the cell. All the remaining parameters of the analysis are the same as that was used previously. Due to the number of constraints generated by the use of equations to implement the periodic boundary conditions the computational time increased drastically and hence this analysis was carried out for applied strain of approximately 20%.

In Fig. 5.8 the results from this finite element simulation and that obtained in the previous section (displacement boundary condition) are plotted for comparison. It can be seen that periodic boundary conditions capture the experimental behavior more closely when compared to the more restrictive zero outward displacement boundary conditions. This comparison plot also shows that for applied strains greater than 5% there is a notable difference between the responses predicted by the two approaches. The displacement boundary conditions restrain the normal displacements and thus are found to over predict the stress-strain response when compared to the periodic boundary conditions which couple the displacements of matching nodes on each pair of the surface to imitate an infinitely large material bulk.

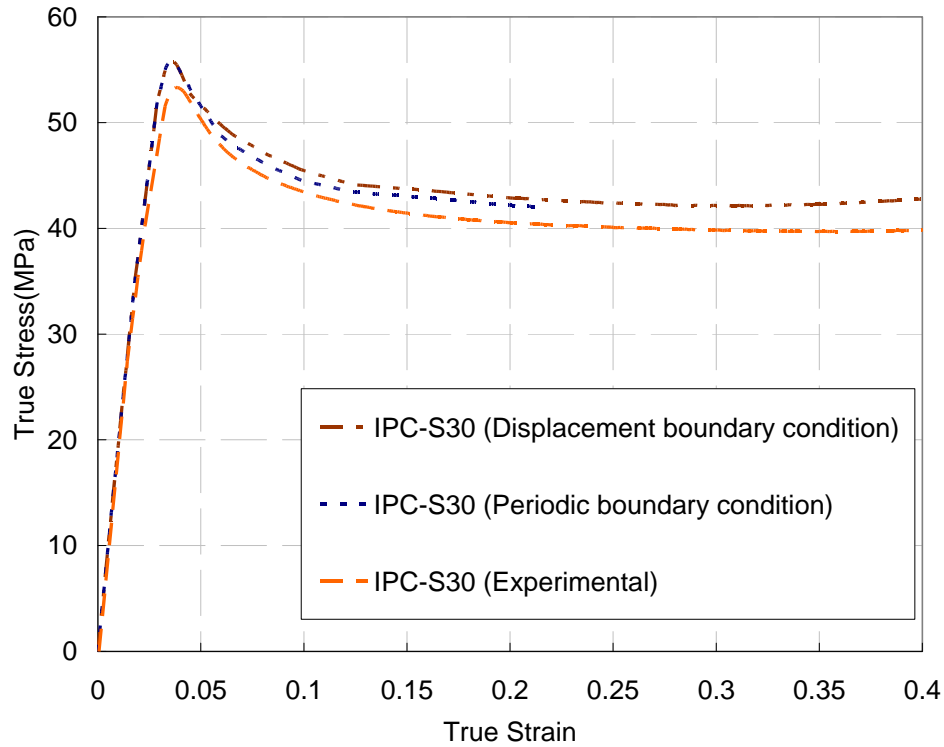


Figure 5.8: Effect of boundary condition on stress-strain response of IPC

### 5.3 Finite element modeling of syntactic foam-filled honeycombs

Full scale finite element simulations were carried out to study the in-plane failure characteristics of the syntactic foam filled composites and also to compare results with those obtained from experiments. In order to simulate the compression response of the composite the finite element model was developed under plane strain assumptions and had the same specimen dimensions (25 mm x 25 mm x 16 mm) as the ones used in experiments. The structure of composite was modeled in MATLAB® and was subsequently imported into ABAQUS® for carrying out finite element analysis.

### 5.3.1 FEA model description

The geometry for the finite element model of syntactic foam-filled honeycomb composite was generated using an array of hexagonal cells in MATLAB®. First, an array of 8 x 8 hexagonal cells was generated such that each cell had a cell size of 3.25 mm (or, 1/8<sup>th</sup> of an inch) (Fig.5.9). Next, the aluminum honeycomb structure was generated such that the area fraction of the aluminum honeycomb was 8% since the relative density of the aluminum honeycomb used in the experimental study was ~8%.

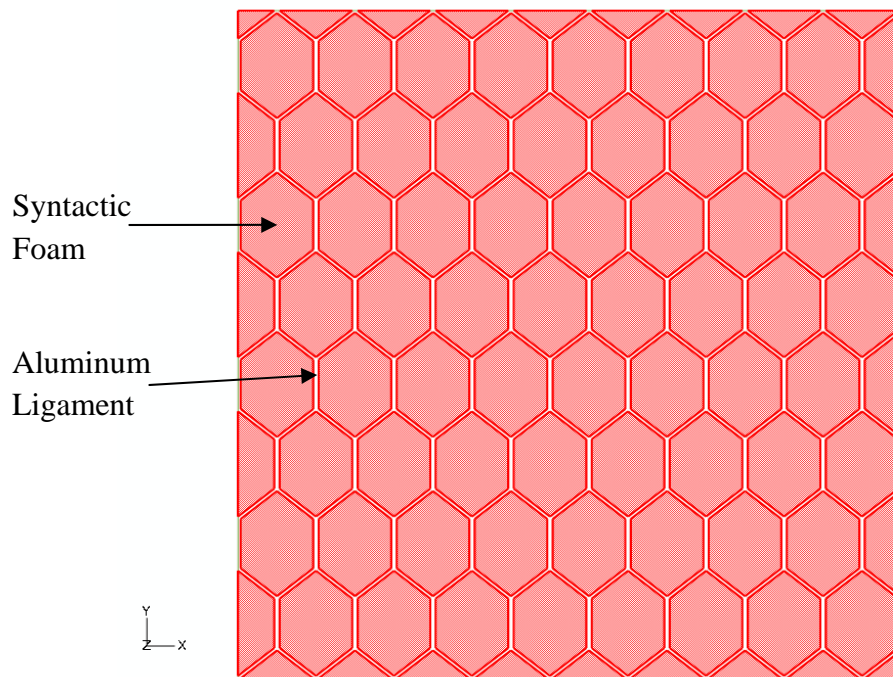


Figure 5.9: Geometry of honeycomb specimen used in analysis

The honeycomb sheets used in this work were manufactured using an expansion process and thus each cell had the two vertical walls of double the thickness when compared to the other (inclined) sides of the cell. Therefore, a regular honeycomb structure with

double wall thickness in vertical direction was generated to represent the aluminum honeycomb structure. The relative density of the honeycombs was estimated by dividing the area of the cell walls by the total area of a unit cell. The material inside these cells was assumed to be filled with syntactic foam, thus resulting in the structure of the syntactic foam-filled honeycomb composite.

The honeycomb sheet used for the preparation of foam-filled honeycomb composite (Al 5052-H39) is the same as that was experimentally tested and numerically modeled by Papka et al [38]. These authors have developed finite element models to simulate the crushing of this honeycomb sheet by assuming the stress-strain response of aluminum as a bilinear function with a post-yield modulus of  $E/100$ ,  $E$  being the elastic modulus. Accordingly, in the current study the elastic-plastic behavior of aluminum was modeled in same way as described in Ref. [38]. The measured stress-strain responses for syntactic foams containing different volume fractions of microballoons were used to model the material surrounding the aluminum ligaments. The material model described in Section 5.1 was once again used to model the plastic behavior of syntactic foam. The platen of the testing machine was modeled as a rigid surface by specifying its value of elastic modulus to be approximately 100 times that of aluminum. MATLAB® was used to construct the model which was then imported into ABAQUS® finite element software for analysis purposes. Adaptive automatic stabilization scheme available in ABAQUS/Standard can be used to solve unstable static problems involving geometric or material nonlinearity and thus is also used in the current analysis [39]. This scheme is used for stabilizing unstable quasi-static problems through the automatic addition of

volume-proportional damping to the model. In the current work the default value of the dissipated energy fraction ( $2 \times 10^{-4}$ ) was used for the calculation of the damping factor. In the adaptive automatic stabilization scheme the value of the damping factor can vary spatially and with time and depends on the ratio of energy dissipated by viscous damping to the total strain energy of the model. It has a default value of 0.05 and was used in the current work. A contact pair was defined between the top and bottom surfaces of the specimen that were in contact with the platen surface. The platen surface was chosen as the master surface and the specimen surface that was in contact with the platen surface was chosen as the slave surface. The normal behavior of these contact pairs was modeled using a hard contact relationship which minimizes the penetration of the slave surface into the master surface. In this relationship, any contact pressure can be transmitted between the surfaces when they are in contact and the surfaces separate if the contact pressure reduces to zero. The tangential behavior was assumed to be frictionless. Figure 5.10 shows boundary conditions used in the model. In order to simulate the experiments uniaxial compression was carried out carried out by applying uniform vertical displacements to the top platen, as shown in Fig. 5.10. The applied strain was increased from 0 to 40%.

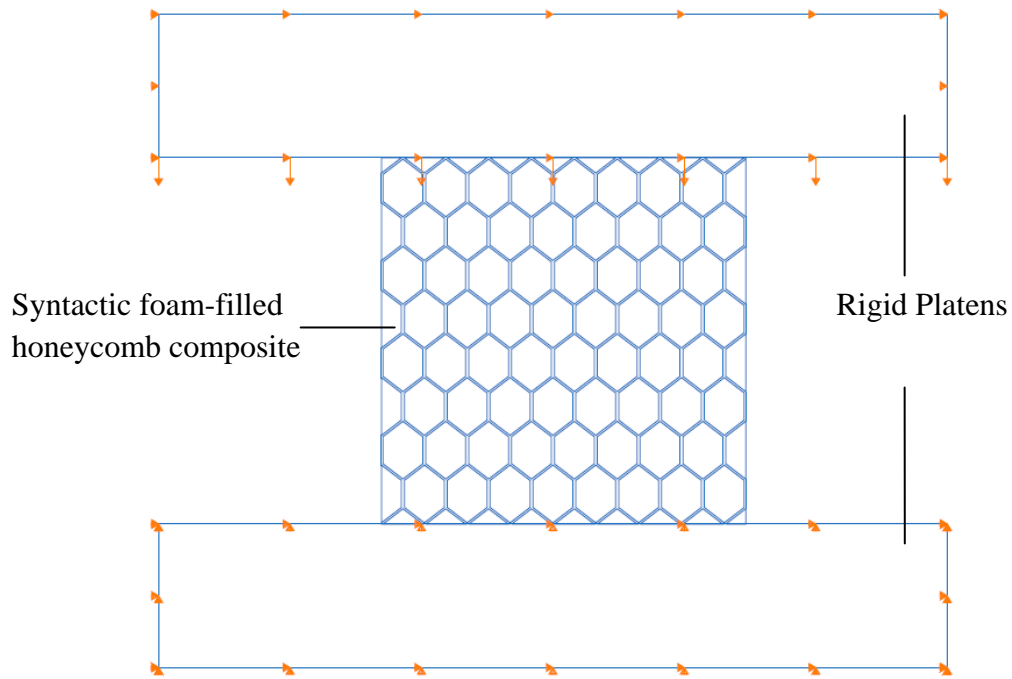


Figure 5.10: Loads and boundary conditions used during the analysis

A representative finite element mesh used in the simulations is shown in Fig. 5.11. A mesh convergence study was carried out to ensure the mesh refinement in the composite structure. The number of elements used in the finite element model for this study was varied (11140, 14354 and 16760 elements) and it was found that the model with 16760 elements successfully captured the overall behavior of the composite. The model was discretized using generalized plane strain elements and a typical finite element mesh consisted of 16,760 linear interpolation quadrilateral and triangular elements.

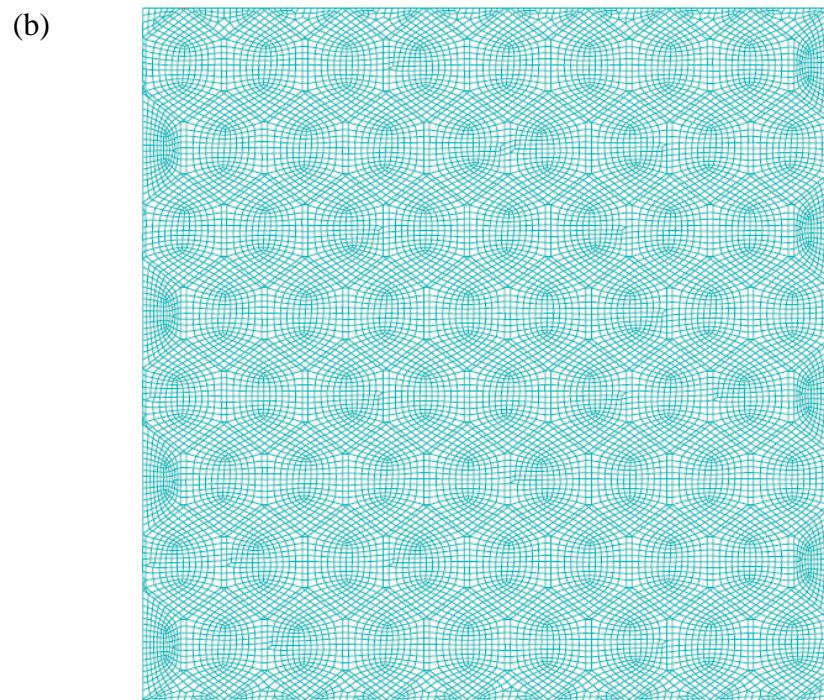
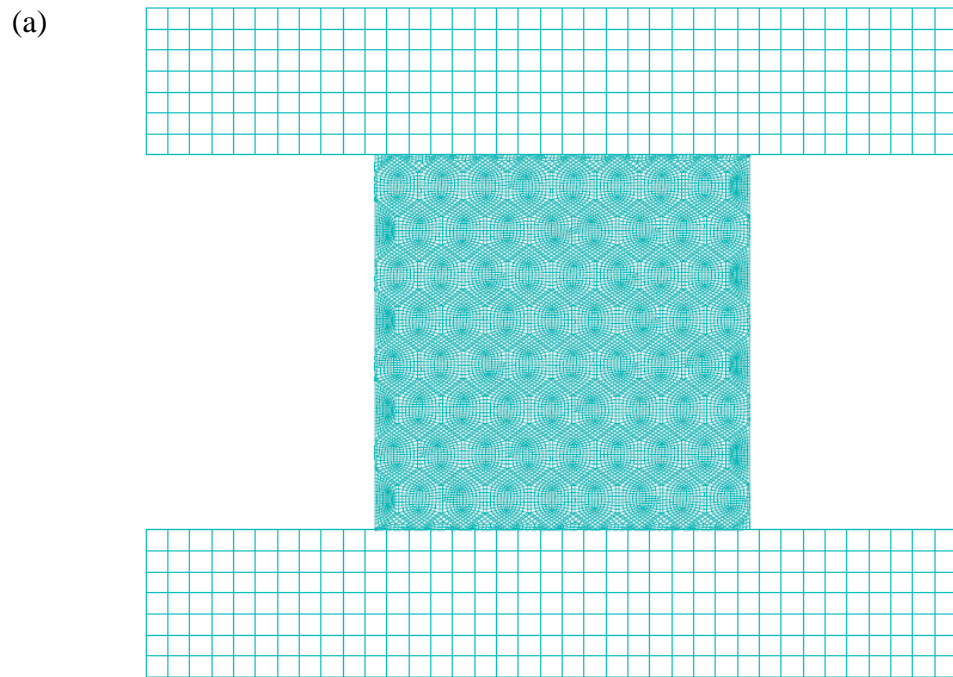


Figure 5.11: (a) Finite element mesh of the model (b) enlarged view showing finite element mesh of the composite

### 5.3.2 Results

Figure 5.12 shows the deformation stages of a foam-filled honeycomb composite with 30% volume fraction of microballoons which is compressed along the L-direction and the stress-strain response of this composite is shown in Fig. 5.13(b). Uniform vertical displacement is applied to the top platen while the bottom one is fixed. This results in crushing of the sample placed in between the platens. At relatively low strains uniform deformation of the sample can be seen. As strain increases the deformations start to localize in a narrow band of cells in a dominant shear mode at  $\sim 45^\circ$  to the loading direction, as in Fig. 5.12(c). This mode of deformation then leads to the formation of multiple shear bands that act as failure planes. At applied strain of  $\sim 15\%$  these shear bands coalesce and deformation starts spreading to the neighboring cells and the specimen begins to deform in an unsymmetric manner as in Fig. 5.12(d). The deformation process also seems to be highly localized, as observed in experiments. By the end of Fig. 5.12(e) the deformation propagates to the neighboring cells with much greater compressive deformation of the material near the top half as compared to the bottom half of the specimen. This mode of failure then continues with certain cells heavily deforming in an unsymmetric manner while some cells remain relatively undeformed. The final configuration which is at an applied strain of 40% clearly reveals shear bands that have dominated the deformation process in syntactic foam-filled aluminum honeycomb composite.



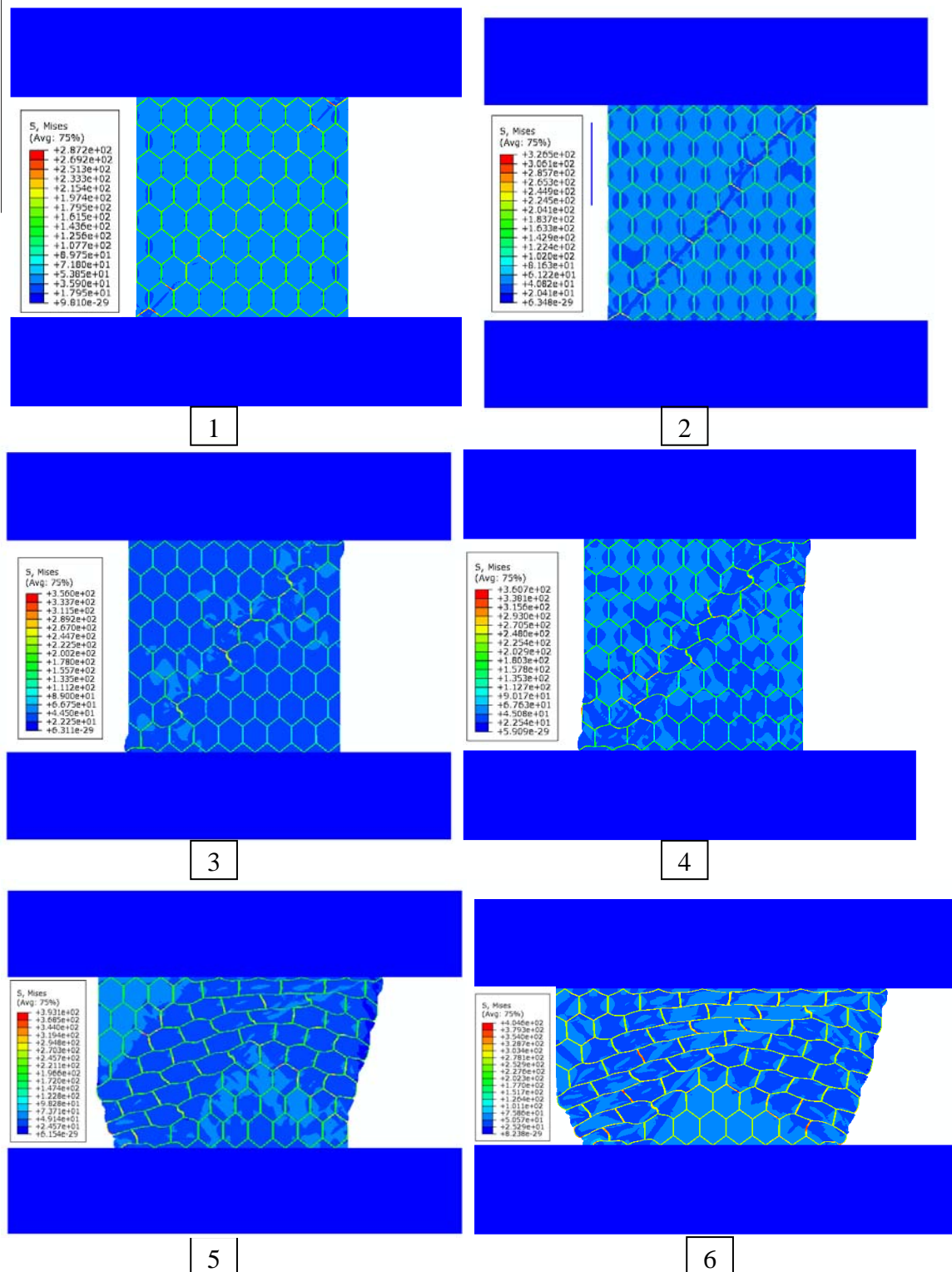
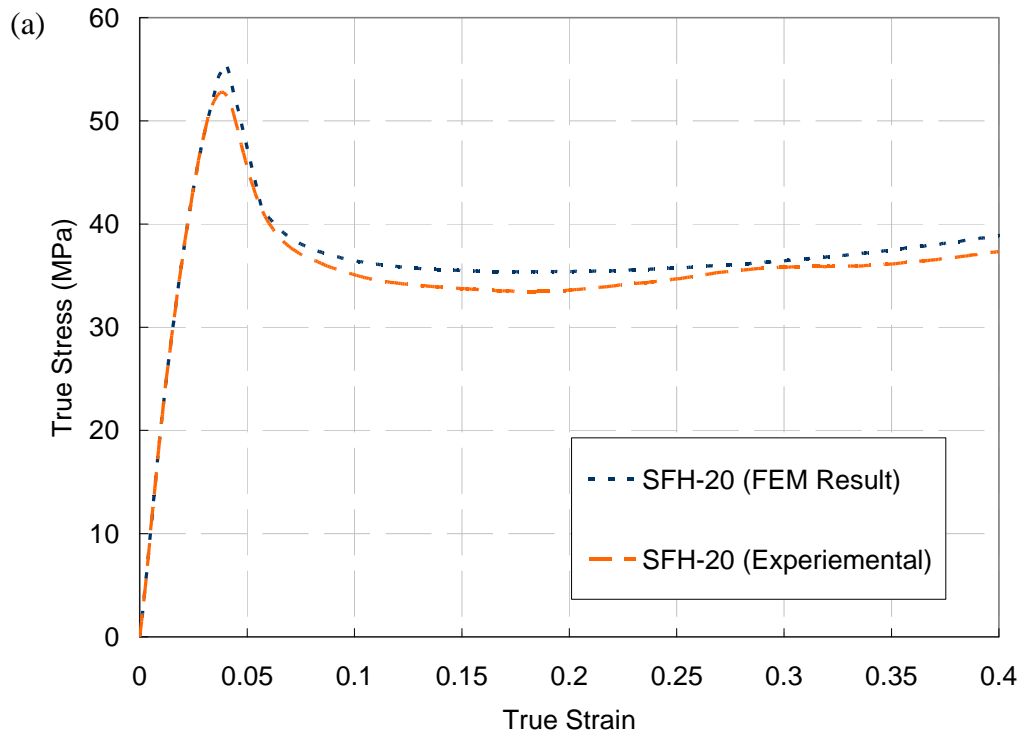


Figure 5.12: Sequence of deformation at applied strain of (1): 1.8%, (2):5.4%, (3): 8.2%, (4): 14.6%, (5):32.8%, (6)40%

The deviations between the sequence of events observed during experiments and as seen in the numerical simulation can be attributed to manufacturing imperfections, and anomalies in cell sizes of real sample. That is, the honeycomb with a smaller cell size will have an additional amount of adhesive that will affect the mechanical response. The expansion process through which the honeycombs are manufactured introduces changes in material properties and also leaves behind residual stresses as identified in Ref. [40]. The idealized cell geometry assumed in the finite element model does not actually exist in the honeycomb structure where the cell geometry and the cell size differ on a microscopic level. As the sequence of collapse largely depends on the cell geometry and is one of the main reasons for the observed deviations.



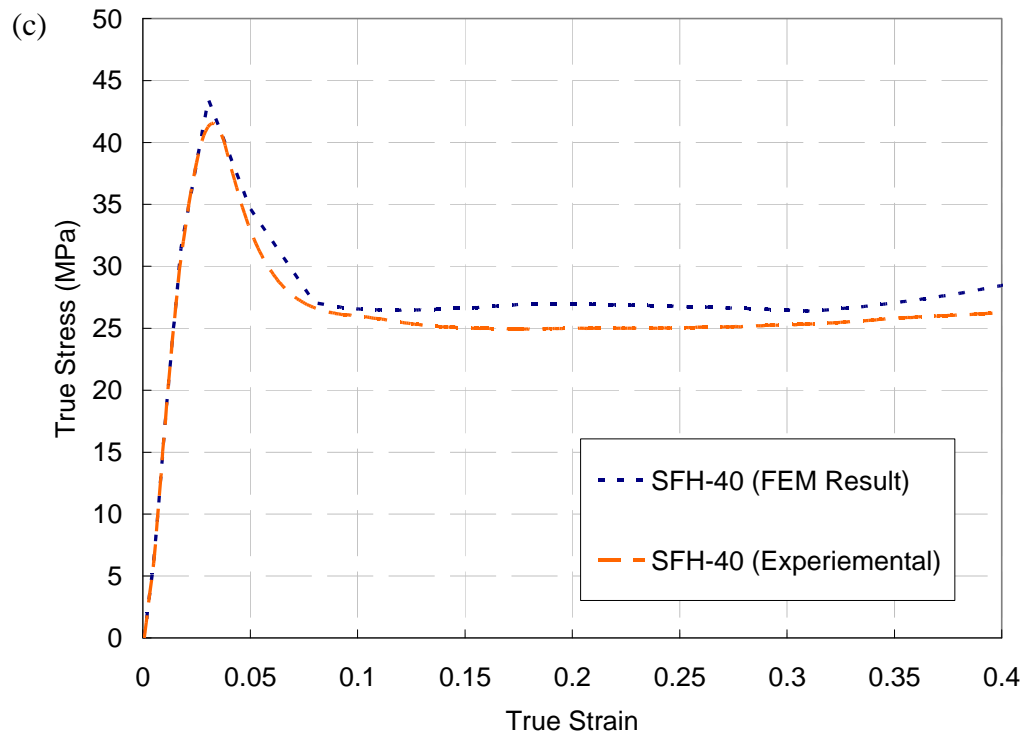
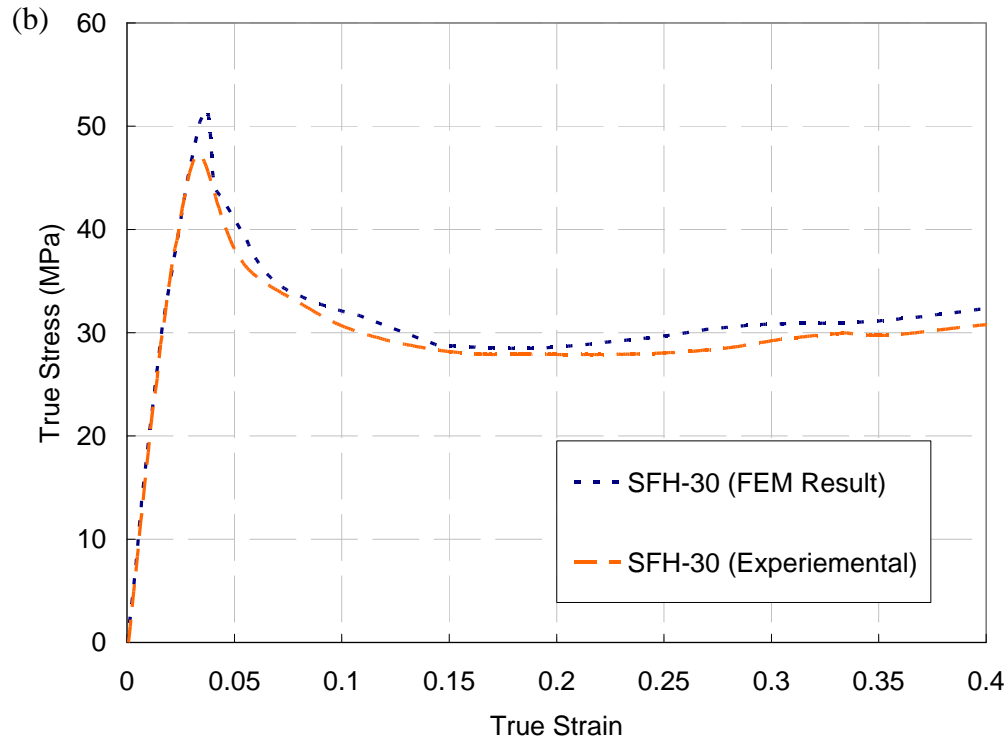


Figure 5.13: Comparison of numerical and experimental results for Syntactic foam-filled honeycomb composites (a) 20% volume fraction, (b) 30% volume fraction, (c) 40% volume fraction of microballoons

In Fig. 5.13 the finite element results for syntactic foam-filled honeycomb composite with 20%, 30% and 40% volume fraction of microballoons are compared with the experimentally obtained true stress-strain curves. From the graphs it is evident that the computational model captures the overall stress-strain response of the composite quite well even though there are some differences in the sequence of deformation between that observed during experiments and that predicted by finite element analysis. The values of elastic modulus and plateau stress predicted by the finite element model are found to be in good agreement with that from experiments. From Fig. 5.13 it can be clearly seen that the numerical model successfully captures the stress-strain response of the syntactic foam-filled honeycomb composite having varying volume fraction of microballoons. The deviations between the two responses especially in the post yield regime can be attributed to the reasons as discussed above.

## **CHAPTER 6**

### **MICROMECHANICS BASED ELASTIC MODULUS PREDICTION**

In this chapter, the feasibility of predicting the elastic modulus of syntactic foams and syntactic foam-filled composites is discussed. This is done by evaluating measurements relative to the micromechanics models reported in the literature. Several models have been developed to predict the elastic properties of composites based on known properties of the constituents, typically the matrix and the filler. The mixing laws used to estimate elastic moduli of such composites can be grouped into two categories. In the first category, the composite structure is an assembly of discontinuous and random inclusions which cannot be modeled using a unit cell based analysis. In the second category, the composite structure is usually modeled by a repeating geometry and the rule-of-mixtures based on isostress and isostrain approximations.

Effective mechanical properties of two phase particulate composites have been under investigation for many years and several micromechanical models have been developed to predict the elastic properties [41-44]. These models are based on the assumption that tractions and displacements are continuous (or the individual phases are assumed to be ideally bonded) at the interface between matrix and filler phases and the composite is assumed to be homogenous and isotropic on a macroscopic scale.

In the current work, a few models are used to predict the effective elastic properties of syntactic foams, IPC foams and foam-filled honeycombs and compare them with measurements.

## 6.1 Micromechanics model for elastic modulus prediction

In this section some of the micromechanics models that are used for estimating the elastic modulus of foam-filled composites are reviewed.

### 6.1.1 Hashin-Shtrikman model

This model is based on the minimum energy principle to predict the upper and lower bounds of elastic modulus of a composite [41]. For a two phase mixture comprising of matrix and spherical fillers, the upper bounds of bulk ( $K$ ) and shear moduli ( $G$ ) can be represented as,

$$K_c^{UB} = K_1 + \frac{V_2}{\frac{1}{K_2 - K_1} + \frac{3V_1}{3K_1 + 4G_1}} \quad (6.1)$$

$$G_c^{UB} = G_1 + \frac{V_2}{\frac{1}{G_2 - G_1} + \frac{6(K_1 + 2G_1)V_1}{5G_1(3K_1 + 4G_1)}} \quad (6.2)$$

where  $V$  is the volume fraction of the constituents and subscripts 1 and 2 represent the stiff and compliant phases, respectively. The lower bounds of bulk and shear modulus can be calculated by switching the subscripts in the above equations.

The elastic modulus is then computed using the relation,

$$E = \frac{9KG}{3K + G} \quad (6.3)$$

where the upper and lower bulk modulus ( $K$ ) and shear modulus ( $G$ ) values are substituted to get the respective bounds on the elastic modulus.

### 6.1.2 Tuchinskii model

This model can be used to predict the upper and lower bounds of the elastic modulus for the composite with an interpenetrating skeletal structure [42]. In this model the composite is modeled by a repeating hollow cubic skeletal structure (ligaments aligned along the edges of the cube) of height ( $H$ ), which represents the first phase. The cavity of this skeleton is filled with a second cubic phase of height ( $h$ ) as shown in fig.6.1. The upper and lower bounds on the elastic modulus of the composite are given by equations,

$$E_c^{UB} = E_1 \left[ \frac{1-c}{(1-c^2) + \left(\frac{E_2}{E_1}\right)c^2} + \frac{c}{(1-c)^2 + \left(\frac{E_2}{E_1}\right)(2-c)c} \right]^{-1} \quad (6.4)$$

$$E_c^{LB} = E_1 \left[ (1-c)^2 + \left(\frac{E_2}{E_1}\right)c^2 + \frac{2\left(\frac{E_2}{E_1}\right)c(1-c)}{c + \left(\frac{E_2}{E_1}\right)(1-c)} \right] \quad (6.5)$$

$$f_2 = (3 - 2c)c^2 \quad (6.6)$$

where  $E_c^{UB}$  and  $E_c^{LB}$  are the upper and lower bounds for elastic modulus of the composite, respectively,  $E_i$  is the Young's modulus of the  $i^{th}$  phase,  $f_2$  is the volume fraction of phase 2 and  $c$  is a geometric parameter ( $c = h/H$ ). The value of  $c$  in Eqs. (6.4) and (6.5) are obtained by solving Eq. (6.6).

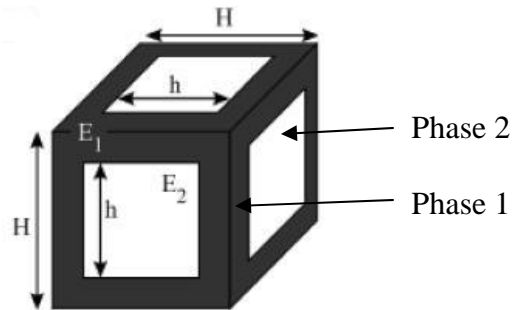


Figure 6.1: Schematic representation of phase geometry for a Tuchinskii model [13]

### 6.1.3 Ravichandran Model

This model considers a continuous matrix phase surrounded by a periodic arrangement of uniformly distributed cubic inclusions. The repeating cell structure is characterized by inclusion size ( $v$ ) and the size of the matrix material ( $w$ ) as shown in fig.6.2. Here a unit cell based description of the material microstructure along with isostress and isostrain configurations (rule-of-mixtures) is used to derive expressions for the upper and lower bounds of elastic modulus of a two phase composite [43]. The two bounds of elastic moduli are given by,



$$E_c^U = \frac{[E_p E_m + E_m^2(1+c)^2 - E_m^2](1+c)}{(E_p - E_m)c + E_m(1+c)^3} \quad (6.7)$$

$$E_c^L = \frac{(cE_p E_m + E_m^2)(1+c)^2 - E_m^2 + E_p E_m}{(cE_p + E_m)(1+c)^2} \quad (6.8)$$

where  $E_c^U$  and  $E_c^L$  are the upper and lower bounds of elastic modulus of the composite, respectively. In the above,  $E_p$  and  $E_m$  denote elastic modulus of the inclusion and matrix phases and  $c$  is a non-dimensional parameter given by,

$$c = \left( \frac{1}{V_p} \right)^{1/3} - 1 \quad (6.9)$$

where  $V_p$  is the volume fraction of the inclusion phase.

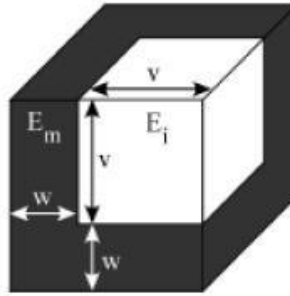


Figure 6.2: Schematic representation of cell geometry for a Ravichandran model [13]

## 6.2 Modulus prediction for syntactic foams

The microballoons used in this work have an extremely small wall thickness (relative to the diameter) and hence the mixture can be modeled reasonably well as a porous material. In order to check the feasibility of predicting the elastic modulus of syntactic foam by modeling the mixture as a porous material, the results from the experiments were compared with those published in ref.[45] where a homogenization technique is used to take into account the presence of void space inside the filler and wall thickness of the filler particles. In Fig. 6.3 the experimental data from the current study and the ones tabulated in ref.[45] are used to plot normalized Young's modulus of the mixture as a function of microballoon volume fraction.

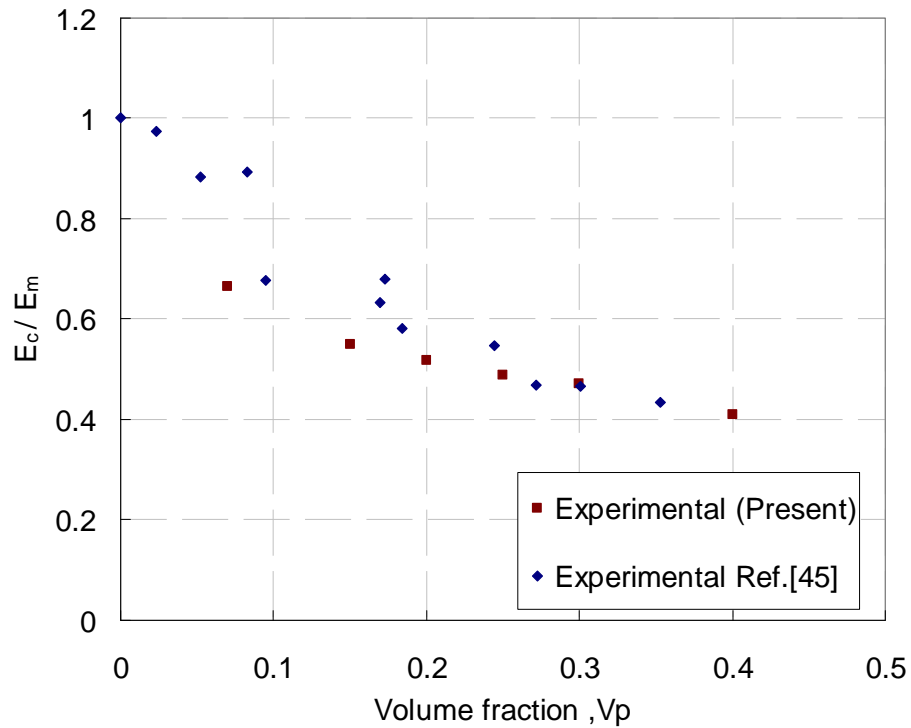


Figure 6.3: Variation of measured young's moduli with microballoon volume fraction

The Young's modulus at a particular volume fraction is normalized by the ones for the neat matrix material. (The normalization was carried out because the matrix material used in Ref. [45] is polyester whereas the current work employs epoxy.) From the figure it can be seen that both sets of data have similar trends and the values are also found to be in good agreement with each other. A high degree of accuracy can be noted between the values predicted using the theoretical models and experimental measurements. Based on the above evidence, the role of microballoon wall in very low-density (or, very small microballoon wall thickness) mixtures in question is indeed negligible.

In order to predict the elastic properties of syntactic foams by approximating the mixture as a porous material, the values of bulk modulus and shear modulus of the filler phase are set equal to zero in equations used for determining the upper and lower bounds of elastic modulus. The comparison between micromechanics prediction and experimental measurements are shown in Fig. 6.4. From the plots, it is evident that the Hashin-Shtrikman and Ravichandran bounds seem to agree modestly with the measured modulus values at higher volume fractions but deviate significantly, by as much as 39%, at lower volume fractions. Further, the lower bounds of both these models are found to over predict the elastic modulus consistently. Interestingly, the Tuliniskii model which describes a co-continuous (interpenetrating) phase microstructure provides a better estimate of the elastic modulus of the syntactic foam over the entire range of compositions investigated. The lower bound of this model is found to be in close agreement with measured modulus values over the entire range of compositions.

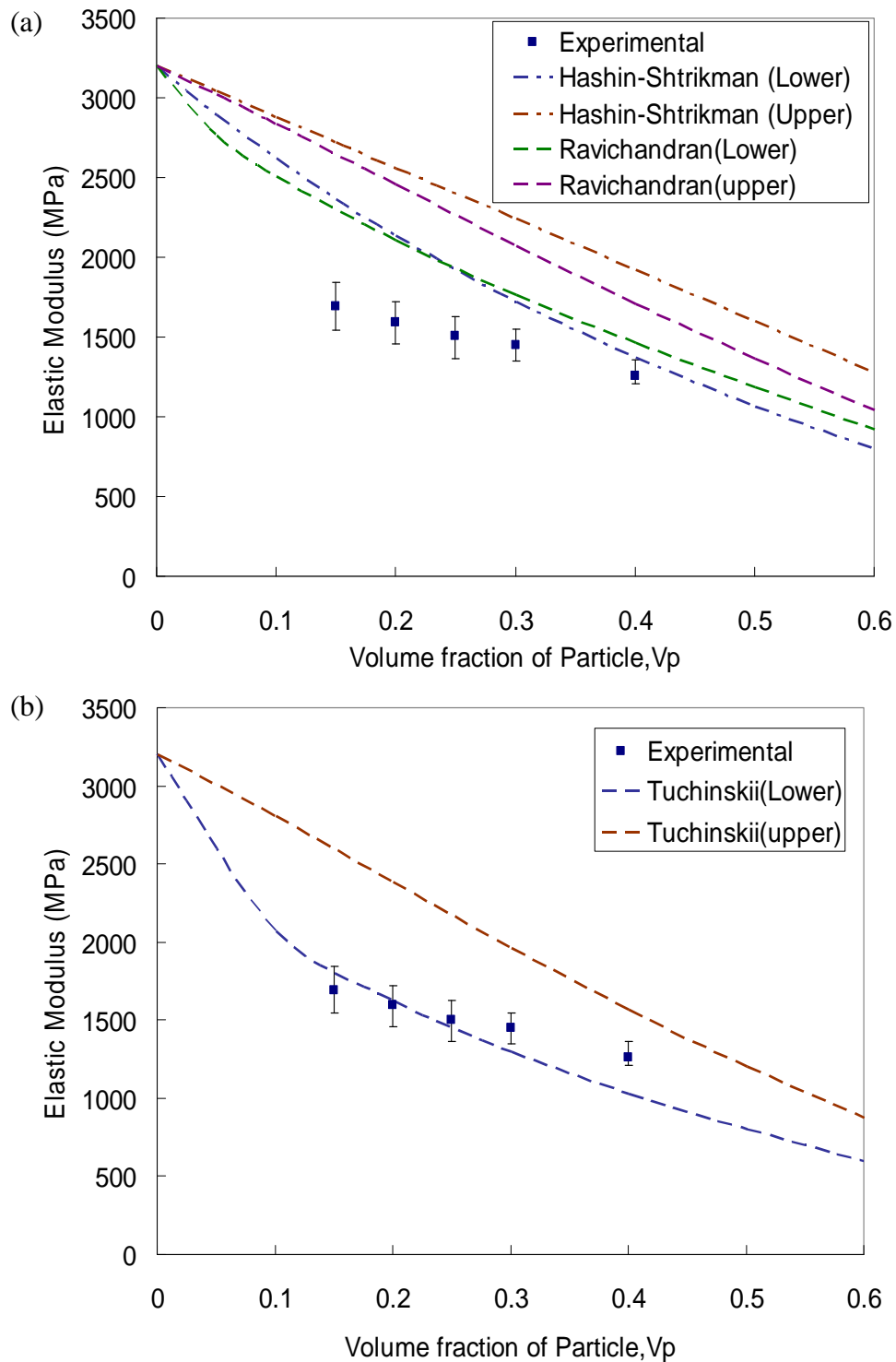


Figure 6.4: Comparison between predicted and measured values of elastic modulus for syntactic foams. (a) Hashin-Shtrikman and Ravichandran bounds, (b) Tughiniskii bounds

The maximum difference between the experimentally measured values and that predicted using the lower bounds of this model was ~14% (for the case of 40% volume fraction of microballoons in the syntactic foam).

### **6.3 Elastic modulus prediction for IPC**

The values of elastic modulus for IPC foam predicted using the above three models by considering IPC foam as a two phase composite are listed in Table 6.1. In doing so, the syntactic foam phase was considered as one of the phases namely the matrix and aluminum as the other. Evidently, experimental results are in close agreement with the lower bound predictions from the Hashin-Shtrikman model. The lower bounds of Ravichandran and Tuchinskii models, however, seem to over predict the elastic characteristic. From Table 6.1 it can also be noted that the elastic modulus of IPC foam with silane coated aluminum preform lies within the Hashin-Shtrikman bounds, whereas this is not true for the IPC foam with uncoated aluminum preform. (This is likely attributed to the weak interfacial adhesion between the preform and the syntactic foam which easily results in debonds during loading, in turn violating the condition of continuity between the phases used in the model.) The maximum difference between the values predicted by the Hashin-Shtrikman lower bounds and experimentally measured ones for the IPC foam with silane coated aluminum preform is approximately 9%. The upper and lower bounds of the Ravichandran model are found to be influenced by the choice of the ‘matrix’ and ‘inclusion’ phases. By using syntactic foam as the matrix material, the difference between the measurements and prediction is about 35%. (The

choice of aluminum as the matrix phase results in upper and lower bounds that overestimate the modulus with deviations of over two fold and should obviously be avoided.) In this context, it is worth noting that the value of elastic modulus of the composite predicted using the Hashin-Shtrikman and the Tuchinskii models were found to be consistent irrespective of the choice of the ‘matrix’ and the ‘inclusion’ phases. The Tuchinskii model which considers a two phase interpenetrating microstructure also over predicts the elastic modulus values. The possible reason for this could be the assumption of a relatively simple cubic geometry adopted by this model, quite different from the complex 3-D structure that exists in the present case. Similar observations regarding such differences have also been made by Moon et al., [13].

Volume fraction of microball-oon in syntactic foam(%)	Measured elastic modulus of IPC foam (MPa)		Ravichandran model		Hashin – Shtrikman model		Tuchinskii model	
	Uncoated aluminum preform	Silane coated aluminum preform	Lower bound (MPa)	Upper bound (MPa)	Lower bound (MPa)	Upper bound (MPa)	Lower bound (MPa)	Upper bound (MPa)
20	1821	2123	2741	3740	1943	5254	3721	4248
30	1573	1852	2505	3397	1765	5105	3569	4086
40	1442	1702	2200	2960	1539	4917	3377	3879

Table 6.1: Comparison between measured and predicted values of elastic modulus for the IPC foam based on different micromechanics models

They also have found the modulus ratio ( $E_1/E_2$ ) of the two phases to have a significant effect on the accuracy of elastic modulus prediction by various theoretical models. In their work, these authors have examined the mechanical properties of alumina-epoxy IPC having a modulus ratio ( $E_1/E_2$ ) of  $\sim 114$ . They have found significant deviations between measured values of Young's modulus and those predicted using Ravichandran and Tuchinskii models. In the current study, the modulus ratio ( $E_1/E_2$ ) being relatively high (between 43 and 54 depending on the volume fraction of microballoons in the syntactic foam) a close agreement between measured Young's moduli and those predicted using the theoretical models was not obtained. Only the Hashin-Shtrikman model predicted the values with a reasonably good accuracy.

#### **6.4 Elastic modulus prediction for syntactic foam-filled honeycombs**

The values of elastic modulus of the syntactic foam-filled aluminum honeycomb composite computed using different models described earlier are reported in Table 6.2. The values of elastic modulus predicted by these models are found to have similar trend as that reported in Table 6.1 for IPC composite. That is, even in this case the experimental results are found to be in close agreement with the lower bound predictions from the Hashin-Shtrikman model and lie between the upper and lower bounds of this model. The Ravichandran model is found to over predict the experimental results but significant difference is seen between the lower bound predictions of the Tuchinskii model and the experimental results. The inability of these models to predict accurate results can be attributed to the reasons discussed in the earlier section and also due to the

following. Ravichandran model considers a continuous matrix phase surrounded by a periodic arrangement of uniformly distributed cubic inclusions which is clearly not the case here and also the Tuchinskii model is used to represent an interpenetrating composite and hence is found to over predict the values significantly. The modulus ratio ( $E_1/E_2$ ) of the two phases has a significant effect on the accuracy of elastic modulus prediction by various theoretical models as discussed in the previous section and is one of the main reasons.

Volume fraction of microball-oon in syntactic foam(%)	Measured elastic modulus of filled honeycombs (MPa)	Ravichandran model		Hashin – Shtrikman model		Tuchinskii model	
		Lower bound (MPa)	Upper bound (MPa)	Lower bound (MPa)	Upper bound (MPa)	Lower bound (MPa)	Upper bound (MPa)
20	2027	2583	3552	1868	4538	3182	3563
30	1989	2361	3225	1697	4390	3032	3402
40	1695	2073	2810	1479	4201	2841	3197

Table 6.2: Comparison between measured and predicted values of elastic modulus for the syntactic foam-filled honeycomb composite based on different micromechanics models



## **CHAPTER 7**

### **CONCLUSIONS**

#### **7.1 Conclusions**

In this work the feasibility of processing a lightweight interpenetrating aluminum-syntactic foam composites and syntactic foam-filled honeycomb composites have been demonstrated. The interpenetrating phase composite (IPC) foams and the foam-filled honeycomb composites were produced by infiltrating uncured epoxy-based syntactic foam into an open-cell aluminum preform and into an aluminum honeycomb structure, respectively. Different varieties of IPC and foam-filled honeycomb composites were prepared by varying the volume fraction of microballoons from 20%-40% in the syntactic foam. Two variants of IPC foams were also produced by using aluminum preform in 'as-recieved' condition and by coating it with silane to increase adhesion between the metal scaffold and polymer foam.

The IPC foam samples and syntactic foam-filled honeycomb composites were mechanically tested in uniaxial compression and responses were examined relative to the conventional syntactic foams with the same volume fraction of microballoons. The syntactic foam-filled composites had stress-strain responses similar to the ones for

conventional structural foams. An initial linear elastic response was followed by a noticeable softening caused by the onset of collapse of microballoons leading to a plateau stress and compaction behaviors at the end. The IPC foam samples in general and the silane coated ones in particular showed improvement in elastic modulus, compression strength and plateau stress values by 28-35%, 20-25% and 37-42% respectively, when compared to the conventional syntactic foams. On the other hand, the foam-filled honeycomb composites had approximately 26-31% and 36-39% increase in the elastic modulus and plateau stress, respectively, when the composites were compressed along the W-direction. More importantly, the IPC foam samples had 15-20 MPa increase in the plateau stress and this value was found to be in the range of 4-8 MPa for the foam-filled honeycomb samples relative to the corresponding syntactic foam samples. Interestingly, in case of IPC foam this increase in the plateau stress was found to be significantly higher than the plateau stress of ~2.5 MPa for an unfilled preform. This was attributed to the existence of synergistic mechanical constraint between the syntactic foam and aluminum preform of the IPC foam. This also produced a rather pronounced improvement in the energy absorption in IPC foam relative to the corresponding syntactic foam samples. The Silane treated IPC samples consistently showed ~50% higher energy absorption per unit volume and 33% higher energy absorption per unit mass relative to the corresponding syntactic foam. When preforms were untreated, the percentage increase in energy absorption was found to be somewhat lower. However, the maximum increase in the energy absorption per unit volume and energy absorption per unit mass for syntactic foam-filled honeycomb composite was found to be 48% and 26%, respectively,

when compressed in the W direction. The results also showed that the syntactic foam-filled honeycomb had isotropic linear elastic response for L and W directions and also significant deviations between the two responses was seen in the post yield region.

Finite element models were also developed to capture the major experimental observations and the overall compressive response of foam-filled composites. A Kelvin cell based 3-D elasto-plastic finite element model was developed by adopting unit cell analysis approach to examine the feasibility of predicting both the elastic and plastic characteristics of the IPC foam. This analysis was aimed at validating the case of the IPC foam with silane treated preform where adhesion between the metal ligaments and polymer foam was relatively strong. Two different types of boundary conditions namely periodic displacement boundary conditions and outward displacement constraint were employed in the unit-cell simulations. The numerical model based on measured elasto-plastic compression response of the corresponding syntactic foam and stress-strain response of bulk aluminum was found to successfully capture the overall IPC foam behavior well up to 40% imposed strain. Next, finite element method was also used to simulate experiments performed on foam-filled honeycomb. The stress-strain response of syntactic foam-filled honeycomb composite was predicted by developing a full-scale 8 x 8 array finite element model representing the actual experimentally studied specimens. The numerical model had the same honeycomb relative density and cell size as the one used in experiments. The simulations were fully validated by comparing the results with the experimentally obtained data for L-direction and were also subsequently used to explain the in-plane mechanical behavior of foam-filled honeycomb composites. The

computational model was found to successfully capture the overall stress-strain response of the composite even though there were some differences in the sequence of deformation.

Comparison of elastic modulus of syntactic foam and syntactic foam-filled composites relative to a few micromechanics models was also attempted. Hashin-Shtrikman and Ravichandran bounds were found to agree only modestly with the measured elastic modulus values of syntactic foams the lower bounds of both these models were found to over predict the elastic modulus of syntactic foam consistently. The Tuchinskii model was found to provide a better estimate of the elastic modulus of syntactic foams over the entire composition range that was investigated. The silane coated IPC foam measurements agreed quite well with the lower bound Hashin-Shtrikman two-phase model when syntactic foam and aluminum ligaments are considered as the two constituents. The same measurements, on the other hand, fell below the lower bound predictions of both Tuchinskii' and Ravichandran models. The elastic modulus measurements for IPC foam made with uncoated preform however, were found to be significantly lower than the lower bound predictions of all the three models in view of weak adhesion between the metal and polymer phases leading to premature micro scale debond formations during loading. The micromechanics predictions for foam-filled honeycomb composites showed the experimental results to be in close agreement with the lower bound predictions from the Hashin-Shtrikman model and the experimental data was between the upper and lower bounds of this model. The Ravichandran model was found to over predict the experimental results and significant differences were seen

between the lower bound predictions of the Tuchinskii model and the experimental results.

## **7.2 Future work**

This work focused primarily on understanding the failure behavior of the interpenetrating aluminum syntactic foam composites and syntactic foam-filled honeycomb composites under quasi static loading conditions. The experimental results showed the IPC composite to have enhanced compression response and hence improved energy absorption characteristics when compared to the corresponding syntactic foam samples. These lightweight materials have the potential to be used in automotive, packaging, military and armored vehicle because of its excellent energy absorption characteristics. Accordingly, it would be interesting to examine the deformation behavior and failure characteristics of this material system under dynamic compression. The deformation behavior generally tends to have a wide variation between static and high strain-rate conditions. Since engineering structures often undergo a combined tensile/compression loading, it will be valuable to study the tensile and flexural properties of this material system. Foams and honeycombs are also commonly used as core materials in sandwich construction and hence the possibility of using the syntactic foam-filled composites could also be explored.

Additional work on examining variations to cell structures of both IPC and foam-filled honeycombs needs to be explored. Some preliminary effort in this regard using

Voronoi tessellation approach seems to work under 2D frame work. Examining its feasibility in a 3D framework using polyhedra should be of interest.

Due to the complexity and computational enormity of 3D elastic-plastic simulation of a full-scale IPC, only a unit-cell based analysis was undertaken in this work. It will be of interest to extend this to full-scale analysis and compare the results with the measurements under static and dynamic loading conditions.

## BIBLIOGRAPHY

1. Gibson, L.J., Ashby, M.F., 2001. Cellular solids: Structure and properties, second ed. Cambridge University Press.
2. Wu, C., Weeks, C., Sun, C., 1995. Improving honeycomb-core sandwich structures for impact resistance. *Journal of advanced materials* 26, 41-47.
3. Vaidya, U., Kamath, M., Mahfuz, H., Jeelani, S., 1998. Low velocity impact response of resin infusion molded foam filled honeycomb sandwich composites. *Journal of Reinforced Plastics and Composites* 17(9), 819-849.
4. Vaidya, U., Ulven, C., Pillay, S., Ricks, H., 2003. Impact Damage of Partially Foam-filled Co-injected Honeycomb Core Sandwich Composites. *Journal of Composite Materials* 37(7), 611-626.
5. Clark, D.R., 1992. Interpenetrating phase composites. *Journal of the American Ceramic Society* 75(4), 739-759.
6. Breslin, M.C., Ringnalda, J., Xu, L., Fuller, M., Seeger, J., Daehn, G.S., Otani, T., Fraser, H.L., 1995. Processing, microstructure and properties of co-continuous alumina-aluminum composites. *Journal of Materials Science and Engineering – A195*, 113-119.
7. Daehn, G.S., Starck, B., Xu, L., Elfishawy, K.F., Ringnalda, J., Fraser, H.L., 1996. Elastic and plastic behavior of a co-continuous alumina/aluminum composite . *Acta Materialia* 44(1), 249-261.
8. Imagawa, A., Qui, T.C., 1995. Structure-property relationship of polymer blends with co-continuous structures prepared by photo-cross-linking .*Macromolecules* 28(24), 8388-8394.
9. Skirl, S., Hoffman, M., Bowman, K., Wiederhorn, S., Rodel, J., 1998. Thermal expansion behavior and microstrain of  $Al_2O_3/Al$  composites with interpenetrating networks . *Acta Materialia* 46(7), 2493-2499.

10. Veenstra, H., Verkooijen, P.C.J., Van lent, B.J.J., Dam, J.V., De boer, A.P., Nijhof, A.P.H.J., 2000. On the mechanical properties of co-continuous polymer blends: Experimental and modeling. *Polymer* 41, 1817-1826.
11. Wegner, L.D., and Gibson, L.J., 2000. The mechanical behavior of interpenetrating phase composites-I: Modeling. *International Journal of Mechanical Sciences* 42, 925-942
12. Etter, T., Kuebler, J., Frey, T., Schulzc, P., Löffler, J.F., Uggowitz, P.J., 2004. Strength and fracture toughness of interpenetrating graphite/aluminium composites produced by the indirect squeeze casting process. *Materials Science and engineering –A386*, 61-67.
13. Moon,R.J.,Tilbrook,M., Hoffman,M., 2005. Al-Al<sub>2</sub>O<sub>3</sub> composites with interpenetrating network structures: Modulus estimation. *J. Am. Ceram. Soc.* 88(3), 666-674.
14. Mayer, H., Papakyriacou, M., 2006. Fatigue behavior of graphite and interpenetrating graphite-aluminum composite up to 10<sup>9</sup> load cycles . *Carbon* 44, 1801-1807.
15. Yu, L., Xiao-lu, G., 2006.Compressive behavior and energy absorption of metal porous polymer composite with interpenetrating network structure. *Transactions of Nonferrous Metals Society of China* 16, s439-s443.
16. Kim, J., Kwon, Y., Lomovsky, O., Korchagin, M., Mali, V., Dudina, D., 2006. A synthetic route for metal--ceramic interpenetrating phase composites. *Materials Letters* 60, 3723-3726.
17. Han, J., Hong, C., Zhang, X., Wang, B., 2005. Thermal shock resistance of TiB<sub>2</sub>--Cu interpenetrating phase composites. *Composites Science and Technology* 65, 1711-1718
18. Del Rio, E., Nash, J., Williams, J., Breslin, M., Daehn, G., 2007. Co-continuous composites for high-temperature applications. *Materials Science & Engineering-A* 463, 115-121.
19. Shutov F.A., 1991.Syntactic polymer foams. In: Klempner D, Frisch KC, editors. *Handbook of polymeric foams and foam technology*. New York: Hanser Publishers.
20. Kirugulige, M. S., Kitey, R., and Tippur, H. V., 2005. Dynamic Fracture Behavior of Model Sandwich Structures with Functionally Graded Core: A Feasibility Study, *Composites Science and Technology*, 65, 1052-1068 .
21. Material Datasheet .ERG Materials and Aerospace Corporation, USA.
22. Material Datasheet .Hexcel Corporation, USA.



23. Wegner, L.D., Gibson, L.J., 2001. The mechanical behaviour of interpenetrating phase composites- III: resin-impregnated porous stainless steel. *International Journal of Mechanical Sciences* 43, 1061–1072.
24. Mattern, A., Huchler, B., Staudenecker, D., Oberacker, R., Nagel, A., Hoffmann, M.J., 2004. Preparation of interpenetrating ceramic–metal composites. *Journal of the European ceramic society* 24, 3399–3408.
25. Saravanan, R.A., Surappa, M.K., 2000. Fabrication and characterisation of pure magnesium-30 vol.% SiC<sub>P</sub> particle composite. *Materials Science and Engineering- A* 276, 108–116.
26. Song, B., Chen, W., Frew, D.J., 2004. Dynamic compressive response and failure behavior of an Epoxy Syntactic foam. *Journal of Composite Materials* 38(11), 915-936.
27. Gupta, N., Kishore, Woldsenbet, E., Sankaran, S., 2001. Studies on Compressive Failure features in Syntactic foam Material. *Journal of Materials Science* 36 (18), 4485-4491.
28. Kim, H.S., Plubrai, P., 2004. Manufacturing and Failure mechanisms of Syntactic foam under compression. *Composites Part A: Applied Science and Manufacturing* 35(9), 1009-1015.
29. Gupta, N., Woldesenbet, E., Kishore., 2002. Compressive Fracture Features of Syntactic Foams – Microscopic Examination. *Journal of Materials Science* 37, 3199–3209.
30. Prakash, O., Bichebois, P., Brechet, Y., Louchet, F., Embury, J., 1996. A note on the deformation behaviour of two-dimensional model cellular structures. *Philosophical Magazine A* 75(3), 739-751.
31. Gong, L., Kyriakides S., Jang, W.Y., 2005. Compressive response of open-cell foams. Part I: Morphology and elastic properties. *International Journal of Solids and Structures* 42, 1355–1379.
32. Gong, L., Kyriakides, S., Triantafyllidis, N., 2005. On the stability of Kelvin cell foams under compressive loads. *Journal of the Mechanics and Physics of Solids* 53, 771–794.
33. Luxner, M.H., Stampfl, J., Pettermann, H.E., 2007. Numerical simulations of 3D open cell structures – influence of structural irregularities on elasto-plasticity and deformation localization . *International Journal of Solids and Structures* 44, 2990–3003.

34. Thomson, W. (Lord Kelvin), 1887. On the division of space with minimal partitioned area. *Philos. Mag.* 24 (5<sup>th</sup> series), 503–514.
35. Li, K., Gao, X., Subhash, G., 2005. Effects of cell shape and cell wall thickness variations on the elastic properties of two-dimensional cellular solids. *International Journal of Solids and Structures* 42, 1777-1795.
36. Laroussi, M., Sab, K., Alaoui, A., 2002. Foam mechanics: nonlinear response of an elastic 3D-periodic microstructure. *International Journal of Solids and Structures* 39, 3599-3623.
37. Gong, L., Kyriakides, S., Jang, W., 2005. Compressive response of open-cell foams. Part I: Morphology and elastic properties. *International Journal of Solids and Structures* 42, 1355-1379.
38. Papka, S., Kyriakides, S., 1998. Experiments and full-scale numerical simulations of in-plane crushing of a honeycomb. *Acta Materialia* 46, 2765-2776.
39. ABAQUS™ User's Manual (Version 6.7). ABAQUS Inc., Providence, RI
40. Papka, S., Kyriakides, S., 1994. In-plane compressive response and crushing of honeycomb. *Journal of the Mechanics and Physics of Solids* 42, 1499-1532
41. Hashin, Z., Shtrikman, S., 1963. A variational approach to the theory of the elastic behaviour of multiphase materials. *Journal of the Mechanics and Physics of Solids* 11, 127–140.
42. Tuchinskii, L.I, 1983. Elastic Constants of Pseudoalloys with a Skeletal Structure. *Poroshk. Metall.*, 7 [247] 85 (Translated in *Powder Metallurgy and Metal Ceramics*, 1983), 588-595.
43. Ravichandran, K.S., 1994. Elastic properties of two-phase composites. *Journal of the American Ceramic Society* 77, 1178–1184.
44. Hashin, Z., 1983. Analysis of composite materials. *Journal of Applied Mechanics* 50, 481–505.
45. Bardella, L., Genna, F., 2001. On the elastic behavior of syntactic foams. *International Journal of Solids and Structures* 38, 7235-7260.

## **APPENDICES**

**APPENDIX A**

**EFFECT OF CELL STRUCTURE ON**

**ELASTIC-PLASTIC RESPONSE OF FOAM-FILLED COMPOSITES**

**A.1 Introduction**

Modeling of 2D cellular solids is generally based on idealized unit cells representing microstructural features of an average cell in a real material. A significant limitation of the unit-cell modeling approach is that it does not account for the natural variations in a typical microstructure. In this context, the objective of this work is to investigate how irregularity of cells affects the elasto-plastic response of syntactic foam-filled aluminum honeycomb composites under uniaxial compression. Although several methods have been developed to consider the effects of microstructural variability on mechanical properties of foams, the method based Voronoi tessellations has gained popularity in recent years. Accordingly, a 2D Voronoi tessellation technique in conjunction with finite element analysis was used to generate cell structures with randomly varying irregularities. The resulting microstructure is subsequently used to study the microstructure-compression response for syntactic foam-filled aluminum honeycomb composite.

## A.2 The approach: Voronoi tessellations

A Voronoi diagram is based on the principle of partitioning the space with  $n$  points such that for each site every point in the region around that site is closer to that site than to any other site.

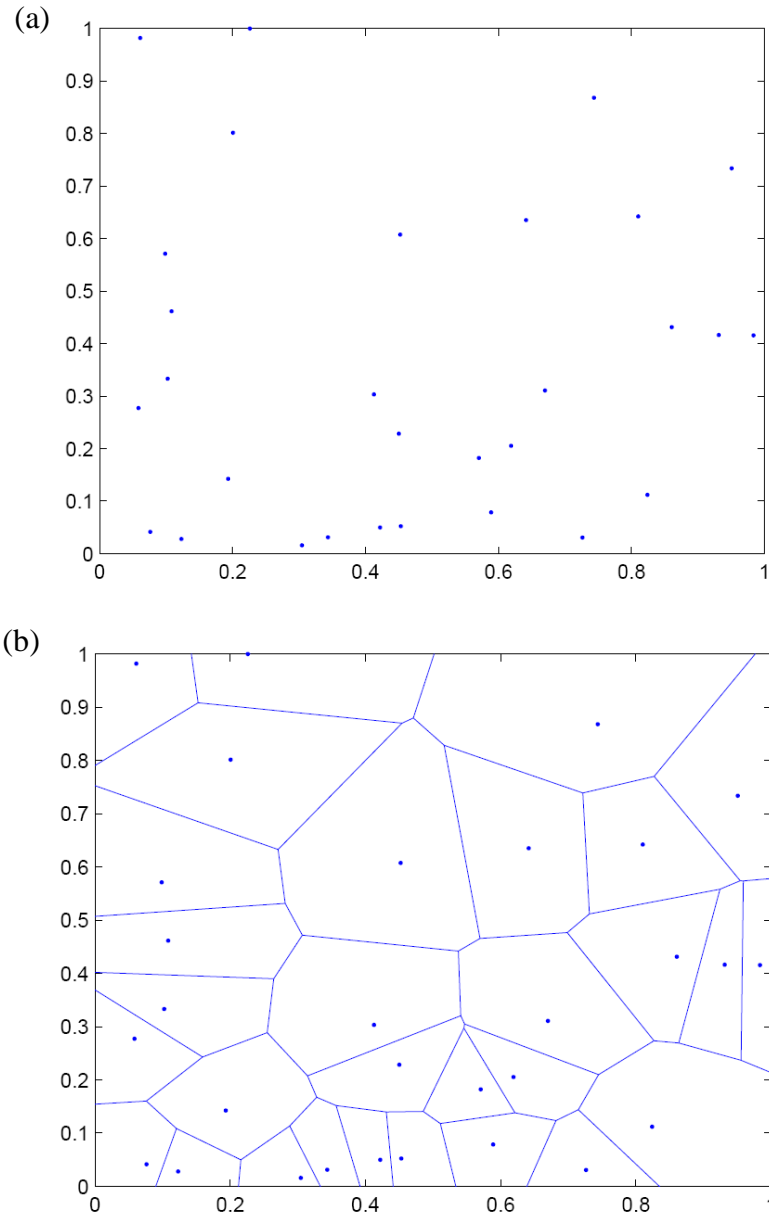


Figure A.1: (a) Set of random points, (b) Voronoi diagram for that set of points

Random 2D models were constructed for the syntactic foam-filled aluminum honeycomb composite using this technique. A set of 30 random points is shown in fig. A.1(a) and the voronoi diagram of this set is generated using voronoi command in MATLAB® is shown in fig.A.1(b). Finite element analysis is then performed on the conceived Voronoi structure to predict the compression response of the corresponding syntactic foam-filled aluminum honeycomb composite.

### **A.3 Irregularity parameter**

A regular hexagonal honeycomb, composed of identical cells having six sides and vertex angles of  $120^\circ$ , is a fully ordered 2D Voronoi tessellation. This basic pattern was used to create the structure for the foam-filled honeycombs described in Chapter 5. The random microstructure of this composite can be described by a 2D Voronoi diagram, which consists of a number of convex polygons. The first step towards creating a random microstructure is to generate an array of  $20 \times 20$  fully ordered hexagonal cells. Next, a random number set with a uniform distribution in the range [0:1] is generated and the coordinates of each of the points of the voronoi diagram are then perturbed using a set of random numbers to achieve varying degrees of irregularity. A unique set of random numbers can also be generated every time to vary the randomness. In the second step, Voronoi diagram is constructed such that the area fraction of the (aluminum) honeycomb is ~8%. The relative density of the honeycombs is estimated by dividing the area of the cell walls by the total area of a unit cell. Here, we define an irregularity parameter  $\alpha$  that is used to quantify the degree-of-irregularity (DOI) of a 2D Voronoi tessellation as,

$$\alpha = (A_l - A_s)$$

where,  $A_l$  and  $A_s$  are the area of the largest and the smallest cell in a particular random structure.

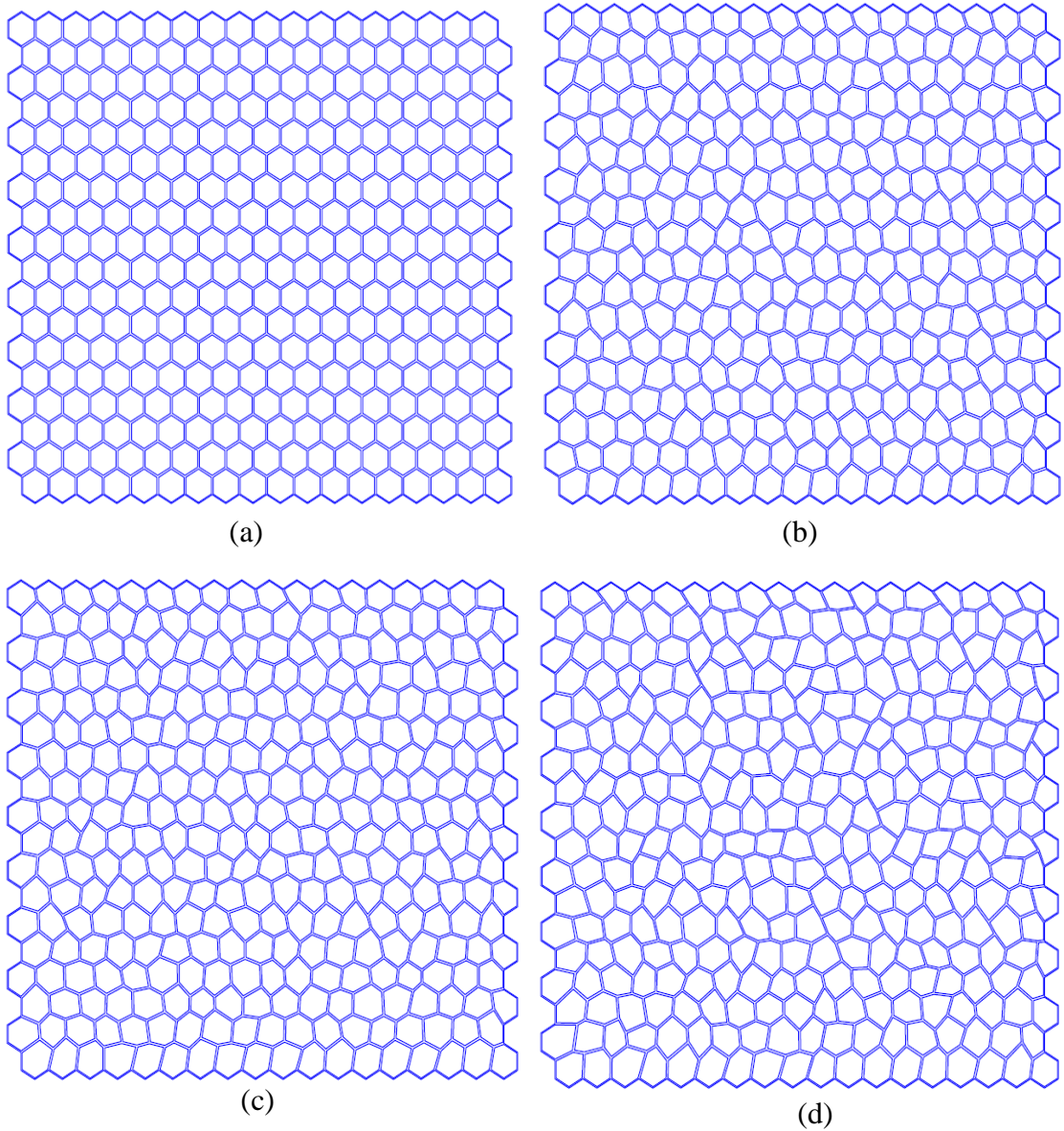


Figure A.2: Syntactic foam-filled honeycomb composite with varying degree-of-irregularity: (a):  $\alpha = 0$ , (b)  $\alpha = 0.2$ , (c)  $\alpha = 0.4$ , (d)  $\alpha = 0.6$

Syntactic foam-filled honeycomb composite with a regular hexagonal honeycomb structure is obtained when  $\alpha = 0$ , and the composite with a completely irregular honeycomb structure are defined when  $\alpha = 1$ . Figure A.1 shows syntactic foam-filled honeycomb samples with different degrees of cell shape irregularity. Each sample includes 324 complete cells. These models were first generated in MATLAB® and finite element analysis were performed using ABAQUS® structural analysis software.

#### **A.4 FEA model description**

Finite element analyses were carried out to obtain the stress-strain relations for syntactic foam-filled honeycombs with 30% volume fraction of microballoons having cell shape irregularities using ABAQUS/Standard. A rate independent plasticity model, described in Chapter 5, based on associated plastic flow rule and von-Mises yield criterion with isotropic hardening was used to model plasticity of both aluminum and syntactic foam phases of the composite. The measured stress-strain response for syntactic foam with 30% volume fractions of microballoons was used to model the infused material around the ligaments of the aluminum honeycomb. The properties of Al 5052-H39 were assigned to regions representing ligaments of the aluminum honeycomb structure. The other parameters used in the analyses were the same as described in Section 5.3.1 of Chapter 5.



### A.5 Effect of cell irregularity on stress-strain response of composites

Finite element analyses were carried out on syntactic foam-filled honeycomb composites with varying degree of cell shape regularity and the effect of cell structure randomness on the stress-strain response of the composites was studied. The results of the finite element simulations are plotted in Fig. A.3. It shows that with an increase in DOI results in a decrease in the elastic modulus. It also affects the overall stress-strain response of the composites in general and inelastic characteristics in particular.

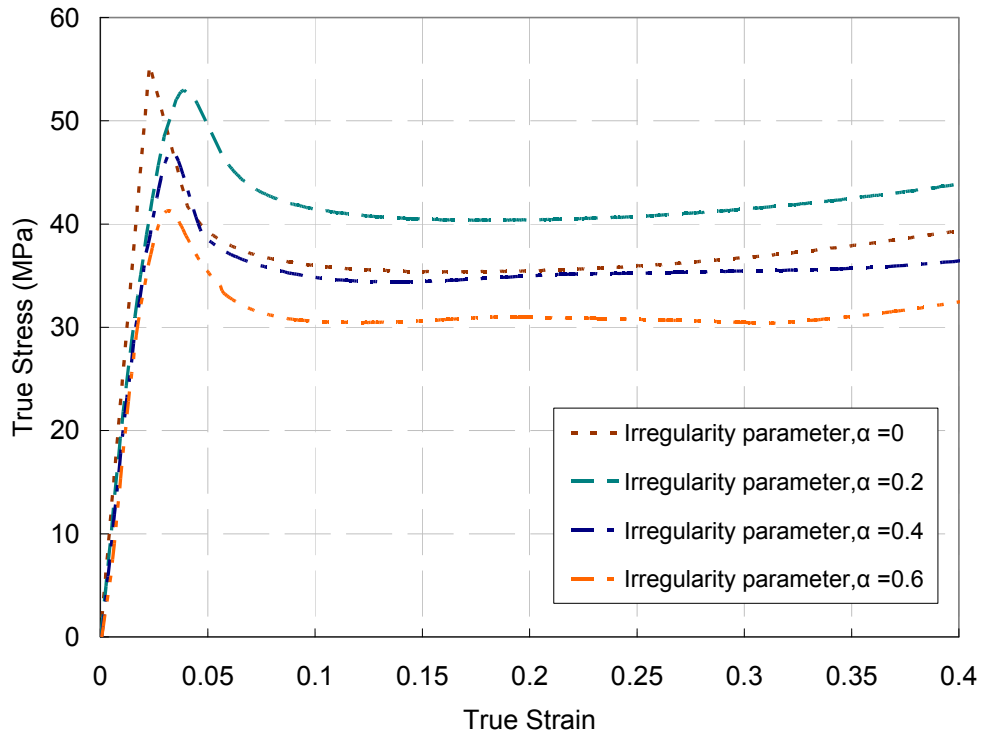


Figure A.3: Effect of cell irregularity on stress-strain response of the composite

The yield stress of syntactic foam-filled honeycomb decreases with increase in the irregularity of cell shapes and thus the syntactic foam-filled honeycomb with a perfectly ordered cell structure has the highest value of yield stress (55.4 MPa) and this decreases

monotonically to  $\sim 53\text{Mpa}$ ,  $47\text{Mpa}$ ,  $41\text{Mpa}$  for  $\alpha = 0.2$ ,  $0.4$  and  $0.6$ , respectively. The plateau stress, however, increases by approximately 14% for  $\alpha = 0.2$  and then decreases for  $\alpha = 0.4$  and  $0.6$  by approximately by 2% and 12% when compared to that of the foam-filled honeycomb with perfectly ordered cell structure. From Fig. A.3 it can be observed that on average elastic modulus increases considerably when cell randomness parameter ( $\alpha$ ) increases from 0 to 0.2 with further increase in  $\alpha$ , the change in elastic modulus is not significant and decreases by  $\sim 6\%$  when degree-of-regularity is increased from 0.4 to 0.6. Syntactic foam-filled honeycomb composite with regular cell structure is found to be strongest in terms of elastic moduli and yield strength.

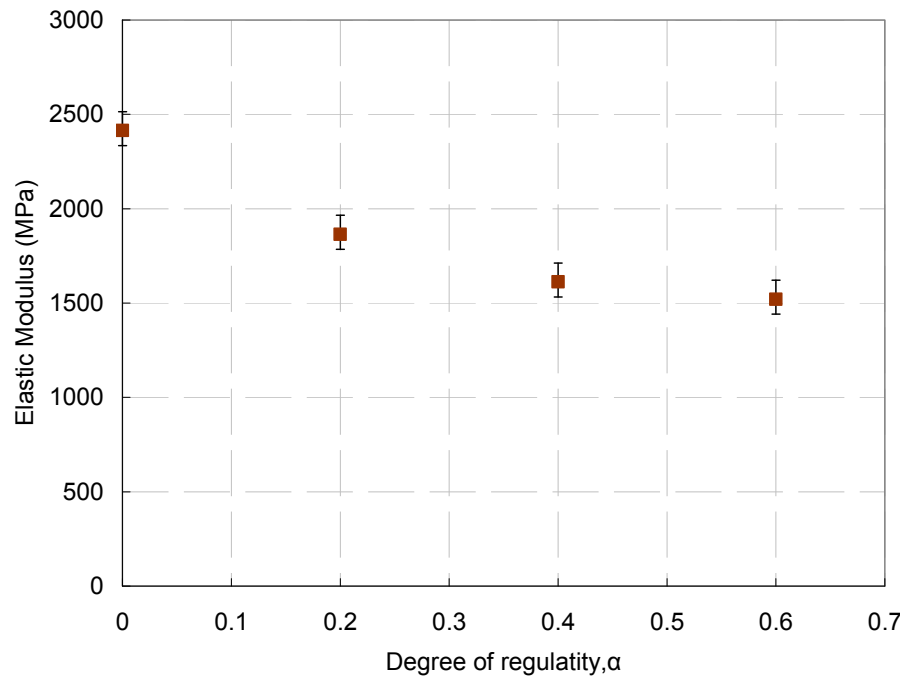


Figure A.4: Effect of cell irregularity on elastic modulus of the composite

The strong dependence of the moduli on initial changes in  $\alpha$  is attributed to the changes in the microstructure as this leads to changes in cell regularity. Initial perturbations in the

shape of regular hexagonal cell structure leads to presence of irregular hexagonal cells in the microstructure, as shown in Fig. A.1(b). The stiffness of each of these irregular hexagons is significantly less than that of a regular hexagon, thereby leading to a significant decrease in the elastic modulus of the foam-filled honeycomb with perturbed cell shapes when compared to that with a regular cell shape.

#### **A.6 Effect of relative density on stress-strain response of composites**

Finite element models of foam-filled honeycomb composite with different relative densities of the (aluminum) honeycomb were generated by changing the cell wall thickness. As before, the model consisted of 324 regular hexagonal cells. The analyses were limited to models having low relative densities ( $\rho \leq 0.2$ ). The results are shown in Fig. A.5. The compression responses indicate that the elastic modulus, plateau stress and yield stress decrease with increasing relative density. With increase in the relative density there is decrease in the area of the cell and hence the area fraction of syntactic foam is also less and this results in a stiffer response of the composite. The plateau stress increases from 35MPa for a relative density of 8% to 53MPa for 20% relative density. The yield stress and the elastic modulus are also found to be increasing monotonically by 26% and 31% respectively. The stress-strain response of composite is found to be fairly consistent with the changes in the relative density of the aluminum honeycomb sheet.

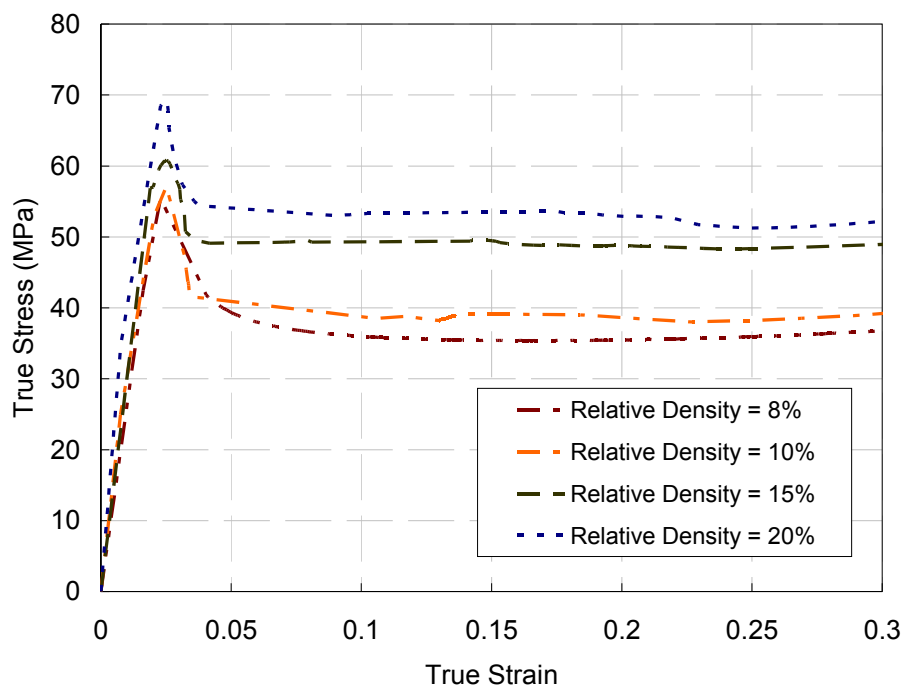


Figure A.5: Effect of relative density on stress-strain response of the composite.

**APPENDIX B**  
**MATLAB CODES**

**(1) This code is used to generate numerical model for syntactic foam-filled honeycomb composite**

```

%-----
This program is used to create cell array (8x8) with a cell size of 1/8
inch
%-----
clear all;
close all;
clc;

%-----
This is to generate a hexagonal grid
%-----
pos = hextop(10,10);
pos1=pos';
x=pos1(:,1);      % x-ccordinate of center points of cells
y=pos1(:,2);      % y-ccordinate of center points of cells
figure(1);

%-----
Construct a voronoi diagram
%-----
h=voronoi(x,y,[]);
[vx,vy] = voronoi(x,y,[]); % Vertices of voronoi edges so that
"plot(VX,VY,'-',X,Y,'.')" plots cell
axis equal;
[cord,c]=voronoin([x(:) y(:)]);
conn=zeros(length(c),6); % assign zero to the unassigned Index
for i=1:length(c),
temp=c{i};
for j=1:length(c{i})
conn(i,j)=temp(j);
end
end
close all;
nen=6;
nodes=length(cord); %defining the coordinates of the nodes (stored in
                    cord)
elems=length(conn); % defining the no. of nodes in each cell (6)

```

```

%-----
Checking for 0 and 1 in the cell array and deleting that array
%-----
icount=1;
for i=1:length(conn),
count=0;
for j=1:6,
if (and(conn(i,j)~=0,conn(i,j)~=1))
count=count+1;
end
if count==6,
connect(icount,:)=conn(i,:); % connect consists of cells whose index
                             are not 0 and 1
icount=icount+1;
end
end
end

% Assigning the x and y values as the first and second column of the
cord array
xo=cord(:,1);
yo=cord(:,2);

% To get the Actual cell size(8x8 in 1 inch)
x1=2.98823*xo;
y1=3.51932*yo;
xo=x1;
yo=y1;
cord(:,1)=x1;
cord(:,2)=y1;

% Matrix z with xo and yo
d=[1:length(xo)];
s=d';
zo=[s xo yo];
z=zo';

%-----
Creating the input file for writing the data
%-----
fid = fopen('box1_nodep.py', 'wt');
fprintf(fid,'from abaqus import *\n');
fprintf(fid,'from abaqusConstants import *\n');
fprintf(fid,'myModel=mdb.Model(name='Model-1')\n');
fprintf(fid,'import part, material, section, assembly, step,
interaction \n');
fprintf(fid,'import regionToolset, displayGroupMdbToolset as dgm, mesh,
load, job \n');

% For plotting and calculating the area of cells
for i=1:length(connect)
for j=1:nen
k=connect(i,j);
xxo(j)=xo(k);
yyo(j)=yo(k);

```

```

end
xxo(nen+1)=xxo(1);
yyo(nen+1)=yyo(1);
hold on;

plot(xxo,yyo,'-');
B(i)=polyarea(xxo,yyo);
end

% For Collecting values along xmin
n=1;
for i=1:length(cord)
if and(cord(i,1)<3.05,cord(i,1)>0);
if(cord(i,2)>2.04);
x2(n)=cord(i,1);
y2(n)=cord(i,2);
n=n+1;
end
end
end
% plot(x2,y2,'+');

% For Collecting values along ymax
n=1;
for i=1:length(cord)
if and(cord(i,2)>25.3,cord(i,1)<26.5);
if (cord(i,1)>2);
x3(n)=cord(i,1);
y3(n)=cord(i,2);
n=n+1;
end
end
end
% plot(x3,y3,'.');

% For Collecting values along xmax
n=1;
for i=1:length(cord)
if and (cord(i,1)>25.3,cord(i,1)<27);
if and(cord(i,2)<25,cord(i,2)>1);
x4(n)=cord(i,1);
y4(n)=cord(i,2);
n=n+1;
end
end
end
% plot(x4,y4,'+');

% For Collecting values along ymin
n=1;
for i=1:length(cord)
if and (cord(i,2)>1,cord(i,2)<2.1);
if (cord(i,1)>2.8);

```

```

x5(n)=cord(i,1);
y5(n)=cord(i,2);
n=n+1;
end
end
end
%plot(x5,y5);

% For defining xmin values
m2=[x2; y2];
m2= m2';
m21=sortrows(m2,2);
mx2=m21(:,1);
my2=m21(:,2);
plot(mx2,my2);
hold on;

%For defining ymax values
m3=[x3;y3];
m3=m3';
m31 = sortrows(m3,1);
mx3=m31(:,1);
my3=m31(:,2);
plot(mx3,my3);

%For defining xmax values
m4=[x4;y4];
m4=m4';
m41 = sortrows(m4,2);
mx4=m41(:,1);
my4=m41(:,2);
plot(mx4,my4);

%For defining ymax values
m5=[x5;y5];
m5=m5';
m51 = sortrows(m5,1);
mx5=m51(:,1);
my5=m51(:,2);
plot(mx5,my5);

% Scaling the values
xmin=min(x1); xmax=max(x1); ymin=min(y1); ymax=max(y1);
xint=(xmax-xmin)/10; yint=(ymax-ymin)/10;
xl=xmin-xint;
xu=xmax+xint;
yl=ymin-yint;
yu=ymax+yint;
axis equal;
axis([xl xu yl yu]);

% To create the inner cell
for i=1:length(connect)
    for j=1:6,

```



```

xs(i,j) = cord(connect(i,j),1);
ys(i,j) = cord(connect(i,j),2);
end
for j=1:6
xavg=mean(xs(i,:));
yavg=mean(ys(i,:));
xn(i,j) = xs(i,j)-xavg;
yn(i,j) = ys(i,j)-yavg;
xn1(i,j) = xn(i,j).*0.95;
yn1(i,j) = yn(i,j).*0.95;
xn2(i,j) = xn1(i,j)+xavg;
yn2(i,j) = yn1(i,j)+yavg;
end
end

for i=1:length(connect)
for j=1:nen
xxol(j)=xn2(i,j);
yyol(j)=yn2(i,j);
end
xxol(nen+1)=xxol(1);
yyol(nen+1)=yyol(1);

hold on;
plot(xxol,yyol,'-');
A(i)=polyarea(xxol,yyol);
end

%-----
Writing the data for ABAQUS input file
%-----
k=1000;
% For reading the points of the lines
for i=1:length(xn2),
k=k+1;
fprintf(fid,'mySketch%d = myModel.Sketch
(name='HexShape%d',sheetSize=200)\n',k,k);
for j=1:6,
if (j~=6)
fprintf(fid,'mySketch%d.Line(point1=( %6f, %6f),point2=( %6f, %6f
)\n',k, xn2(i,j), yn2(i,j), xn2(i,j+1), yn2(i,j+1));
else
fprintf(fid,'mySketch%d.Line(point1=( %6f, %6f),point2=( %6f, %6f
)\n',k, xn2(i,j), yn2(i,j), xn2(i,1), yn2(i,1));
end
end

% For defining Areas for the cells
fprintf(fid,'myHex%d =
myModel.Part(name='h%d',dimensionality=TWO_D_PLANAR,\n',k,k);
fprintf(fid,'type=DEFORMABLE_BODY)\n');
fprintf(fid,'myHex%d.BaseShell(sketch=mySketch%d)\n',k,k);
end

```

```

% Define remaining area
% To define the area of the cells
k=k+1;
fprintf(fid, 'mySketch%d =
myModel.Sketch(name=' 'HexShape%d' ',sheetSize=200.)\n',k,k);
for i=1:length(xn2),
for j=1:6,
if (j~=6)
fprintf(fid, 'mySketch%d.Line(point1=( %6f, %6f),point2=( %6f, %6f
))\n',k, xn2(i,j), yn2(i,j), xn2(i,j+1), yn2(i,j+1));
else
fprintf(fid, 'mySketch%d.Line(point1=( %6f, %6f),point2=( %6f, %6f
))\n',k, xn2(i,j), yn2(i,j), xn2(i,1), yn2(i,1));
end
end
end

% For defining the boundary and the area of inner cells
for i=1:length(mx2)
j=1;
if (i<length(mx2))
fprintf(fid, 'mySketch%d.Line(point1=( %6f, %6f),point2=( %6f, %6f
))\n',k, mx2(i,j), my2(i,j), mx2(i+1,j), my2(i+1,j));
else if (i==length(mx2))
end
end
end
for i=1:length(mx3)
j=1;
if (i<length(mx3))
fprintf(fid, 'mySketch%d.Line(point1=( %6f, %6f),point2=( %6f, %6f
))\n',k, mx3(i,j), my3(i,j), mx3(i+1,j), my3(i+1,j));
else if (i==length(mx3))
end
end
end
for i=1:length(mx4)
j=1;
if (i<length(mx4))
fprintf(fid, 'mySketch%d.Line(point1=( %6f, %6f),point2=( %6f, %6f
))\n',k, mx4(i,j), my4(i,j), mx4(i+1,j), my4(i+1,j));
else if (i==length(mx4))
end
end
end
for i=1:length(mx5)
j=1;
if (i<length(mx5))
fprintf(fid, 'mySketch%d.Line(point1=( %6f, %6f),point2=( %6f, %6f
))\n',k, mx5(i,j), my5(i,j), mx5(i+1,j), my5(i+1,j));
else if (i==length(mx5))
end
end
end
end

```

```

fprintf(fid,'myHex%d = myModel.Part(
name=' 'h%d' ',dimensionality=TWO_D_PLANAR,\n',k,k);
fprintf(fid,' type=DEFORMABLE_BODY)\n');
fprintf(fid,'myHex%d.BaseShell(sketch=mySketch%d)\n',k,k);

% For reading the points of the lines of one cell(outer cell)
for i=1,
k=k+1;
fprintf(fid,'mySketch%d =
myModel.Sketch(name=' 'HexShape%d' ',sheetSize=200.)\n',k,k);
for j=1:6,
if (j~=6)
fprintf(fid, 'mySketch%d.Line(point1=( %6f, %6f),point2=( %6f, %6f
))\n',k, cord(connect(i,j),1), cord(connect(i,j),2),
cord(connect(i,j+1),1), cord(connect(i,j+1),2));
else
fprintf(fid, 'mySketch%d.Line(point1=( %6f, %6f),point2=( %6f, %6f
))\n',k, cord(connect(i,j),1), cord(connect(i,j),2),
cord(connect(i,1),1), cord(connect(i,1),2));
end
end

% For defining Areas for the cell
fprintf(fid,'myHex%d =
myModel.Part(name=' 'h%d' ',dimensionality=TWO_D_PLANAR,\n',k,k);
fprintf(fid,' type=DEFORMABLE_BODY)\n');
fprintf(fid,'myHex%d.BaseShell(sketch=mySketch%d)\n',k,k);
end

% To define the inner and outer cell as a set
% For reading the points of the lines of one cell (outer cell)
for i=1,
k=k+1;
fprintf(fid,'mySketch%d =
myModel.Sketch(name=' 'HexShape%d' ',sheetSize=200.)\n',k,k);
for j=1:6,
if (j~=6)
fprintf(fid, 'mySketch%d.Line(point1=( %6f, %6f),point2=( %6f, %6f
))\n',k, cord(connect(i,j),1), cord(connect(i,j),2),
cord(connect(i,j+1),1), cord(connect(i,j+1),2));
else
fprintf(fid, 'mySketch%d.Line(point1=( %6f, %6f),point2=( %6f, %6f
))\n',k, cord(connect(i,j),1), cord(connect(i,j),2),
cord(connect(i,1),1), cord(connect(i,1),2));
end
end
end

%For reading the points of the lines of one cell(inner cell)
for i=1,
for j=1:6,
if (j~=6)
fprintf(fid, 'mySketch%d.Line(point1=( %6f, %6f),point2=( %6f, %6f
))\n',k, xn2(i,j), yn2(i,j), xn2(i,j+1), yn2(i,j+1));
else

```

```

fprintf(fid, 'mySketch%d.Line(point1=( %6f, %6f),point2=( %6f, %6f
))\n',k, xn2(i,j), yn2(i,j), xn2(i,1), yn2(i,1));
end
end
end

% For Assembly
fprintf(fid,'a1 = mdb.models[''Model-1''].rootAssembly\n');
fprintf(fid,'a1.DatumCsysByDefault(CARTESIAN)\n');
for i=1001:k
fprintf(fid,'a1 = mdb.models[''Model-1''].rootAssembly \n');
fprintf(fid,'p = mdb.models[''Model-1''].parts[''h%d'']\n',i);
fprintf(fid,'a1.Instance(name='''h%d''', part=p, dependent=ON)\n',i);
fprintf(fid,'a1.Instance(name='''h%d''', part=p)\n',i);
end
fprintf(fid,'session.viewports[''Viewport:
1''].setValues(displayedObject=a1)\n');
fclose(fid);

```

## (2) This code is used to generate voronoi model

```
%-----  
%Program generates the voronoi model for 20x20 cell array  
%-----  
  
clear all;  
close all;  
clc;  
  
%-----  
This is to generate a hexagonal grid  
%-----  
pos = hextop(20,20);  
pos1=pos';  
x=pos1(:,1);      % x-ccordinate of center points of cells  
y=pos1(:,2);      % y-ccordinate of center points of cells  
figure(1);  
h=voronoi(x,y,[]);  
[vx,vy] = voronoi(x,y,[]); % Vertices of voronoi edges so that  
"plot(VX,VY,'-',X,Y,'.')" plots cell  
axis equal;  
[cord,c]=voronoin([x(:) y(:)]);  
conn=zeros(length(c),6); % assign zero to the unassigned Index  
for i=1:length(c),  
temp=c{i};  
for j=1:length(c{i})  
conn(i,j)=temp(j);  
end  
end  
close all;  
nen=6;  
nodes=length(cord); %defining the coordinates of the nodes (stored in  
cord)  
elems=length(conn); % defining the no. of nodes in each cell (6)  
  
%-----  
Checking for 0 and 1 in the cell array and deleting that array  
%-----  
icount=1;  
for i=1:length(conn),  
count=0;  
for j=1:6,  
if (and(conn(i,j)~=0,conn(i,j)~=1))  
count=count+1;  
end  
if count==6,  
connect(icount,:)=conn(i,:); % connect consists of cells whose index  
are not 0 and 1  
icount=icount+1;  
end  
end  
end
```

```

% Assigning the x and y values as the first and second column of the
cord array
xo=cord(:,1);
yo=cord(:,2);

% Matrix z with xo and yo
d=[1:length(xo)];
s=d';
zo=[s xo yo];
z=zo';

%-----
Creating the input file for writing the data
%-----
fid = fopen('connect_pert.py', 'wt');
fprintf(fid,'from abaqus import *\n');
fprintf(fid,'from abaqusConstants import *\n');
fprintf(fid,'myModel=mdb.Model(name='Model-1')\n');

%-----
To perturb the nodes
%-----
rand('state',10);      % use different states to get a unique random
                        number set every time

x7=rand(1,length(cord));
y7=rand(1,length(cord));
x8=x7*0.3;
y8=y7*0.3;
x8=x8';
y8=y8';

% Not perturbing the side nodes
for i=1:length(cord)
if (cord(i,2)<=0.5774)
y9(i)=cord(i,2);
x9(i)=cord(i,1);
elseif or(cord(i,1)==0.5,cord(i,1)==1)
x9(i)=cord(i,1);
y9(i)=cord(i,2);

elseif or(cord(i,1)==18.5,cord(i,1)==19)
x9(i) = cord(i,1);
y9(i)= cord(i,2);

elseif (cord(i,2)>=15.8771)
y9(i)= cord(i,2);
x9(i)= cord(i,1);

else
x9(i)=x8(i)+xo(i);
y9(i)=y8(i)+yo(i);
end
end

```

```

%-----
To assign values after perturbation
%-----
x9=x9';
y9=y9';
cord1(:,1)=x9;
cord1(:,2)=y9;

% For Collecting values along xmin
n=1;
for i=1:length(cord)
if and(cord(i,1)<1.1,cord(i,1)>0);
if(cord(i,2)>0.289);
x2(n)=cord(i,1);
y2(n)=cord(i,2);
n=n+1;
end
end
end

% For Collecting values along ymax
n=1;
for i=1:length(cord)
if and(cord(i,2)>15.80,cord(i,1)<18.6);
if (cord(i,1)>0.8);
x3(n)=cord(i,1);
y3(n)=cord(i,2);
n=n+1;
end
end
end

% For Collecting values along xmax
n=1;
for i=1:length(cord)
if and (cord(i,1)>18,cord(i,1)<19.1);
if and(cord(i,2)<16,cord(i,2)>0.29);
x4(n)=cord(i,1);
y4(n)=cord(i,2);
n=n+1;
end
end
end

% For Collecting values along ymin
n=1;
for i=1:length(cord)
if and (cord(i,2)>0.28,cord(i,2)<0.58);
if (cord(i,1)>0.5);
x5(n)=cord(i,1);
y5(n)=cord(i,2);
n=n+1;
end
end
end

```

```

%For defining xmin values
m2=[x2; y2];
m2= m2';
m21=sortrows(m2,2);
mx2=m21(:,1);
my2=m21(:,2);
plot(mx2,my2);
hold on;

%For defining ymax values
m3=[x3;y3];
m3=m3';
m31 = sortrows(m3,1);
mx3=m31(:,1);
my3=m31(:,2);
plot(mx3,my3);

%For defining xmax values
m4=[x4;y4];
m4=m4';
m41 = sortrows(m4,2);
mx4=m41(:,1);
my4=m41(:,2);
plot(mx4,my4);

%For defining ymax values
m5=[x5;y5];
m5=m5';
m51 = sortrows(m5,1);
mx5=m51(:,1);
my5=m51(:,2);
plot(mx5,my5);

% scaling the values
xmin=min(x); xmax=max(x); ymin=min(y); ymax=max(y);
xint=(xmax-xmin)/10; yint=(ymax-ymin)/10;

xl=xmin-xint;
xu=xmax+xint;
yl=ymin-yint;
yu=ymax+yint;
axis equal;
axis([xl xu yl yu]);

%For perturbing the outer cells to get the inner area
for i=1:length(connect)
for j=1:6,
xs(i,j) = cord1(connect(i,j),1);
ys(i,j) = cord1(connect(i,j),2);
end
for j=1:6
xavg=mean(xs(i,:));
yavg=mean(ys(i,:));
xn(i,j) = xs(i,j)-xavg;

```



```

yn(i,j) = ys(i,j)-yavg;
xn1(i,j) = xn(i,j).*0.93;
yn1(i,j) = yn(i,j).*0.93;
xn2(i,j) = xn1(i,j)+xavg;
yn2(i,j) = yn1(i,j)+yavg;
end
end

% Plotting the inner cells after creating the cells
for i=1:length(connect)
for j=1:nen
xxol(j)=xn2(i,j);
yyol(j)=yn2(i,j);
end
xxol(nen+1)=xxol(1);
yyol(nen+1)=yyol(1);
hold on;

plot(xxol,yyol,'-');
A(i)=polyarea(xxol,yyol);
end

%-----
Writing the data for ABAQUS input file
%-----
k=1000;
% for reading the points of the lines
for i=1:length(xn2),
k=k+1;
fprintf(fid,'mySketch%d =
myModel.Sketch(name='HexShape%d',sheetSize=200.)\n',k,k);
for j=1:6,
if (j~=6)
fprintf(fid,'mySketch%d.Line(point1=( %6f, %6f),point2=( %6f, %6f
))\n',k, xn2(i,j), yn2(i,j), xn2(i,j+1), yn2(i,j+1));
else
fprintf(fid,'mySketch%d.Line(point1=( %6f, %6f),point2=( %6f, %6f
))\n',k, xn2(i,j), yn2(i,j), xn2(i,1), yn2(i,1));
end
end

% For defining Areas for the cells
fprintf(fid,'myHex%d =
myModel.Part(name='h%d',dimensionality=TWO_D_PLANAR,\n',k,k);
fprintf(fid,'      type=DEFORMABLE_BODY)\n');
fprintf(fid,'myHex%d.BaseShell(sketch=mySketch%d)\n',k,k);
end

% Define remaining area
% To define the area of the cells
k=k+1;
fprintf(fid,'mySketch%d =
myModel.Sketch(name='HexShape%d',sheetSize=200.)\n',k,k);

```

```

for i=1:length(xn2),
for j=1:6,
if (j~=6)
fprintf(fid, 'mySketch%d.Line(point1=( %6f, %6f),point2=( %6f, %6f
))\n',k, xn2(i,j), yn2(i,j), xn2(i,j+1), yn2(i,j+1));
else
fprintf(fid, 'mySketch%d.Line(point1=( %6f, %6f),point2=( %6f, %6f
))\n',k, xn2(i,j), yn2(i,j), xn2(i,1), yn2(i,1));
end
end
end

% For defining the boundary and the area of inner cells
for i=1:length(mx2)
j=1;
if (i<length(mx2))
fprintf(fid, 'mySketch%d.Line(point1=( %6f, %6f),point2=( %6f, %6f
))\n',k, mx2(i,j), my2(i,j), mx2(i+1,j), my2(i+1,j));
else if (i==length(mx2))
end
end
end

for i=1:length(mx3)
j=1;
if (i<length(mx3))
fprintf(fid, 'mySketch%d.Line(point1=( %6f, %6f),point2=( %6f, %6f
))\n',k, mx3(i,j), my3(i,j), mx3(i+1,j), my3(i+1,j));
else if (i==length(mx3))
end
end
end

for i=1:length(mx4)
j=1;
if (i<length(mx4))
fprintf(fid, 'mySketch%d.Line(point1=( %6f, %6f),point2=( %6f, %6f
))\n',k, mx4(i,j), my4(i,j), mx4(i+1,j), my4(i+1,j));
else if (i==length(mx4))
end
end
end

for i=1:length(mx5)
j=1;
if (i<length(mx5))
fprintf(fid, 'mySketch%d.Line(point1=( %6f, %6f),point2=( %6f, %6f
))\n',k, mx5(i,j), my5(i,j), mx5(i+1,j), my5(i+1,j));
else if (i==length(mx5))
end
end
end

```

```

fprintf(fid,'myHex%d =
myModel.Part(name='h%d',dimensionality=TWO_D_PLANAR,\n',k,k);
fprintf(fid,' type=DEFORMABLE_BODY)\n');
fprintf(fid,'myHex%d.BaseShell(sketch=mySketch%d)\n',k,k);

% For reading the points of the lines of one cell(outer cell)
for i=1,
k=k+1;
fprintf(fid,'mySketch%d =
myModel.Sketch(name='HexShape%d',sheetSize=200.)\n',k,k);
for j=1:6,
if (j~=6)
fprintf(fid,'mySketch%d.Line(point1=( %6f, %6f),point2=( %6f, %6f
))\n',k, cord(connect(i,j),1), cord(connect(i,j),2),
cord(connect(i,j+1),1), cord(connect(i,j+1),2));
else
fprintf(fid,'mySketch%d.Line(point1=( %6f, %6f),point2=( %6f, %6f
))\n',k, cord(connect(i,j),1), cord(connect(i,j),2),
cord(connect(i,1),1), cord(connect(i,1),2));
end
end

% For defining Areas for the cell
fprintf(fid,'myHex%d =
myModel.Part(name='h%d',dimensionality=TWO_D_PLANAR,\n',k,k);
fprintf(fid,' type=DEFORMABLE_BODY)\n');
fprintf(fid,'myHex%d.BaseShell(sketch=mySketch%d)\n',k,k);
end

% For Assembly
fprintf(fid,'a1 = mdb.models[''Model-1''].rootAssembly\n');
fprintf(fid,'a1.DatumCsysByDefault(CARTESIAN)\n');
for i=1001:k
fprintf(fid,'a1 = mdb.models[''Model-1''].rootAssembly \n');
fprintf(fid,'p = mdb.models[''Model-1''].parts['h%d']\n',i);
fprintf(fid,'a1.Instance(name='h%d', part=p, dependent=ON)\n',i);
fprintf(fid,'a1.Instance(name='h%d', part=p)\n',i);
end
fprintf(fid,'session.viewports[''Viewport:
1''].setValues(displayedObject=a1)\n');
fclose(fid);

```